Chapman - Jouguet deflagrations and their transition to detonations

Doctoral thesis by
Willstrong Rakotoarison

Thesis supervised by **Pr. Matei I. Radulescu**
submitted to the **University of Ottawa**
in partial fulfillment of the requirements for the **Ph.D. degree**

Department of Mechanical Engineering
Faculty of Engineering
University of Ottawa

uOttawa

Publications

Journal articles

W. Rakotoarison and M. I. Radulescu, "A dynamic system approach for solving the steady structure of high speed deflagrations", 2023, *Proceedings of the Combustion Institute*

W. Rakotoarison, A. Pekalski, and M. I. Radulescu, "Detonation transition criteria from the interaction of supersonic shock-flame complexes with different shaped obstacles", 2020, *Journal of Loss Prevention in the Process Industries*, vol. 64, p. 103963

W. Rakotoarison, B. Maxwell, A. Pekalski, and M. I. Radulescu, "Mechanism of flame acceleration and detonation transition from the interaction of a supersonic turbulent flame with an obstruction: Experiments in low pressure propane–oxygen mixtures", 2019, *Proceedings of the Combustion Institute*, vol. 37, no. 3, pp. 3713–3721

In preparation

W. Rakotoarison, H. Yang, and M. I. Radulescu "A one-dimensional model for CJ-deflagrations and their transition to detonations", in preparation for *Combustion and Flame* (2023)

W. Rakotoarison, Y. Vilende, A. Pekalski, and M. I. Radulescu "Model for Chapman-Jouguet deflagrations in open ended tubes with varying vent ratios", in preparation for *Combustion and Flame* (2023)

Conference papers and presentations

W. Rakotoarison, and M. I. Radulescu, "A dynamic system approach for solving the steady structure of high speed deflagrations", presented at the *39th International Symposium on Combustion*, 2022, Dublin, Ireland

W. Rakotoarison, Y. Vilende, and M. I. Radulescu, "Model for CJ deflagrations in open ended tubes with varying vent ratios", presented at the *27th International Colloquium on the Dynamics of Explosions and Reactive Systems*, 2019, Beijing, China

W. Rakotoarison, A. Pekalski, and M. I. Radulescu, "Detonation transition criteria from the interaction of supersonic shock-flame complexes with different shaped obstacles", presented at the *12th International Symposium on Hazards, Prevention, and Mitigation of Industrial Explosions*, Kansas City, 2018, Missouri - USA

W. Rakotoarison, B. Maxwell, A. Pekalski, and M. I. Radulescu, "Mechanism of flame acceleration and detonation transition from the interaction of a supersonic turbulent flame with an obstruction:

Experiments in low pressure propane–oxygen mixtures", presented at the *37th International Symposium on Combustion*, 2018, Dublin, Ireland

W. Rakotoarison, M. I. Radulescu, B. Maxwell, and A. Pekalski, "Experimental investigation of the deflagration to detonation transition of a supersonic shock - turbulent flame complex in an obstructed channel", presented at the *2018 Combustion Institute/Canadian Section Spring Technical Meeting*, 2018, Toronto, Ontario - Canada

W. Rakotoarison, A. Pekalski, and M. I. Radulescu, "Propagation of a shock-flame complex around a cylinder", poster presented at the *26th International Colloquium on the Dynamics of Explosions and Reactive Systems*, 2017, Boston, Massachusetts - USA

Abstract

This thesis by articles addresses the role played by Chapman-Jouguet (CJ) deflagrations in deflagration to detonation transition (DDT) events. By definition, CJ deflagrations are flames propagating with a sonic flow in the burned gases, and are theoretically the fastest subsonic combustion waves able to propagate steadily, predicted using conservation of mass, momentum and energy. DDT is difficult to describe, as many complex phenomena and their interaction take place, including flame instabilities, turbulent combustion, and combustion in compressible medium, among others. Recent experiments and numerical simulations however showed that, prior to transition to detonations, deflagrations plateau at the CJ regime before rapid acceleration.

In the present thesis, multiple aspects of the last stages of DDT are studied, and are each presented in published articles or articles in preparation. The two articles presented in Chapter 2 focus on experiments performed on the transition of a shock-flame complex to a detonation downstream of a single obstacle, in a stoichiometric propane-oxygen mixture at low pressure, mimicking the common configuration found at the last stages of DDT in experiments and numerical simulations performed in a channel filled with obstacles. The relative large size of the obstacle and the low gas initial pressure permitted to visualize the details of the initiation of the detonation around the obstacle. Transition to detonation was found to occur in a similar fashion for variously shaped obstacles, after flame acceleration due to the interaction with reflected shocks. This acceleration process was found to occur rapidly in the case where the incident flame propagated with a burning rate close to the Chapman-Jouguet value.

The third article presented in Chapter 3 describes a model aimed to predict the properties of shocks followed by a CJ deflagration, in experimental configurations where the burned gases can be vented. The formulation is similar to the double discontinuity problem adapted from the work of Chue (1993), extended to cases where the burned gases are not confined by a rear wall anymore, but can be vented through an opening of known dimensions. The properties of the shock / CJ-deflagration complex could then be predicted and compared to flame measurements done prior the initiation of detonations, obtained on a selection of large scale DDT experiments. The good agreement suggests that DDT occurs when deflagrations reach the CJ regime, corroborating with observations done in shock tubes.

The article presented in Chapter 4 is aimed to present a consistent method for calculating the structure of flames propagating at arbitrary burning velocities, from the low-Mach case (isobaric) up to the CJ deflagration regime. The method uses a dynamical system approach to calculate the steady wave structure, described by ordinary differential equations. A stability analysis near the burned and unburned gases permitted to develop a numerical shooting technique, which was used

to obtain the flame structure and burning rate eigenvalue.

Chapter 5 is a numerical study of the deflagration to detonation transition problem in one-dimension. By linearly increasing the burning rate eigenvalue to increase the flame burning velocity, the flame first reached the CJ condition. Subsequent increase in the burning rate leads to the self-organization of the flame into a CJ deflagration - shock complex. This self-organization triggers a pulsating gasdynamic instability leading to the transition of the flame to detonation.

Résumé

Cette thèse par articles traite du rôle des déflagrations Chapman-Jouguet (CJ) dans les problèmes de transition déflagration-détonation (TDD). Par définition, ces déflagrations se propagent avec un écoulement sonique dans les gaz brûlés, et sont théoriquement les flammes subsoniques les plus rapides pouvant se propager de façon stationnaire, prédites par les lois de conservation de masse, quantité de mouvement et énergie. La TDD est difficile à décrire car elle implique des mécanismes complexes et leurs interactions, telles que les instabilités de combustion, et combustion turbulente en milieu compressible, entre autres. De récentes expériences et simulations ont cependant montré que, précédant leur transition vers des détonations, les déflagrations stagnent au régime CJ avant une rapide accélération.

Dans cette thèse, différents aspects des dernières étapes de la TDD sont étudiés, chacun étant présentés dans un articles publiés ou en préparation. Les deux articles présentés au Chapitre 2 portent sur des expériences de transition de complexes chocs-flammes vers des détonations en aval d'un obstacle, dans des mélanges propane-oxygène stœchiométriques à basse pression, imitant la configuration d'écoulement ayant lieu aux dernières étapes de la TDD, dans des expériences et simulations numériques réalisées dans des canaux à obstacles. La relative grande taille de l'obstacle et la faible pression initiale a permis de visualiser les détails de l'initiation de la détonation autour de l'obstacle. Il a été trouvé que la transition vers une détonation a lieu de manière similaire pour une variété de formes d'obstacles, causée par l'accélération de la flamme après interaction avec des chocs réfléchis. De plus, le processus d'accélération de flamme a lieu plus rapidement dans les cas où la flamme incidente se propageait à un taux de combustion proche de celui Chapman-Jouguet.

Le troisième article présenté au Chapitre 3 décrit un modèle destiné à prédire les propriétés de chocs suivis de déflagrations CJ, dans des expériences où les gaz brûlés peuvent être évacués. Cette formulation est similaire au problème de la double discontinité adaptée du travail de Chue (1993), étendue au cas où les gaz brulés ne sont pas confinés, mais peuvent être évacués à travers une ouverture aux dimensions connues. Les propriétés des complexes chocs / déflagrations CJ peuvent alors être prédites puis comparées aux mesures faites sur des flammes, juste avant leur transition vers des détonations, obtenues dans des expériences de TDD à grande échelle. Leur bon accord suggère que la TDD a lieu quand les déflagrations ont atteignent le régime CJ, corroborant les observations faites dans des tubes à chocs.

L'article présenté au Chapitre 4 a pour but de présenter une méthode capable de calculer la structure de flammes se propageant à des vitesses de combustion arbitraires, du cas bas nombre de Mach (isobare) jusqu'au régime de déflagration CJ. Cette méthode traite les flammes stationnaires, dont la structure est décrite par des équations différentielles ordinaires, comme un système

dynamique. Une analyse de la stabilité linéaire aux gaz frais et brûlés a permis de développer une *shooting method* dédiée, utilisée pour obtenir la structure des flammes ainsi que leur valeur propre de combustion.

Le Chapitre 5 est une étude numérique du problème de TDD en une dimension. En augmentant linéairement la valeur propre de combustion de la flamme pour augmenter son taux de combustion, la flamme atteint dans un premier temps les conditions CJ. Une augmentation supplémentaire du taux de combustion mène à la formation d'un complexe choc - déflagration CJ. Cette organisation déclenche une instabilité de combustion, se manifestant par une pulsation du taux de combustion, menant à la transition de la déflagration vers une détonation.

Acknowledgments

I started this thesis with a lot of excitement. Learning cool stuff, experiencing another country, practicing the language, making new friends were what I had in mind when I decided to start this chapter of my life. After all these years and with a lot of help, I can confidently say that I found what I looked for. This part is dedicated to the people who were here close, and those who were, although out of sight, definitely not out of mind.

My first words go to Prof. Matei Radulescu. For hosting me in his group, guiding me in my research, being patient in teaching, providing advice during our conversations, bringing me around the world, helping me grow up as a scientist and a human ... and whatever else I cannot think of that has been decisive in the realization of this thesis. For all that, there is barely any word to express how thankful I am. Please know that your lessons were not taught in vain, and will be put to good use in my personal and professional life.

With him, I would like to thank all the people of the DRDL and other research fellow. It is hard to express how fortunate I am to get along with you, from the office to out in the wild. Hongxia, Farzane, Max, Qiang, Ramki, Kevin, Shem, Sarthak, Aliou, Pr. Ashwin Chinnayya, I wish you to do great in your lives, just as you wished me to do great in mine. I would also like to thank Dr. Andrjez Pekalski from Shell for useful discussions, and for permitting part of this research to be done. Finally, I would like to thank Prof. Pierre Vidal for being the one to introduce me to the field of detonations, making me like it, and helping me at key steps of this adventure.

Because a good adventure does not come without good fellows, I would like to express my gratitude to the family Gasparyan, Lilit, Hovhannes, Arpine, their brothers and parents, who cared for me like one of theirs. Please know that your blessings reached me, and how much I will value the time I spent with you. I would also like to let *Les Bogoles*, Nala, Zenfull, Clochette, Khalessi, Melina, Gino, Marie, Ema, Fred, Said, Ivan, Alexis, Kenzo and Kate know that your support helped me go through life far from home. More than just friends, you helped me grow *strong* (in all the sense of the term) and kept my heart warm, even in the coldest nights of the Canadian winter. I would also like to thank Laura, Paul and Jacob for hosting me and being so helpful during my first year in Ottawa. The same goes to Marge and Dave, who have been wonderful hosts during the following years, and made my stay very comfortable.

To all of you and those I did not mention, but that have been at some point part of my journey. You may think this work is mine *only*, but be aware. I would not have been able to put it all together without your love, support, and faith in what I am capable of. I hope these few words can express how grateful I am to have you by my side.

Willstrong

Pour vous Maman, Papa, Flowave, Alix.

Votre amour inconditionnel m'a fait aller bien plus loin que je ne m'en serais cru capable.

Contents

Chapter 1

Introduction

1.1 Deflagration to detonation transtion

Deflagration to detonation transition (DDT) is one of the major topics in the field of combustion, owing to its relevance in application to safety in the process industry [1], the design of detonation base power generation and propulsion devices, or the formation of supernovae when applied to thermonuclear reaction systems [2]. It relates to the sudden change of the propagation mechanism of combustion waves in premixed reactive mixtures. Deflagrations are expansion waves, for which the propagation mechanism relies on the diffusion of heat and chemical species through the reaction zone. They propagate at subsonic burning velocities of the order of 10 cm/s when they are laminar, and up to 200 m/s when they are highly turbulent. On the other hand, detonations are supersonic compression waves in which reactions are self-initiated. This occurs due to the presence of a precursor shock, downstream of which conditions of pressure and temperature are favorable to the gas thermal ignition on short time scales. Both the reaction zone and the precursor shock are coupled, as the expansion of the burned gases provides the thrust required to drive the shock. Hence, the detonation wave is self-sustained, and propagates at the so-called Chapman-Jouguet (CJ) detonation speed, typically of the order 2000 m/s for stoichiometric fuel-air mixtures.

Owing to their differences in their respective propagation mechanism, deflagration to detonation transition requires the description of many individual phenomena, occurring over a wide range of space and time scales, as well as their interactions. This statement is what makes DDT a complex event to study. Nevertheless, detailed description of the mechanisms of flame acceleration from low speed laminar flames to transition to detonation, based on extensive experimental and numerical investigation, can be found in the review papers [3–5], from which a typical sequence of events can be summarized as follow. A laminar deflagration is initiated from a mild ignition source. Its

front being intrinsically unstable, hydrodynamic and thermal-diffusive instabilities quickly cause it to wrinkle and increase its surface area. This latter effect is further amplified in non-smooth channels, caused by the stretching of the laminar flame front as it is convected through constrictions provided by inner walls or obstacles [4, 6], resulting in an even stronger increase of its front surface area. This provides the main mechanism of flame acceleration at early stages. The substantial flame acceleration results in the formation of acoustic waves, eventually coalescing to form shocks, downstream of which the flame burning rate is increased owing to the higher temperature of the compressed fresh gases. Moreover, these shocks can reflect to interact back with the flame front, and further destabilize it. The turbulence generated by such events, together with the interaction of the flame front with turbulent wakes, pressure gradients and boundary layers [7, 8], contribute to further increase the flame burning rate. At the late stages of its acceleration, the deflagration drives a shock in the fresh gases ahead of it, in a so-called *shock-flame complex*, representative of the propagation regime preceding transition to detonation [9, 10].

The subsequent acceleration of the shock-flame complex and its possible transition to detonation is not as easily described from first principles. The prime difficulty lies in the fact that the flame, at its last stages of acceleration, is no longer laminar but turbulent, and its burning rate is strongly coupled with the compressible features of the flow field, like shocks and strong pressure waves. It is nonetheless commonly found and accepted that detonations are ignited from local explosions at hot spots [5, 11], via the so-called *shock wave amplification by coherent energy release* (SWACER), or the Zel'dovich-Lee gradient mechanism [3]. Based on the work of Zel'dovich [12], it relies on the presence of a favorable gradient of induction time in the flow field, that permits the formation of a spontaneous reaction front that, under certain circumstances, can cause shock waves to strengthen enough to support the formation of a self-sustained detonation. The SWACER mechanism succeeds to describe, at least qualitatively, the formation of detonations in a large amount of experimental and numerical configurations, such as *knocking* in internal combustion engines, and flame propagation in obstructed tubes. In the latter case, flame acceleration and the onset of a detonation is commonly promoted by inner walls, offering support for turbulence generation and shock reflection, leading to the formation of hot-spots and rapid transition to detonation [13–17].

1.2 Chapman-Jouguet deflagrations

A large set of DDT experiments in closed tubes report that, prior to the initiation of the detonation, the flame reaches a terminal apparent velocity, i.e. relatively to the tube walls, comparable to the speed of sound in the burned gases [7]. This feature, together with the fact that the burned gases

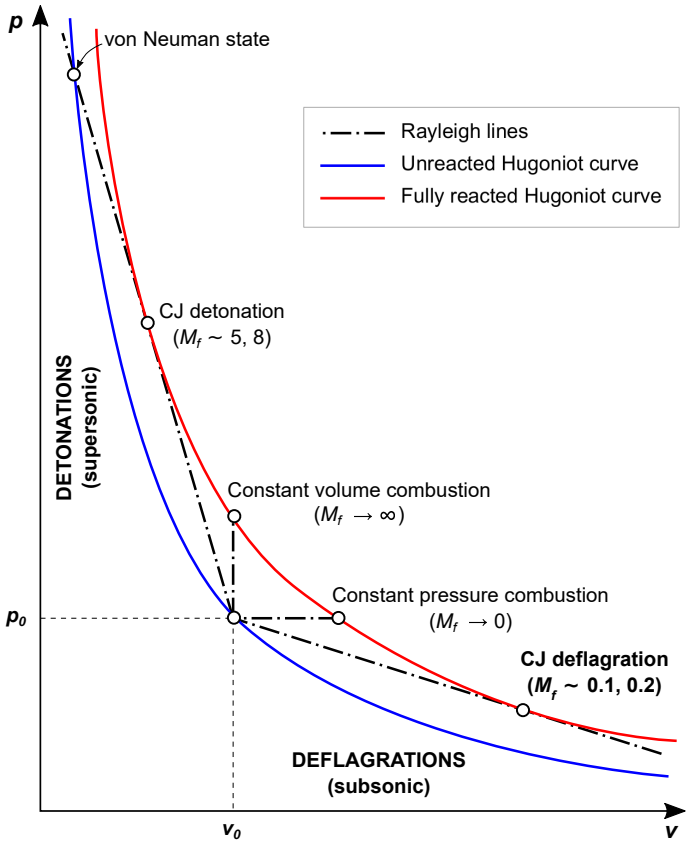

Figure 1.1: Pressure - specific volume ($p - v$) diagram of deflagrations and detonations. State (0) corresponds to the fresh state in which the flame propagates.

are at rest owing to the closed end of the tubes in which they are observed, states that, in a frame attached to the flame, the velocity of the burned gases is equal to their speed of sound. This property of a sonic flow in the burned gases is what characterizes *Chapman-Jouguet (CJ) deflagrations*. The definition of such flames arises naturally from first principles of thermodynamics and their properties (burning velocity, jump relations) can easily be computed using the Rankine-Hugoniot relations, derived from the conservation relations across a fully reacted discontinuity, if the initial state, gas properties and equation of state are provided. They are formally identified in a pressure - specific volume diagram (Figure 1.1), lying at the single intersection between the fully reacted Hugoniot and the single Rayleigh curve, the latter being evaluated at the wave speed that causes it to be tangent to the Hugoniot curve, on the deflagration side. Defined this way, CJ deflagrations thus correspond to flames propagating at the maximum speed admissible for subsonic flames, as faster flames cannot satisfy the conservation relations between the fresh and reacted states unless they are detonations, i.e. supersonic combustion waves.

The study of CJ deflagrations and other fast flames differs from the study of more common, low-speed deflagrations, generally associated to planar laminar flames, in that they propagate at relatively high burning Mach numbers M_f, the ratio of the flame burning velocity to the speed of sound in the fresh gases just ahead of the flame. For comparison, while the burning Mach number of laminar flames is of order 10^{-3}, CJ deflagrations propagate at burning Mach numbers of about 0.1 - 0.2. While the isobaric assumption applies well to the former, the latter involves significant pressure drops within the reaction zone, down to about 50% of the initial pressure. This adds complexity to the study of high-speed deflagrations, as compressible effects should now be accounted for when studying their behavior and fate in a flow. This topic regarding compressibility effects in the propagation of high speed flames was discussed in the work of Travnikov and co-authors [18, 19], in which linear and non-linear stability of flame fronts burning at high Mach numbers were investigated. The evolution of a sinusoidal disturbance applied to a planar, two-dimensional flame front was tracked over time, for different initial flame burning Mach numbers. It was found that the resulting growth of the initial disturbance strongly depends on its wavelength and on the flame burning rate, caused by hydrodynamic effects through the Landau-Darrieus instability. Notably, the maximum growth rate of the instability was found to increase with the flame Mach number, suggesting that high-speed flames may be subject to higher disturbances amplification. Nevertheless, some conflicting findings were reported by He [20] and confirmed by Bychkov et al. [21], who found that the growth rate of hydrodynamic instabilities is completely suppressed once the flame reaches the CJ condition. The analysis did not allow for shock generation and applied constant fluxes. Shocks were nevertheless observed in the non-linear calculations of Travnikov and Fecteau [22, 23]. These shocks were found sufficient for DDT in their numerical experiments. Stability analysis of CJ deflagrations would thus require to incorporate acoustic wave effects.

High speed deflagrations can also affect the overall features of the medium in which they propagate. For example, accelerating flames can cause the formation of shock waves which strength is influenced by the growth of the flame burning rate. The formation of more or less strong shocks can also be caused by the nature of the confinement downstream of the flame. In most shock-tube experiments for example, the presence of solid walls prevents the burned gases to exhaust to the atmosphere. Their expansion pushes the flame forwards, that acts as a porous piston driving a flow ahead of it, thus forming shocks and compression waves. As a result, realistic states reached by a fluid element experiencing a shock then a CJ deflagration are more likely to be represented by the pressure-volume diagram plotted in Figure 1.2. In it, an unperturbed gas at state (1) is compressed by a shock to reach state (2), then expanded through a deflagration (here a CJ deflagration),

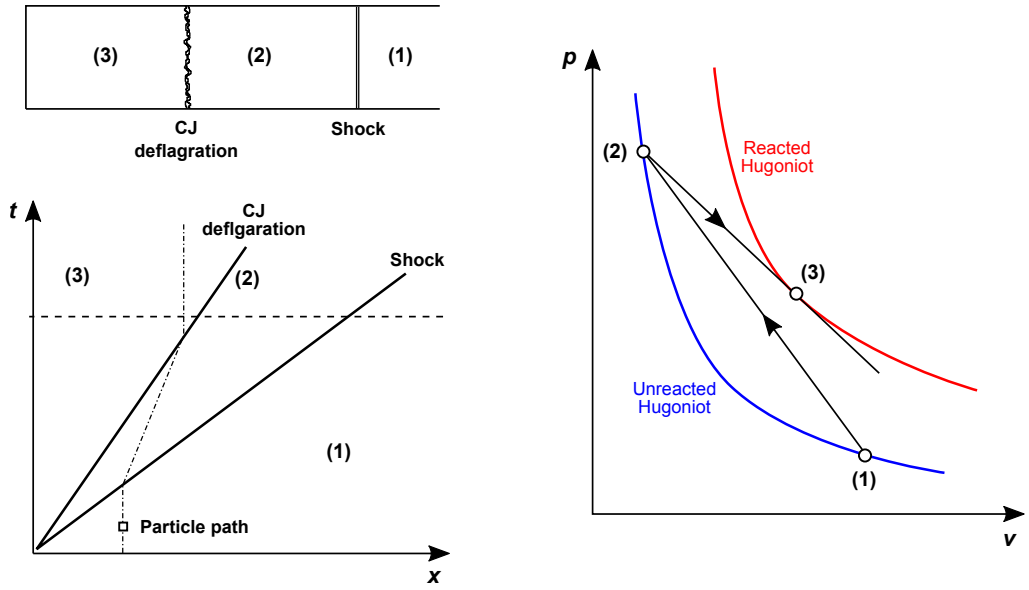

Figure 1.2: Global structure of a shock follow by a CJ-deflagration, represented schematically in a closed-ended tube (top left), in the associated space-time diagram (bottom left), and pressure-volume diagram (right).

yet reaching a higher-than-state-(1) pressure at state (3). Consequently, the post shock region is one that requires appropriate description for proper investigation of the DDT process [24], as it is a region in which the growth of instabilities and the eventual transition to detonation would be affected, especially for near-CJ deflagrations [22].

Further details of the interaction of turbulent combustion with highly compressible flows involving high-speed deflagrations were recently published by Poludnenko and colleagues [25]. In their work, direct numerical simulations were performed of three-dimensional, turbulent, high-speed deflagrations and their transition to detonation. A main conclusion was that fast, turbulent deflagrations reaching the CJ-deflagration regime are intrinsically unstable, in a way that rapid acceleration and transition to detonation is facilitated. The described instability was found to act similarly as the Richtmyer-Meshkov instability, that causes interfaces, in that case the flame front, to fold when interacting with pressure gradients by production of baroclinic vorticity. It however differs in that, pressure gradients originate from the turbulent flame brush itself and not from external sources, as the flame front is alternatively being disrupted by turbulence, then restored by flame collision [26]. The resulting pressure pulses are generally of small amplitude in the case of low-speed flames, but are significant for turbulent flame fronts propagating at nearly the CJ deflagration burning velocity. An argument was made on the ability of such flames to generate these high pressure pulses within the thickness of the flame brush, based on the fact that chemical energy

release (translated by the flame burning velocity) occurs on a time scale comparable to the acoustic waves flame crossing time, primarily permitted by the sonic flow at the burned gases for CJ deflagrations [27]. This coupling between the flame generated turbulence and pressure pulses was found to be a strong mechanism of flame destabilization, causing large fluctuations of its burning velocity, contributing to an overall flame acceleration and eventual transition to detonation. Despite the fact that this process remains to be verified experimentally, it was argued to be the main cause of rapid flame acceleration at its latest stages, in configurations where hot-spots are unlikely to occur, in smooth tubes or unconfined geometries (vapor clouds, type Ia supernovae explosions), or in insensitive premixed gases, characterized by long induction times, for which further flame acceleration and strong shocks are required to allow for the reactive mixture to self-ignite.

The intrinsic flame instabilities occurring at high burning Mach numbers leading to DDT are in apparent contradiction with some experimental and numerical studies of flame acceleration and DDT. The flame acceleration was observed to decrease as the flame reached the CJ deflagration speed. It then propagated quasi-steadily before rapid transition to detonation. Valiev and colleagues, in their numerical work on flames accelerating from realistic laminar burning velocities up to their transition to detonation [24], identified three consecutive regimes of deflagration acceleration prior the initiation of a detonation. The latest one corresponds to a saturating state in which the flame speed reaches a plateau, that may be associated to the CJ deflagration regime. The reason why such behavior occurs was found to be due to purely gasdynamic effects upstream and downstream of the flame front, caused by the gas compression induced by a strong shock propagating ahead of the flame, originating from the early stages of the flame acceleration. This highlights the importance of considering DDT as a whole process from mild flame ignition, consideration that is lacking in other studies in which the flame is generally initially set to propagate at definite stages of its acceleration.

Beyond these numerical and theoretical observations, CJ deflagrations were also observed experimentally as propagating quasi-steadily in congested channels. They were denoted as *choked flames* by Lee and colleagues [28] in their work on the classification of quasi-steady flames propagation regimes in obstructed channels. They were found to correspond to the fastest flames before quasi-detonations can be achieved, in more sensitive mixtures or in obstructed tubes with larger obstacle scaling [29]. Visual inspection using high speed schlieren photography later permitted to observe the structure of such flames, always propagating downstream of a precursor shock. They were argued to be comparable to the coupled shock-flame complex encountered in the experiments performed by Chue et *al.* [30], of accelerated flames propagating as quasi-steady waves in obstacle filled channels, and of shock-flame complexes resulting from the decoupling of detonations, when

these are transmitted through a tube section equipped with porous walls. In their analysis, Chue and co-workers used a model of their own, aimed to characterize the steady flow field involved in the propagation of a shock followed by a CJ-deflagration. Both waves were modeled as discontinuities propagating at constant speeds in a tube closed far downstream of the deflagration (the burned gases are thus at rest), across which the appropriate jump relations apply, in a so-called *double discontinuity* problem. The good agreement they obtained on the predicted flow properties with their experimental observations, was used to conclude on the fact that choked flames and decoupled detonations are CJ deflagrations.

Double discontinuity models were later used in the same manner to model experimental configurations aimed to capture DDT by Radulescu, Saif and co-workers [31, 32]. They proposed a model aimed to predict the quasi-steady, one-dimensional flow resulting from the decoupling of a detonation passing through a porous wall to form a shock followed by a CJ-deflagration. It was compared to a series of experiments designed to study the re-initiation of detonations downstream of porous walls of either 75% or 90% blockage ratio, in low-pressure, hydrocarbon-oxygen mixtures, eventually diluted in argon. The comparison of the resulting deflagration apparent velocity (measured relative to the tube walls) and the one predicted by their model showed that, after passing through the porous wall, the flame propagates quasi-steadily for some time at about the predicted CJ-deflagration speed, from which further flame acceleration or deceleration may occur to allow or not transition to detonation. The authors observed these fast deflagrations to organize into fewer gasdynamic modes while rapidly amplifying transverse and longitudinal waves via localized auto-ignition spots.

These experiments were later replicated numericallly by Maxwell [33] and Jaravel [34], in works which objectives were, among others, to describe the underlying propagation mechanism of the aforementioned fast flames and their transition to detonations. A main finding was regarding the major role turbulent burning plays, to maintain such high flame velocities, as the region of compressed gases ahead of the flame caused by the passage of the precursor shock do not permit self initiation of the reactive mixture. Instead, local, turbulent fluctuations of the burning rate in the flame brush were found to be large enough, roughly an order of magnitude above post-shock, laminar flame burning rate, to generate pressure waves spreading in all directions. Those eventually coalesce and amplify to form longitudinal and transverse shocks of notable strength, that can, through shock collision, form hot spots from which local explosions may occur. This sequence of events occurring repeatedly, could ultimately lead to shock collision strong enough to support the formation of self-sustained detonations.

1.3 Research projects

In this thesis, different projects were conducted to further characterize the flow field preceding the initiation of detonations. These served as a base to discuss the relevance, requirement and/or sufficiency of CJ deflagrations in the DDT process.

The following sections of this introduction briefly describe the mindset in which these projects were started, that treat different aspects of the problem of high-speed deflagrations and their transition to detonations, from experimental and modeling approaches. Because this thesis compiles a series of articles on this topic, a detailed introduction can be found in the respective article associated to each given project.

1.3.1 Interaction of a supersonic shock-flame complex with a single obstacle

Obstacles placed on the path of a propagating deflagration are well known to promote flame acceleration and eventually lead to the transition to detonations. They are used in a large majority of experiments involving the study of detonations, as they permit their rapid initiation, without requiring long detonation tubes. In an industrial context, their presence if flammable gas is released to the atmosphere can be the source of disastrous effects. A mild flame initiated in the reactive vapor cloud can rapidly transit to a detonation, as observed in 2005 at the Buncefield Oil Storage Depot [1]. Understanding the mechanism of transition to detonations is thus of major interest in our ability to predict and mitigate occurrences of such dramatic events, but remains difficult owing to the complexity of the events at play, as seen in Section 1.1.

In tubes filled with obstacles, it is common to observe initiation of detonations from auto-ignition at shock reflection locations in sensitive fuels like hydrogen-oxygen [6, 11]. However in less sensitive mixtures like those involving hydrocarbons, turbulent mixing was found to play an important role in the propagation mechanism of chocked flames in congested channels [33, 35], and extensively in the onset of detonations. We thus proposed here to investigate the details of the interaction between high speed deflagrations and a single obstacle, with the aim to observe the mechanism by which the last stages of flame acceleration and the onset of detonations occur in hydrocarbon-oxygen mixtures. A series of experiments were performed in a thin, rectangular channel characterized by a high aspect ratio cross section of height 203 mm, aimed to approximate two-dimensional wave propagation, as shown in Figure 1.3. The mixture investigated was stoichiometric propane-oxygen, one of the hydrocarbon mixtures used in the former experiments done by Saif et *al.* on the transition to detonation of CJ-deflagrations [32], to which this project was a continuation.

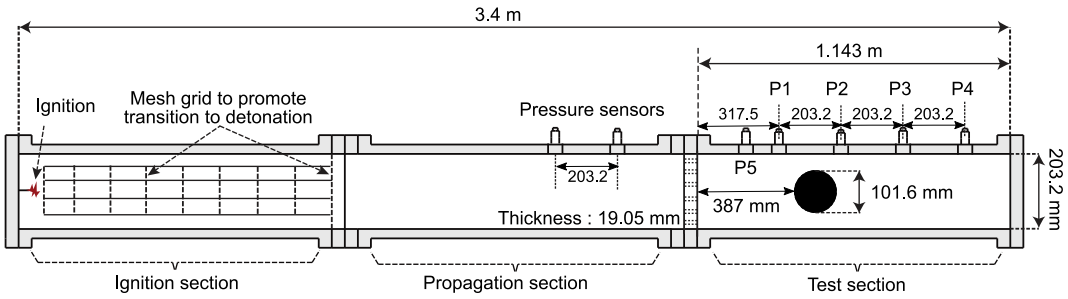

Figure 1.3: Schematic of the shock tube used to perform experiments of DDT over a single obstacle.

The method used to generate turbulent flames propagating at high burning velocities was identical to the one used by Saif, done by decoupling a detonation through a high blockage ratio perforated plate, to form shock-flame complexes, in which the flame is nearly a CJ deflagration [36]. A single obstacle providing a maximum blockage ratio of 50% was placed on the path of the formed shock-flame complex. The large height of the tube (relative to what is commonly found in the literature) and relatively large size of the obstacle, together with our choice to run the experiments at low initial pressure, permitted to conveniently observe the details of the interaction and eventual onset of detonations using high-speed schlieren photography.

Efforts were also put into detailed characterization of the flow field, prior to the flame interaction with the obstacle. Those were set by adjusting the gas initial pressure, that controlled the sensitivity of the mixture to flame propagation. Finally, the shape of the obstacle was varied to investigate the role of the obstruction geometry, hence the nature of the flame interaction with the obstacle. These elements were then processed to discuss the critical conditions by which detonation initiation was likely to occur in the vicinity of the obstacle.

1.3.2 A model for predicting the properties of shock - CJ deflagration complexes in vented DDT experiments

In a large majority of laboratory scale experiments performed in closed tubes, transition to detonation occurs once the flame reaches an *apparent velocity*, i.e. measured in a frame attached to the tube walls, of about the speed of sound in the burned gases. Because those are at rest owing to the non-moving, closed rear end of the tube, such flames propagate with a sonic downstream flow, and are thus CJ deflagrations. In larger scale DDT experiments however, it was found that deflagrations transition to detonations when reaching an apparent velocity smaller than the speed of sound in the burned gases, raising the question of whether they still are CJ deflagrations or not.

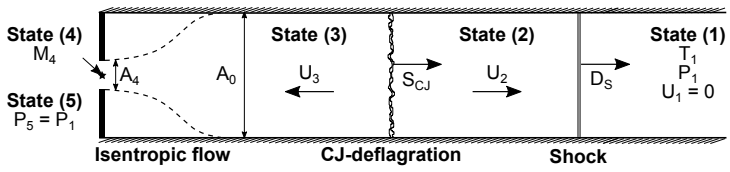

Figure 1.4: Schematic of the double-discontinuity problem in a vented tube.

Investigating this inconsistency first requires to describe the flow phenomenology. In closed-ended tubes, the high apparent velocity of the flame front is permitted by the high velocity of the fresh gases ahead of it. This motion originates from the expansion of the burned gases, that can only occur in the direction of flame, owing to the tube closed rear end. The flame thus acts as a piston driving a shock propagating in the fresh gases ahead of it. Predicting the properties of the resulting shock - flame complex in closed ended tubes was formerly done by Chue et *al.* [30] using a double discontinuity formulation, in the particular case where the flame is a CJ deflagration propagating at its characteristic burning rate. On the other hand, in an industrial context and in large scale DDT configurations, the flame is generally only partially confined. Part of the burned gases can thus be vented to the surrounding medium, resulting in a slower flow induced ahead of the flame, and hence the formation of weaker shocks. This causes the apparent velocity of CJ deflagrations to be smaller than the speed of sound in the burned gases, as their advected component, carried by the flow of fresh gases ahead of them, are smaller than in the closed tube case.

In this thesis, Chue's double discontinuity model was extended to account for the venting of the burned gases through an opening of known size, at the tube's rear end, as shown in Figure 1.4. Such a model was designed to evaluate the apparent velocity of CJ-deflagrations and other properties of the shock-flame complex, propagating in vented tubes. Work was also put into Chue's model to account for gases with realistic thermochemical properties in order to complete his original study, restricted to perfect gases. Numerical methods were thus developed to perform thermochemical equilibrium calculations across CJ-deflagrations, in a manner similar to the work done by Shepherd and co-workers, applied to shocks and detonations [37].

The proposed model was then applied to a selection of non-confined DDT experiments, as found in the work of Pekalski and Davis [38, 39], as well as other similar experiments. In these, a flame was ignited in a gaseous reactive medium, loosely confined by a tarp. The flame front was accelerated as it propagated in an array of obstacles, until it transitioned to a detonation. At the passage of the flame, the expansion of the burned gases forced the loose confinement to be released, allowing them to be vented to the atmosphere through the opening given by the array of obstacles. Unlike experiments in shock tubes, the flame apparent velocity (i.e. measured in a fixed

frame of reference) at which transition to detonation occurs is smaller than the speed of sound in the burned gases. As aforementioned, this statement may be caused by the fact that the flow velocity of the fresh gases just ahead of the flame is smaller than in the case of a closed-ended tube, as part of the burned gases are vented to the atmosphere. Verifying whether these flames are still CJ deflagrations prior to rapid transition to detonation was done by comparison of the actual measurements of flame apparent velocity, shock speed and/or shock pressure (when available), with the values predicted by the proposed model, in order to comment on the involvement of CJ deflagrations in vented DDT experiments.

1.3.3 The structure and stability of one-dimensional, high-speed deflagrations

Knowledge of the properties of high-speed deflagrations is key for the understanding their transition to detonations. Having them characterized is generally done through detailed, multi-dimensional numerical simulations, providing a lot of details regarding the coupling between turbulence, energy release and the compressible features of the flow field. Alternatively, an overall one-dimensional structure can be calculated, if the flame reaction-diffusion parameters are set appropriately to have them propagating at a prescribed burning velocity, in a manner similar to the *thickened flame* model for turbulent flames. Dealing with the one-dimensional structure of high-speed deflagrations has the advantage of being significantly simpler to work with, when willing to investigate their response to a prescribed flow perturbation, at different propagation regimes. Moreover, their chemical-diffusion parameters can be set arbitrarily to model changes of behavior, in order to study their impact on the flow field.

Computation of the one-dimensional structure of flames propagating at finite burning velocities is however a complicated task, owing to the intrinsic mathematical nature of their equilibrium states, namely the fresh and the burned states. Resources dealing with the full structure of high-speed, steady deflagrations are thus limited, and generally focus on characterizing the nature of the flame equilibrium states [40], on advanced numerical methods aimed to solve their structure [22], or on the solution to simpler cases, the most common one being the low-Mach number flame. The latter is characterized by very small burning velocities, resulting in infinitely small pressure drops across their reaction zone, and negligible gas kinetic energies when compared to its enthalpy. Under this approximation, a set of ordinary differential equations (ODEs) can be derived then further simplified from the steady, reactive Navier-Stokes equations. Their structures are well known and methods to compute them are robust and work over a wide range gas parameters,

namely heat release, activation energy, ratio of specific heat and Lewis number [41, 42].

When the reaction rate is modeled using a single-step, irreversible Arrhenius type law, computation of the flame structure rely on numerical, iterative shooting methods aimed to solve the boundary value problem, defined by the flame set of ODEs, with boundary states taken at infinite distances from the reaction zone, being the known fresh and burned states. These shooting methods consist in numerically integrating the flame structure for different values of the Arrhenius law pre-exponential factor, until the unique one that connects the fresh and the burned state is found. Linear analysis of the nature of the fresh and burned states under the low-Mach approximation permits to justify that numerical integration should be and was performed from the burned state to the fresh state, the former being a saddle and the latter a stable node [43]. This statement however breaks down when considering the more general case of flames propagating at finite burning velocities. For those, both equilibrium points are saddles [40], from which no obvious choice on the direction of integration can *a priori* be made. Nevertheless, iterative shooting methods can still be applied if conditions at the boundaries are treated carefully.

In this thesis, a method capable of computing the steady structure of deflagrations, propagating at finite burning velocities was proposed. The approach chosen was also an iterative shooting method aimed to solve the boundary value problem stated by the steady, one-dimensional flame ODEs, with boundary conditions far from the reaction zone being those at the fresh and burned states. It differs from usual shooting methods used to solve low-Mach deflagrations, in that further analysis and treatment of the boundary conditions were performed, in order to overcome their saddle nature. To do so, elements of dynamical systems analysis were used, with extensive use of the eigenvalue/eigenvector decomposition of the linearized set of the flame ODEs, and of the flame ODEs phase space. These results were then used to design strategies for the integration of the flame structure, as well as providing insights in the flame linear stability.

The steady flame profiles obtained can then be used as initial conditions to one-dimensional simulations of high-speed, accelerating deflagrations and their transition to detonation. Those are intended to serve as an alternate model to multi-dimensional simulations. In the latter, flame acceleration is mostly caused by the increase of the flame surface area, or interaction with turbulence or with the compressible features of the flow. Here in the case of one-dimensional flames, the consumption rate of the reactants will be modeled using a one-step, irreversible Arrhenius law, in which the pre-exponential factor can be varied over time to control the flame burning rate. This simple formulation permits to induce a response of the flow, like the formation of compression waves and shocks, and cause an eventual coupling between the shock and the reaction zone, relevant to discuss the conditions required for deflagrations to transit to detonations.

Chapter 2

Shock-flame complexes interaction with a single obstacle

In the present chapter, the interaction of a shock-flame complex with a single obstacle was investigated. Two complementary studies were done. One aimed to identify and characterize the flow field and the sequence of events leading to the transition or not of deflagrations to detonations (Section 2.1). The other focused on the characterization of a criteria for deflagration to detonation transition after the flame interaction with a shaped obstacle (Section 2.2)

2.1 Mechanism of flame acceleration and detonation transition from the interaction of a supersonic turbulent flame with an obstruction

This study seeks to determine the mechanism of flame acceleration and transition to detonation when a turbulent flame preceded by a shock interacts with a single obstruction on its path, here taken as a cylindrical obstacle or a wall. The problem is addressed experimentally in a mixture of propane-oxygen at sub-atmospheric conditions. The turbulent flame was generated by passing a detonation wave through a perforated plate, yielding flames with turbulent burning velocities 10 to 20 times larger than the laminar values and incident shock Mach numbers ranging between 2 and 2.5. Time resolved schlieren videos recorded at approximately 70 kHz and numerical reconstruction of the flow field permitted to determine the mechanism of flame acceleration and transition to detonation. It was found to be the enhancement of the turbulent burning rate of the flame through its interaction with the shock reflection on the obstacle by the Richtmyer-Meshkov instability. The

amplification of the burning rate was found to drive the flame burning velocity close to the speed of sound with respect to the fresh gases, resulting in the amplification of a shock in front of the flame. The acceleration through this regime resulted in the strengthening of this shock. Detonation was observed in regions of non-planarity of this internal shock, inherited by the irregular shape of the turbulent flame itself. Auto-ignition at early times of this process was found to be negligibly slow, suggesting that the relevant time scale for detonation formation is primarily associated with the increase in turbulent burning rate by the interaction with reflected shocks.

This study was published in 2019 in the Proceedings of the Combustion Institute [44], and is attached to this thesis in the following pages. The author conducted the experiments, analysis and wrote the paper. The conceptual planning was performed with the Ph.D. supervisor, Prof. M. I. Radulescu. The second and third authors participated in the discussions during the data reduction phase.

Available online at www.sciencedirect.com

ScienceDirect

Proceedings of the Combustion Institute 37 (2019) 3713–3721

Proceedings of the Combustion Institute

www.elsevier.com/locate/proci

Mechanism of flame acceleration and detonation transition from the interaction of a supersonic turbulent flame with an obstruction: Experiments in low pressure propane–oxygen mixtures

Willstrong Rakotoarison [a], Brian Maxwell [b], Andrzej Pekalski [c], Matei I. Radulescu [a,*]

[a] *Department of Mechanical Engineering, University of Ottawa, Ottawa, ON K1N 6N5, Canada*
[b] *Department of Mechanical Engineering, University of Victoria, Victoria, BC V8W 2Y2, Canada*
[c] *Shell Global Solutions, Concord Business Park, Manchester, United Kingdom*

Received 29 November 2017; accepted 24 August 2018
Available online 22 November 2018

Abstract

The present paper seeks to determine the mechanism of flame acceleration and transition to detonation when a turbulent flame preceded by a shock interacts with a single obstruction in its path, taken as a cylindrical obstacle or a wall in the present study. The problem is addressed experimentally in a mixture of propane–oxygen at sub-atmospheric conditions. The turbulent flame was generated by passing a detonation wave through a perforated plate, yielding flames with turbulent burning velocities 10 to 20 larger than the laminar values and incident shock Mach numbers ranging between 2 and 2.5. Time resolved schlieren videos recorded at approximately 100 kHz and numerical reconstruction of the flow field permitted to determine the mechanism of flame acceleration and transition to detonation. It was found to be the enhancement of the turbulent burning rate of the flame through its interaction with the shock reflection on the obstacle. The amplification of the burning rate was found to drive the flame burning velocity close to the speed of sound with respect to the fresh gases, resulting in the amplification of a shock in front of the flame. The acceleration through this regime resulted in the strengthening of this shock. Detonation was observed in regions of non-planarity of this internal shock, inherited by the irregular shape of the turbulent flame itself. Auto-ignition at early times of this process was found to be negligibly slow compared with the flow evolution time scale in the problem investigated, suggesting that the relevant time scale is primarily associated with the increase in turbulent burning rate by the interaction with reflected shocks.

Keywords: Turbulent flame; Shock–flame interaction; Deflagration-to-detonation transition

* Corresponding author.
E-mail address: matei@uottawa.ca (M.I. Radulescu).

https://doi.org/10.1016/j.proci.2018.08.050
1540-7489 © 2018 Published by Elsevier Inc. on behalf of The Combustion Institute.

1. Introduction

When a flame propagates through a congested area, the flame surface area increases as preferentially directed flow convecting the flame elongates its surface area. This leads to an increase in the rate of reactant consumption, which in turn accelerates more fluid, thereby increasing the global burning rate. This feedback mechanism leads to the acceleration of the flame front in the preferred direction of motion and the generation of a shock wave ahead of the flame. These early dynamics are now very well understood through extensive experiments, theoretical models and numerics [1–4]; accordingly the dynamics are also relatively well predicted at engineering scales of interest via coarse grained models advecting the surface of the flame, given a particular obstruction geometry (e.g., [5]).

The subsequent acceleration of the flame–shock complex and its possible transition to a detonation are not as well understood, and cannot be easily predicted [3,6]. The prime difficulty lies in the fact that the flame at this stage is no longer laminar [2]. Other than the mechanism described above, the turbulent burning rate itself at the flame becomes strongly coupled with the flow field generated by the flame and gasdynamic interactions [6]. Turbulent transport and gas dynamic heating may both participate. In the presence of obstacles, reflected shocks traversing the flame may promote turbulent mixing at the flame, leading to higher burning rates [7] conducive to a more prompt DDT. Experiments and numerical simulations usually agree that the final detonation formation involves the creation of hot-spots, where the Zel'dovich–Lee gradient mechanism [4] can be set up in a variable number of ways: shock reflections on obstacles, turbulent mixing, self-generated shocks wave turbulence [6,8,9]. These complications make it difficult to predict the eventual transition to detonation, which is found to depend on many factors: e.g., turbulence intensity, flame properties, congestion geometry, sensitivity to auto-ignition, memory of the flow field set-up during the early stage of acceleration.

While detailed recent experiments have shown that auto-ignition from shock reflections plays a fundamental role in sensitive fuels like hydrogen–oxygen at the limit of transition between choked flames and quasi-detonations [2,10], indirect observations for less sensitive hydrocarbons-air quasi-detonations at atmospheric conditions suggest that turbulent mixing plays a more important role; see for example [11] for discussion. It is thus worthwhile revisiting the problem of turbulent flame transition to detonations in less sensitive hydrocarbons. We study the interaction of a well defined shock–flame complex in propane–oxygen, as it interacts with a single cylindrical obstacle or a flat wall. Care is exercised to obtain a controllable initial turbulent flame of sufficient intensity, such that the subsequent transition to a detonation occurs rapidly and is reflective of the last stages of the DDT process. The shock–turbulent flame complex in our study was generated using the technique of passing a detonation wave through a perforated plate, which gives rise to a system of interacting shocks yielding a region of intense wave turbulence. This can give rise to an intense turbulent deflagration [8,12,13] approaching the Chapman–Jouguet deflagration speed [9,14] typically observed in fast flame propagation and DDT in tubes with constrictions [3]. This permits to generate flames with high levels of turbulence conducive to transition to detonation from the interaction with a single obstruction, as we will show in the present study.

2. Experimental details

The experiments were conducted in a 3.5-m-long thin rectangular channel with a cross-section of 203 mm by 19 mm (Fig. 1), described in detail elsewhere [15]. The entire tube was filled with the desired test mixture. A detonation was initiated by a high voltage capacitor discharge. An initial obstacle section promoted this transition for less sensitive mixtures. A self-sustained detonation wave was then established in the tube, which propagated at speeds approximately 5% below the Chapman–Jouguet value calculated. This was inferred from time or arrival measurements using a pair of PCB 113B24 pressure transducers. The detonation then transmitted across a perforated plate as a leading shock followed by a turbulent deflagration. The intensity of the turbulent deflagration and the strength of the leading shock were controlled by the perforated plate's blockage ratio, hole geometry and mixture sensitivity. The configuration of the perforated plate investigated is shown in Fig. 1. The resulting high area blockage ratio of approximately 96% was chosen higher than in our previous studies [8,9,14], such that the strength of the transmitted shock was weaker, in order to de-couple the leading shock from the trailing flame, and the turbulent intensity higher.

Two series of experiments are presented in this communication. The first involves the interaction of the shock flame complex with a 101.6-mm-diameter cylinder, which was located 438 mm downstream of the perforated plate. In the second series of experiments, the obstacle was removed in order to monitor the head-on interaction of the turbulent deflagration wave with the shock wave reflected by the end wall. The reactive mixture studied was $C_3H_8+5O_2$, chosen such that it is sensitive enough at the low pressures required for the experimental facility available in our laboratory. The mixture sensitivity was changed by the initial pressure of the gas in the range of 4–10 kPa. The ambi-

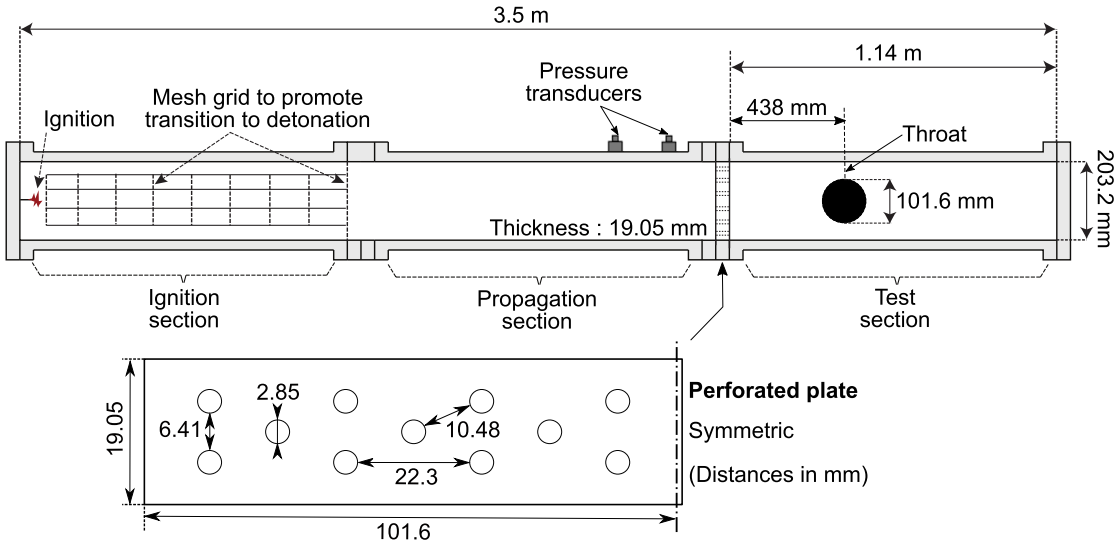

Fig. 1. Schematic of experimental set-up.

ent temperature was 294 K. The experiments were monitored with high speed schlieren visualization [15]. The images acquired with a Phantom V1210 camera had a resolution of 384 by 288 pixels, corresponding to a spatial resolution of 0.8 mm per pixel. All the experiments shown have an interframe time of 12.9 μs, typically providing approximately 100 useful frames per experiment. These sequential frames were then analyzed in order to reconstruct the flow-field, using additional theoretical and numerical tools, as described below.

3. Numerical tools

Partial reconstruction of the flow field measured experimentally relied on the Cantera thermochemical tools and the Shock and Detonation Toolbox developed by Shepherd and his students [16]. Given the shock speeds measured in the experiments, the post shock states can be evaluated using the exact thermo-chemical properties of the reactants. Likewise, laminar burning velocities and characteristic ignition delays can be reliably calculated using these tools at the various thermodynamic states of interest. The current calculations were performed using the San Diego thermochemical database relevant for propane combustion [17].

In some instances, partial numerical reconstruction of the two-dimensional *inert* shock reflection process ahead of the flame was also performed in order to estimate the flow speed in the experiments used for extracting the local burning velocity. The numerical calculations solved the inert Euler equations for a perfect gas with a compressible hydrocode developed by Falle and Giddings [18], which uses an exact Godunov Riemann solver and adaptive mesh refinement. All physical boundaries use a reflective boundary condition, while the back boundary used a zero gradient boundary condition. The initial conditions correspond to a planar shock with uniform state behind it. A contact surface was imposed as initial condition at some distance behind the shock, with a density change corresponding to that of the flame in the experiments. In these calculations, the incident shock Mach number was taken to match that determined in the experiment. The specific heat ratio was taken as $\gamma = 1.22$ evaluated using the method described above at the post-shock state in the experiments.

4. Results

4.1. Flame acceleration past a circular congestion

Whether the interaction of a shock–flame complex with the cylinder resulted in the detonation initiation in the experiment was found to depend on the initial pressure of the mixture, which controlled the strength of the turbulent deflagration produced. The effect of initial pressure on the frequency of detonation formation from the interaction was as follows. At initial pressure of 4.8, 5.5, 6.2, 6.55 and 6.9 kPa, the frequency of detonation formation was respectively 0/9, 2/9, 3/4, 7/7 and 7/8. Table 1 lists the relevant physical properties of interest for the conditions bracketing this critical regime. At each initial pressure, M_I is the Mach number of the incident shock prior to its reflection on the cylinder, S_u is the calculated laminar burning velocity with the unburned gases at the post shock state, S_f is the experimentally measured burning velocity of the flame, T_R is the calculated temperature of the gases behind the normal re-

Table 1
Thermo-chemical parameters for experiments shown.

	p_0 (kPa)	M_I	S_u (m/s)	S_f (m/s)	T_R (K)	τ (μs)
Cyl.	4.8	2.3	5.6	100 ± 24	653	3.9×10^5
Cyl.	6.9	2.5	6.1	140 ± 13	736	9.6×10^4
Wall	4.1	2.0	5.0	56 ± 32	572	9.3×10^6
Wall	4.8	2.1	5.2	46 ± 46	605	1.9×10^6
Wall	6.2	2.2	5.4	210 ± 35	627	6.7×10^5

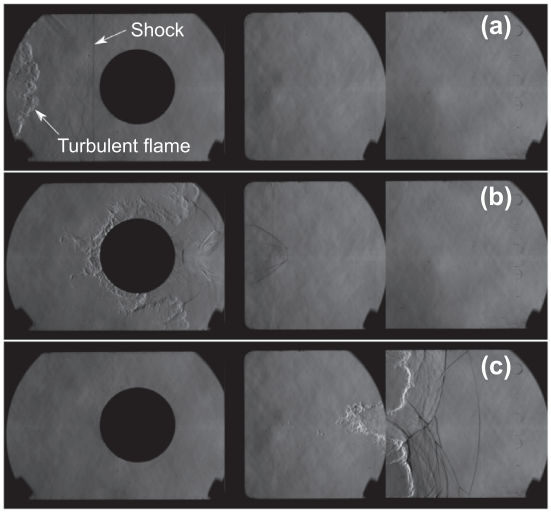

Fig. 2. The interaction of a turbulent flame–shock complex with a cylindrical obstacle in C_3H_8+5O_2 at 4.8 kPa initial pressure, composite images spliced from 3 different experiments; video animations as Supplemental material; the time between successive frames is 425.7 μs.

flected shock, while τ is the ignition delay of the gases behind the reflected shock.

Figure 2 shows an example of a typical flow field evolution for a sub-critical initiation at 4.8 kPa initial pressure. The evolution was obtained by splicing together three experiments, where the schlieren field was displaced progressively downstream of the cylinder. Note the very good merging of the different experiments, which show the good reproducibility of the experiment. In Fig. 2(a), the incoming shock flame complex is visible: a straight shock followed by a turbulent flame. In Fig. 2(b), the leading shock has diffracted around the obstacle ahead of the flame. The flame now has an extended surface, as the flow convects it around the cylinder. In Fig. 2(c), the flame has acquired a V-shape, owing to its preferential convection around the cylinder. Note the series of weak shock waves ahead of the flame, which were generated by the increase in global burning rate owing to the flame surface area increase. In this case, we recover the well-known mechanism of flame acceleration and pressure wave generation due to the enlargement of flame surface area discussed in the introduction. The video animation containing all consecutive frames is given as supplementary material.

In sharp contrast, experiments above 6.9 kPa conclusively showed the prompt detonation initiation, with the detonation formation point moving closer to the point where the first reflected shock from the obstacle interacts with the turbulent flame. At the critical regime, the detonation initiation was sufficiently delayed to clearly reconstruct the dynamics. Figure 3 shows the evolution of the initiation process at 6.9 kPa, when the detonation formation is delayed to the back of the cylinder. In the same figure, we show the numerical reconstruction of the *inert* shock reflection process used to determine the local flow speed ahead of the flame.

The combination of the experimental and numerical sequence first permits us to qualitatively comment on the flow field evolution. Figure 3(b) shows the reflection of the leading shock on the cylinder. In Fig. 3(c), the reflected shock has traversed the flame. Up to this point, the inert calculation and the experiment are in qualitative agreement, since the local burning rate (initially approximately 140 m/s, see below) is relatively small compared to the convective fluid velocities (576 m/s behind the incident shock). Substantial differences arise at later times in Fig. 3(d)–(f) after the reflected shock has interacted with the flame. In the experiments, the flame accelerates substantially, while the contact surface advected with the flow in the inert calculation lags behind. The flame acceleration in the experiments is seen to drive a shock wave ahead of it. Note that a shock is there even in the inert calculation, its origin being the reflection of the reflected shock with the wall close to the flame surface (inert contact surface in the numerics) shown in Fig. 3(d). In the experiments, this internal shock–flame complex rapidly accelerates and transits to a detonation, either directly, or by subsequent shock reflections on the symmetry axis. Both types of re-initiation were observed in the experiment illustrated in Fig. 3. The sequential frames of Fig. 3 permit to reconstruct approximately the flame speed relative to the fresh gas moving ahead of the flame. Analysis of the sequential frames in the experiment permits to determine the speed of the flame in laboratory coordinates D_f along the top wall, shown in Fig. 4. The reconstruction of the flow speed in front of the flame used two methods depending whether it was to estimate the flow speed ahead of the steady flame prior to the reflection or after the reflection. Before reflection, the flame propagates into gas shocked by the incident shock. Using the average shock speed, the gas speed immediately behind the leading shock was obtained by the jump conditions. Since the flow behind the leading shock is not constant, owing to a weak deceleration of the leading shock in this case, a linear correction can be applied if the speed gradient was known. This speed gradient behind the shock can be evaluated exactly from the shock jump equations and Euler equations and expressed in terms of the speed (D) and decay rate ($\dot{D}$) of the leading shock, yielding

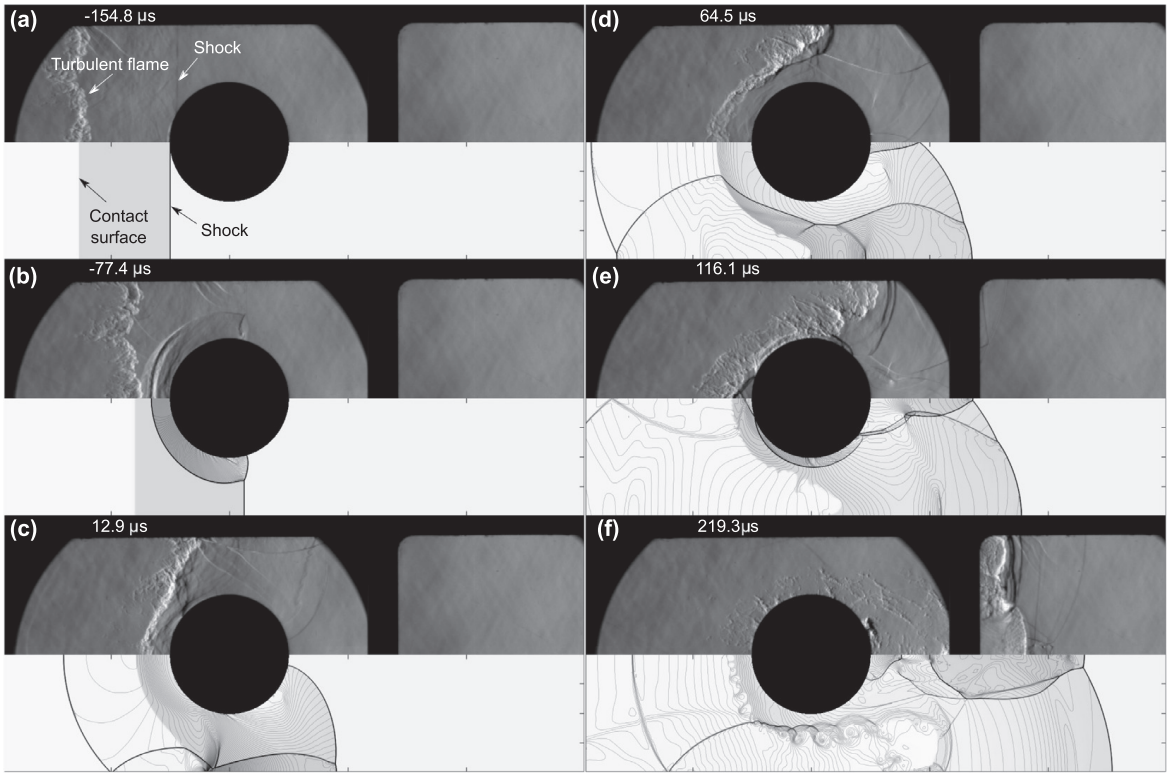

Fig. 3. The interaction of a turbulent flame–shock complex with a cylindrical obstacle in C_3H_8+5O_2 at 6.9 kPa initial pressure (top row in each frame) and the numerical reconstruction of an inert flow field (bottom row) showing a composite image of density field overlayed with pressure contours (video as Supplemental material).

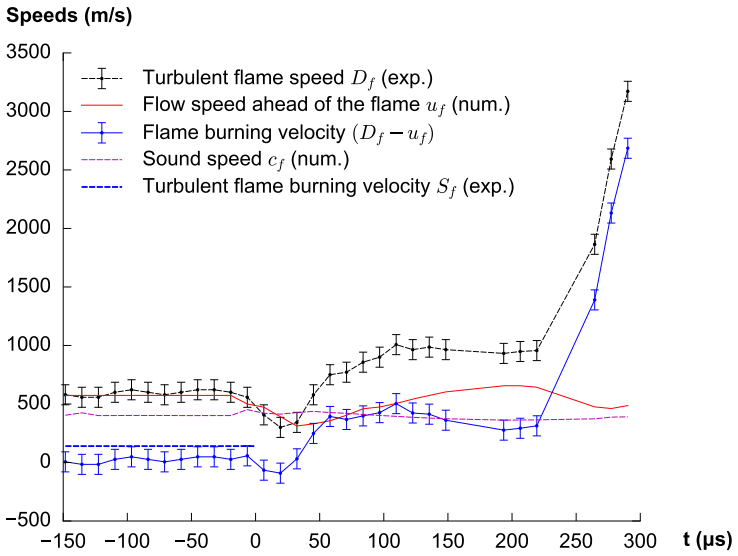

Fig. 4. The speed of the flame D_f, the flow speed ahead of the flame u_f and the resulting flame speed relative to the inert flow ahead of it for the experiment of Fig. 3; time 0 corresponds to the first interaction between the flame and the reflected shock.

the so-called *shock change* equation [19]:

$$\frac{\partial u}{\partial x} = \frac{\left(1 + \rho_0 D\left(\frac{du}{dp}\right)_H\right)\frac{1}{\rho}\left(\frac{dp}{dD}\right)_H \dot{D}}{(D-u)^2 - c^2} \qquad (1)$$

where the pressure p, density ρ and flow speed in the absolute frame u are evaluated at the post shock state. ρ_0 is the density of the undisturbed medium ahead of the shock and the subscript H denotes a derivative taken along the shock Hugoniot. In applying this relation, the deceleration of the leading shock $\dot{D}$ was measured experimentally by fitting a trajectory of constant acceleration to the experimentally determined $x(t)$ data. The deriva-

tives along the shock Hugoniot were evaluated numerically by perturbing the shock jump calculations by 1% in shock speed. The resulting burning velocity obtained is tabulated in Table 1. The standard error reported for the burning velocity is associated with the error of the fitted parameter $\dot{D}$, obtained using the non-linear Levenberg–Marquardt least squares algorithm. This error provides the largest source of error in our model estimate. For this experiment, we obtain a turbulent flame burning velocity prior to the reflection of approximately 140 m/s, or approximately 22 times the laminar burning velocity calculated for this mixture at the post shock thermodynamic state.

After the shock–flame interaction, the flame speed relative to the gases ahead was obtained by making use of the numerical calculations, which permitted to estimate the flow speed just ahead of the flame. Indeed, since the flame develops initially a weak shock in the experiments, the region ahead of the shock is not affected by the flame, and the inert calculation provides a good measure for the local speed of the flow. In the experiments, the flame speed was measured along the top wall, such that the flow speed (away from boundary layers) was always directed in the mean direction of motion. The spatial and temporal evolution of these two speeds are shown in Fig. 4. While the absolute measured flame speed continuously increases, marking the transition to detonation at the end of the record, the advection of the flame by the flow is responsible for a large portion of this speed. Indeed, the flow speed increase in the inert simulations is due solely to the acceleration of the flow passing through a narrower open region (the throat).

The difference between the absolute flame speed and the calculated flow speed, shown in blue, is more meaningful. It shows a rapid increase to approximately 400 m/s by the time the flame is at the throat. Note that this speed corresponds closely to the local sound speed in the gas ahead of the flame. Past the throat, this effective turbulent burning velocity is slightly dropping, to only significantly reaccelerate once the flame has passed the cylinder. The view that emerges from this analysis is that the flame burning velocity is augmented by the shock flame interaction approximately three-fold.

It is pertinent at this point to comment on the relative importance of auto-ignition at the early stages of this flame acceleration process. Following the inert shock reflection, the temperature behind the reflected shock, before substantial volumetric expansion, is calculated from the exact shock jump conditions to be 736 K (see Table 1). At this state, the constant volume ignition delay is approximately 100 ms. This time scale is 3 orders of magnitude longer than the flow evolution and flame acceleration time scales apparent in Figs. 3 and 4, thus ruling out the mechanism of auto-ignition at a hot spot driven by shock reflection. The flame acceleration is thus due to the increased burning rate by the passage of the reflected shock. Note that the constant volume ignition delay is a lower bound estimate. Since the leading shock was found to decay, the resulting expansion of the gases after being shocked signifies that their ignition time will be longer as compared to this estimate. Likewise, the expansion of the gases as they expand over the cylinder will also make the ignition delay longer than calculated for constant volume.

4.2. Flame shock head-on interactions

In order to better determine the mechanism responsible for the rapid increase in burning velocity after the shock flame interaction, the second series of the experiments focused on the problem of normal reflected shock interaction with the flame. These series of experiments were performed by removing the cylinder from the shock tube, and allowing the incident shock to reflect on the end wall of the shock tube and interact with the flame following it.

Figure 5 shows the evolution of the flame resulting from the interaction with the reflected shock at the critical regime, at an initial pressure of 4.1 and 4.8 kPa, for two cases where a transition to detonation was not observed and observed, respectively. In both cases, the dynamics follow the same sequence. The first frames show the structure of the wrinkled flame and the bifurcated structure of the reflected shock [20]. The interaction between the two significantly disturbs the flame structure. The flame structure is now broken up into smaller individual pockets of non-reacted gas. The mechanism for this break-up is consistent with the Richtmyer–Meshkov instability, augmented by the 3D structure of the reflected bifurcated shock [21]. Note also that the compression of turbulent gas ahead of the flame by the reflected shock is also expected to reduce the length and time scales of the turbulence.

The resulting increase in the surface area between burned and unburned gas augments significantly the burning velocity of the flame, and the flame accelerates forward driving a series of compression waves, which eventually form a shock. In the case of Fig. 5(2), this acceleration is faster, and the acceleration can proceed in the gas available ahead of the flame. In this case, the detonation forms near the sides, where the reflection of the non-planar leading shock, inherited by the non-planarity of the flame itself, gives rise to local shock reflections favoring the transition.

The acceleration is best seen on the space time diagram of Fig. 6, where the evolution of the experiment at 4.1 kPa is tracked along a central band 3-pixels-wide in each of the sequential frames, yielding a “streak” photograph. The speed of the reaction front in the absolute frame is shown in Fig. 7. Evident from the reconstruction of Fig. 6 is the backward acceleration of the gases

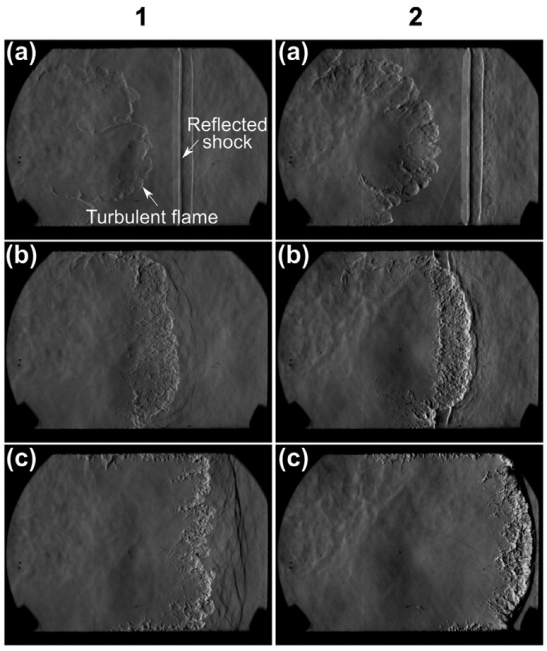

Fig. 5. The interaction of the reflected shock with a turbulent flame in C_3H_8+5O_2 leads to the flame break-up and its subsequent acceleration; (1) at 4.1 kPa initial pressure, frames shown every 206 μs apart and (2) and 4.8 kPa, frames shown 129 μs apart (videos as Supplemental material).

processed by the flame. The non-reacted pockets of Fig. 5 trace out rear facing streaks, the slope of these streaks is proportional to the local flow speed. Also evident is the forward facing acceleration of the flame leading edge. The acceleration generates forward facing compression waves, seen distinctly in this reconstruction. The flame path becomes parallel with the forward facing waves, indicating that the flame burning velocity is now comparable with the local sound speed, approximately 410 m/s; this is compatible with the mechanism deduced from the cylinder experiments. This suggests that the mechanism at play for the acceleration in this case is one for which the burning velocity is increased beyond the sonic condition. This implies that the local pressure increase can no longer be relaxed gasdynamically sufficiently fast, and an internal shock forms ahead of the flame. This internal shock is subsequently strengthened by further acceleration of the burning rate. In the experiment of Fig. 5(2) (see also Fig. 7), the shock observed becomes consistent with rapid auto-ignition such that the flame motion can be effected by shock motion itself, i.e., the transition to detonation. This transition mechanism is similar to the conventional reactivity gradient mechanism. In the present case, the acceleration of the flame is first due to the enhancement of the burning rate by RM instability, which makes the flame itself in phase with acoustic waves and results in pressure amplification and internal shock formation. Experiments at higher pressures yielded significantly higher burning velocities (in excess of 20 times the laminar burning velocity) in the flame following the incident shock, and transition to detonation was observed with time scales less than 100 μs. An example is shown in Fig. 8. Here, the transition to detonation was found internally to the disturbed flame brush by the reflection of the internally formed shocks, owing to the initial non-planarity of the leading shock. This was again consistent with the experiments performed with the cylinder.

Note that the induction delay times behind the reflected shock reported in Table 1 are three orders of magnitude longer than the evolution time observed. This again out-rules autoignition as the main mechanism for the first flame acceleration. Instead, the flame turbulization is responsible for its acceleration. This culminates in the formation of a strong shock, as in Fig. 5(2). The nonhomogeneous and extremely rapid transient did not permit us to measure the shock strength and estimate the ignition delay immediately prior to DDT.

5. Acceleration mechanism and DDT

The picture that emerges from the experiments performed with the interaction of the shock flame complex with a cylinder and a flat wall is that the re-

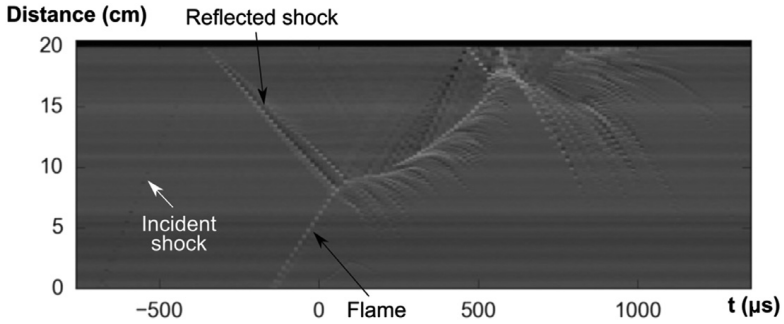

Fig. 6. A space-time diagram evolution of the interaction of Fig. 5 along the center of the channel illustrating the flame acceleration to the sonic condition.

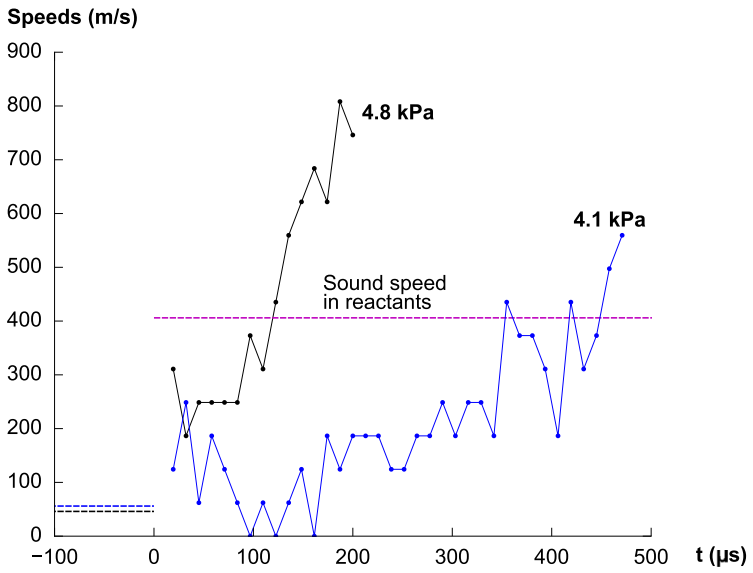

Fig. 7. The speed of the turbulent flames corresponding to Fig. 5 after the interaction with the reflected shock; broken lines denote the burning velocity measured prior to the interaction; time 0 corresponds to the first interaction between the flame and the reflected shock.

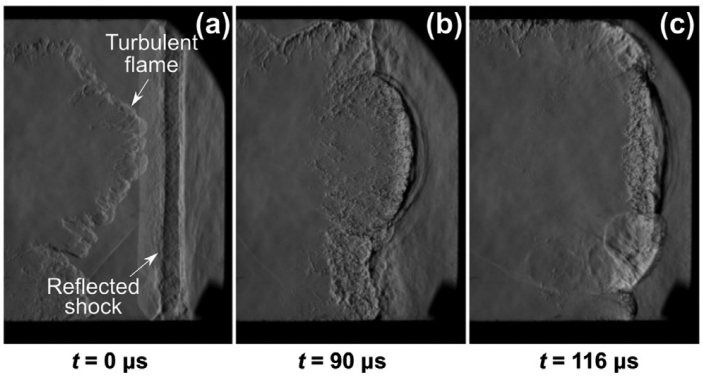

Fig. 8. The interaction of the reflected shock with a turbulent flame at 6.2 kPa illustrating the onset of detonation from the confluence of shocks driven by the flame acceleration (video as Supplemental material).

flected shock, in both cases, significantly enhances the burning rate of the flame. The origin of this enhancement is the disruption of the flame structure by the passage of the shock, with auto-ignition being negligibly slow at early times. The exact mechanism of flame disruption is difficult to assess with certainty. While the Richtmyer–Meshkov instability may disrupt the original turbulent flame, the reflected shock in all the cases investigated has a bifurcated structure, with a re-circulation bubble. This structure may also significantly disturb the flame. Shock–turbulence interaction may also be responsible for the reduction of the smaller scales of the turbulence.

Once the flame burning velocity approaches the sonic condition in the fresh gases, the flame motion is in phase with pressure waves and a strong shock is eventually driven in front of the flame. There appears a quasi-steady period at this state. Subsequent increase in burning rate amplifies the leading shocks, which can trigger auto-ignition, usually through shock reflections. This picture of flame acceleration in very turbulent flames appears to be consistent with the picture borne out from the numerical calculations of Poludnenko et al. [22], who investigated the fate of flames with arbitrarily high turbulent burning velocities. That such high turbulent burning velocities are possible has been shown in the present study, consistent with previous indirect observations of Khokhlov et al. [21].

The acceleration time scales determined in the wall experiments at critical conditions correspond approximately to the conditions in the cylinder experiments, suggesting a possible correlation between two time important time scales of the phenomenon: the flow time associated with gas dynamic cooling as the flame gets convected downstream of the obstacle, and the characteristic time

for flame acceleration. When the characteristic time for flame acceleration is smaller than the flow time of the flame over the obstacle, the flame is expected to have a sufficient time to exploit the amplification of the burning rate by the passage of the shock. When the time scale for flame amplification is much longer than the flow passage time over the obstacle, the flame does not have sufficient time to accelerate. This is in accord with the flow fields observed in the experiments where a clear demarcation between regimes of very fast amplification and regimes with negligible amplification was established.

In conclusion, the mechanism identified as controlling the transition to detonation when a sufficiently strong turbulent flame–shock complex propagates in a congested area is the enhancement of the burning rate by the reflected shocks. Autoignition from the reflected shocks in the current experiments has been found negligible until a much stronger shock is generated by flame amplification. It thus appears that a criterion for DDT in a congestion giving rise to reflected shocks could likely be established in terms of a time scale for the 1D problem of flame acceleration following the head-on shock–flame interaction. Future study should focus on experiments and analysis of this canonical problem, to determine if this problem itself admits simple scaling laws.

Acknowledgments

M.I.R acknowledges the financial support from both Shell and NSERC via a Collaborative Research and Development Grant, “Quantitative assessment and modeling of the propensity for fast flames and transition to detonation in methane, ethane, ethylene and propane”.

Supplementary material

Supplementary material associated with this article can be found, in the online version, at doi:10.1016/j.proci.2018.08.050.

References

[1] V. Bychkov, D. Valiev, L.E. Eriksson, *Phys. Rev. Lett.* 101 (2008) 4.
[2] M. Kellenberger, G. Ciccarelli, *Proc. Combust. Inst.* 35 (2015) 2109–2116.
[3] G. Ciccarelli, S. Dorofeev, *Prog. Energy Combust. Sci.* 34 (2008) 499–550.
[4] J.H.S. Lee, I.O. Moen, *Prog. Energy Combust. Sci.* 6 (1980) 359–389.
[5] C. Johansen, G. Ciccarelli, *J. Loss Prev. Process Ind.* 26 (2013) 571–585.
[6] E.S. Oran, V.N. Gamezo, *Combust. Flame* 148 (2007) 4–47.
[7] G. Thomas, R. Bambrey, C. Brown, *Combust. Theory Model.* 5 (2001) 573–594.
[8] L. Maley, R. Bhattacharjee, S.M. Lau-Chapdelaine, M.I. Radulescu, *Proc. Combust. Inst.* 35 (2015) 2117–2126.
[9] M. Saif, W. Wang, A. Pekalski, M. Levin, M.I. Radulescu, *Proc. Combust. Inst.* 36 (2017) 2771–2779.
[10] M. Kellenberger, G. Ciccarelli, *Combust. Flame* 191 (2018) 195–209.
[11] L.S. Gu, R. Knystautas, J. Lee, A.L. Kuhl, J.R. Bowen, J.-C. Leyer, A. Borisov, in: Dynamics of Explosions, Volume 114 of Progress in Astronautics and Aeronautics, American Institute of Aeronautics and Astronautics, 1988, pp. 232–247.
[12] J.C. Chao, *Critical Deflagration Waves that Lead to the Onset of Detonation*, McGill University, 2006 Ph.D. thesis.
[13] J.S. Grondin, J. Lee, *Shock Waves* 20 (2010) 381–386.
[14] B. Maxwell, A. Pekalski, M. Radulescu, *Combust. Flame* 192 (2018) 340–357.
[15] R. Bhattacharjee, *Experimental Investigation of Detonation Re-initiation Mechanisms Following a Mach Reflection of a Quenched Detonation*, University of Ottawa, 2013 Master’s thesis.
[16] D.G. Goodwin, H.K. Moffat, R.L. Speth, Cantera: An object- oriented software toolkit for chemical kinetics, thermodynamics, and transport processes. http://www.cantera.org, 2015. Version 2.2.0. doi:10.5281/zenodo.170284.
[17] F. Williams, San Diego Mechanism, *Technical report, University of California San Diego*, 2014. 2014-10-04 mechanism available at http://web.eng.ucsd.edu/mae/groups/combustion/mechanism.html.
[18] S.A.E.G. Falle, J.R. Giddings, Numerical Methods for Fluid Dynamics IV, Oxford University Press, 1993, pp. 337–343.
[19] W. Fickett, W.C. Davis, *Detonation Theory and Experiment*, Dover Publication Inc., 1979.
[20] H. Mark, in: The Interaction of a Reflected Shock Wave with the Boundary Layer in a Shock Tube, NACA, 1958. TM 1418
[21] A.M. Khokhlov, E.S. Oran, G.O. Thomas, *Combust. Flame* 117 (1999) 323–339.
[22] A.Y. Poludnenko, T.A. Gardiner, E.S. Oran, *Phys. Rev. Lett.* 107 (2011) 4.

2.2 Detonation transition criteria from the interaction of supersonic shock-flame complexes with different shaped obstacles

The present study is an experimental investigation of the last stages of the deflagration-to-detonation transition. A fast flame following a lead shock was generated by passing a detonation wave through a perforated plate. The shock flame complex then interacts with an obstacle of different shape. We study the influence of the obstacle shape on the transition mechanism to a detonation. The obstacles studied are a single round or square obstacle, a flat plate, a C-shaped and an H-shaped obstacle. The experiments were performed in a thin transparent channel permitting high speed schlieren visualization. Stoichiometric propane-oxygen was investigated at sub-atmospheric conditions. For each obstacle configuration, the initial pressure was changed to modify the flame burning velocity and the Mach number of the leading shock. The burning velocity prior to the interaction was measured experimentally from the displacement velocity of the flame in the videos. This required estimating the speed of the gas ahead of the flame. A linear correction to the speed immediately behind the lead shock was applied using the shock change equations and the measured pressure gradient behind the lead shock in order to account for the non-steadiness of the lead shock and viscous losses to the walls. Three main findings were that the obstacle shape had a minimal influence on the critical flame strength required for transition, although obstacles with a forward facing cavity were able to suppress the transition by isolating the re-initiation event inside the cavity. The main transition mechanism for all geometries was the enhancement of the flame burning velocity through the flame interaction with the shock reflected on the obstacle leading to Richtmyer-Meshkov instability. Finally, it was found that the flame burning velocity of the initial flame required for transition was closely approximated by the Chapman-Jouguet burning velocity. Consistent with the visual observations, this supports the view that transition is favored when the flame is in phase with the acoustic waves, and strong internal pressure waves can be amplified.

This study was published in 2019 in the Journal of Loss Prevention in the Process Industries [45], and is attached to this thesis in the following pages. The author conducted the experiments, analysis and wrote the paper. The conceptual planning was performed with the Ph.D. supervisor, Prof. M. I. Radulescu. Dr. A. Pekalski participated in the discussions during the data reduction phase.

Journal of Loss Prevention in the Process Industries 64 (2020) 103963

Contents lists available at ScienceDirect

Journal of Loss Prevention in the Process Industries

journal homepage: http://www.elsevier.com/locate/jlp

Detonation transition criteria from the interaction of supersonic shock-flame complexes with different shaped obstacles

Willstrong Rakotoarison [a], Andrzej Pekalski [b], Matei I. Radulescu [a,*]

[a] Department of Mechanical Engineering, University of Ottawa, Ottawa, ON, K1N 6N5, Canada
[b] Shell Global Solutions, UK

ARTICLE INFO

Keywords:
Deflagration to detonation transition
Richtmyer-meshkov instability
Supersonic flames
Shock amplification
Congestion shape

ABSTRACT

The present study is an experimental investigation of the last stages of the deflagration-to-detonation transition. A fast flame following a lead shock was generated by passing a detonation wave through a perforated plate. The shock flame complex then interacts with an obstacle of different shape. We study the influence of the obstacle shape on the transition mechanism to a detonation. The obstacles studied are a single round or square obstacle, a flat plate, a C-shaped and an H-shaped obstacle. The experiments were performed in a thin transparent channel permitting high speed schlieren visualization. Stoichiometric propane-oxygen was investigated at sub-atmospheric conditions. For each obstacle configuration, the initial pressure was changed to modify the flame burning velocity and the Mach number of the leading shock. The burning velocity prior to the interaction was measured experimentally from the displacement velocity of the flame in the videos. This required estimating the speed of the gas ahead of the flame. A linear correction to the speed immediately behind the lead shock was applied using the shock change equations and the measured pressure gradient behind the lead shock in order to account for the non-steadiness of the lead shock and viscous losses to the walls. Three main findings were that the obstacle shape had a minimal influence on the critical flame strength required for transition, although obstacles with a forward facing cavity were able to suppress the transition by isolating the re-initiation event inside the cavity. The main transition mechanism for all geometries was the enhancement of the flame burning velocity through the flame interaction with the shock reflected on the obstacle leading to Richtmyer-Meshkov instability. Finally, it was found that the flame burning velocity of the initial flame required for transition was closely approximated by the Chapman-Jouguet burning velocity. Consistent with the visual observations, this supports the view that transition is favored when the flame is in phase with the acoustic waves, and strong internal pressure waves can be amplified.

1. Introduction

Accidental release of combustible gas in the atmosphere presents significant explosion risks. In the presence of air, the mixture can be ignited to generate a flame. Initially propagating at subsonic velocity in the fresh gases, it may accelerate due to interaction with turbulence and transit to the supersonic combustion regime of detonation, through the commonly named deflagration to detonation transition (DDT) event. In the latter case, consequences can be devastating due to the sudden increase of pressure across the detonation front and the trailing blast wave. It is now well understood that DDT is more likely in the presence of obstructions or rough walls, as these promote the turbulization of the flow ahead of the flame.

The early stages of the flame acceleration following the ignition are well understood from extensive experimental studies. The type of obstructions, their size, shape and disposition were found to play a role in this process, as they change the nature of the flow with which the flame interacts (Hall et al., 2009; Park et al., 2007, 2008; Gubba et al., 2011). Early flame acceleration is equally well predicted via numerical and theoretical models (Ciccarelli and Dorofeev, 2008). Comprehensive reviews of the DDT process in both confined and unconfined media have been published (Ciccarelli and Dorofeev, 2008; Valiev et al., 2009; Lee and Moen, 1980; Oran and Gamezo, 2007; Lee, 2008; Breitung et al., 2007).

However, instants preceding the transition to the detonation regime are not as well understood. These instants are characterized by the

* Corresponding author.
E-mail address: matei@uottawa.ca (M.I. Radulescu).

https://doi.org/10.1016/j.jlp.2019.103963
Received 4 April 2019; Received in revised form 12 September 2019; Accepted 12 September 2019
Available online 28 February 2020
0950-4230/

formation of a shock-flame complex, due to coalescence of compression waves as the flame accelerates. This shock-flame complex propagates at supersonic velocities in the frame attached to the unperturbed fresh-gases and large turbulent burning velocities approaching the Chapman-Jouguet value are observed (Chue et al., 1913; Eder and Brehm, 2001; Saif et al., 2017). Recently, we have studied the interaction of such a shock-flame complex with a single cylindrical obstacle (Rakotoarison et al., 2019) for high intensity turbulent deflagrations with typical turbulent burning velocities of approximately 10–20 times the local laminar values. The experiments and numerical reconstruction of the flow-field permitted to identify the key mechanism of detonation transition. It was found that the shock wave reflections from the obstacle enhanced the burning velocity of the turbulent flame by the Richtmyer-Meshkov instability. This gave rise to burning velocities approaching the sound speed in the unburned gas just ahead of the flame, which led to the formation and amplification of shocks, eventually igniting a detonation.

It is thus of interest to determine if this mechanism remains valid for other types of obstacles. The present study is thus an extension of our previous work (Rakotoarison et al., 2019) to obstacles with different shapes. We adopt the same experimental technique as Chao et al. (2005), Grondin and Lee (2010) and Saif et al. (2017) to generate a high speed turbulent deflagration through the interaction of a detonation wave with a perforated plate. This gives rise to a shock-flame complex downstream of the perforated plate with controllable turbulent burning velocity. The question we would like to address is whether the shape of the obstacle plays an important role in the detonation transition criterion of a fast flame/shock complex. Indeed, engineering type calculations of DDT cannot resolve the scales of the obstacle, which is usually replaced by an empirical model. In the present study we consider cylindrical, square, rectangular, C and H-shaped obstacles.

2. Experimental details

Experiments were conducted in a 3.4 m long shock tube of a rectangular 19.05 by 203.2 mm cross-section (Fig. 1), filled with the desired reactive mixture at a controlled pressure. A flame was initiated at one end of the tube by a high voltage spark plug. It transits to a detonation in the first third of the tube (the ignition section) as it passes through a series of obstacles, and becomes a self-sustained detonation by the end of the second third of the tube (the propagation section), propagating at approximately 5% below the Chapman-Jouguet (CJ) detonation speed calculated. This was inferred from time of arrival measurements of the incident wave, using a pair of pressure transducers placed at the end of the propagation section. The detonation was transmitted to the last third of the tube (the test section) across a 96% blockage ratio perforated plate, to become a shock followed by a turbulent deflagration in the test section. This complex propagates at a supersonic velocity in the gases at filling initial conditions, and corresponds to the propagation regime just prior the onset of a detonation in the DDT process (Chao et al., 2005). In our previous studies (Rakotoarison et al., 2019), it was found that the strength of the turbulent deflagration can be controlled by the initial operating pressure, which controls essentially the strength of the detonation wave incident to the perforated plate and its transmission as a high-speed deflagration. The test section was obstructed by shaped obstacles, chosen cylindrical, square, rectangular, C-shaped and H-shaped, placed such that their leading edge is located 387 mm downstream of the perforated plate. These obstacles have a height of 101.6 mm, giving a blockage ratio of 50%.

The reactive mixture studied was $C_3H_8+5O_2$ at the initial temperature 294 K and in a range of initial pressure from 4 to 9 kPa, for the overall set of experiments. The experiments were monitored with a Z-type schlieren set-up with a 305 mm field of view. Images were acquired using a high-speed camera giving an inter-frame time of 12.9 μs The resolution was 384 by 288 pixels, corresponding to a spatial resolution of approximately 0.8 mm per pixel. The monitoring was completed with a row of 4 pressure sensors P1, P2, P3 and P4 placed on the top wall of the tube. They were located at equal 203.2 mm intervals, starting at 317.5 mm from the perforated plate. Signal output is the overpressure given in kPa for a sample rate of 1.538 MHz, filtered in post-process at 100 kHz using an order 6 Butterworth filter.

3. Characterization of the incident shock-flame complex

The shock-flame complex transmitted downstream of the perforated plate is characterized by the shock Mach number and the flame burning velocity, i.e., its velocity relative to the flow of fresh gases just ahead of it. They are controlled by the initial pressure for an experiment, and are plotted in Fig. 2.

The flame burning velocity was estimated by subtracting the flow velocity just ahead of the flame, to the absolute flame velocity measured on the schlieren videos. This was done first by calculating the flow velocity just behind the shock using the velocity jump condition, with the shock propagating at velocity D in the initial state at rest. Owing to the weak deceleration of the shock, the flow behind it is not uniform and expands, as seen on the overpressure signals recorded. A linear correction to the flow velocity calculated just behind the shock was applied using the shock-change equations (Fickett and Davis, 2000), by relating $\partial p/\partial t$ measured experimentally behind the shock at a fixed gauge location to the speed gradient behind the shock $\partial u/\partial x$ required to deduce the

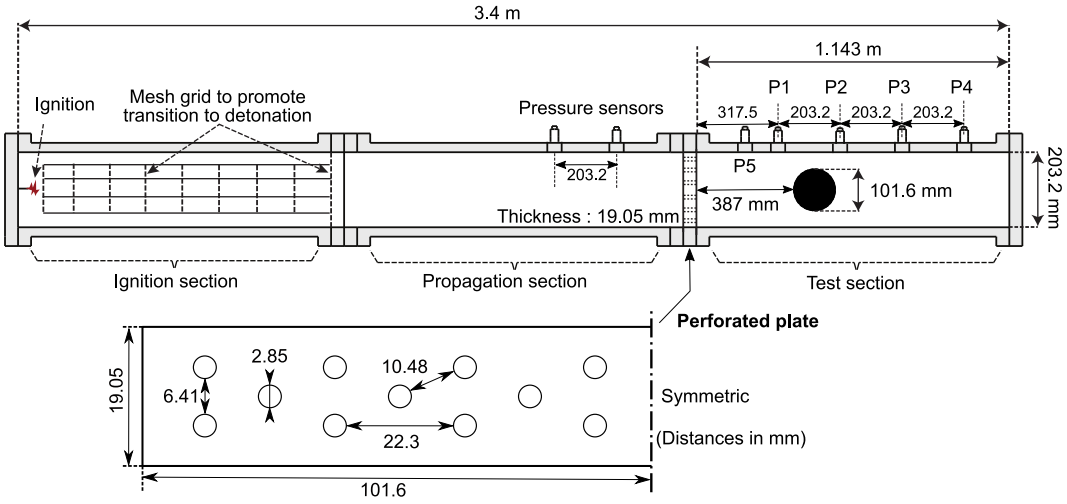

Fig. 1. Schematic of the experimental configuration.

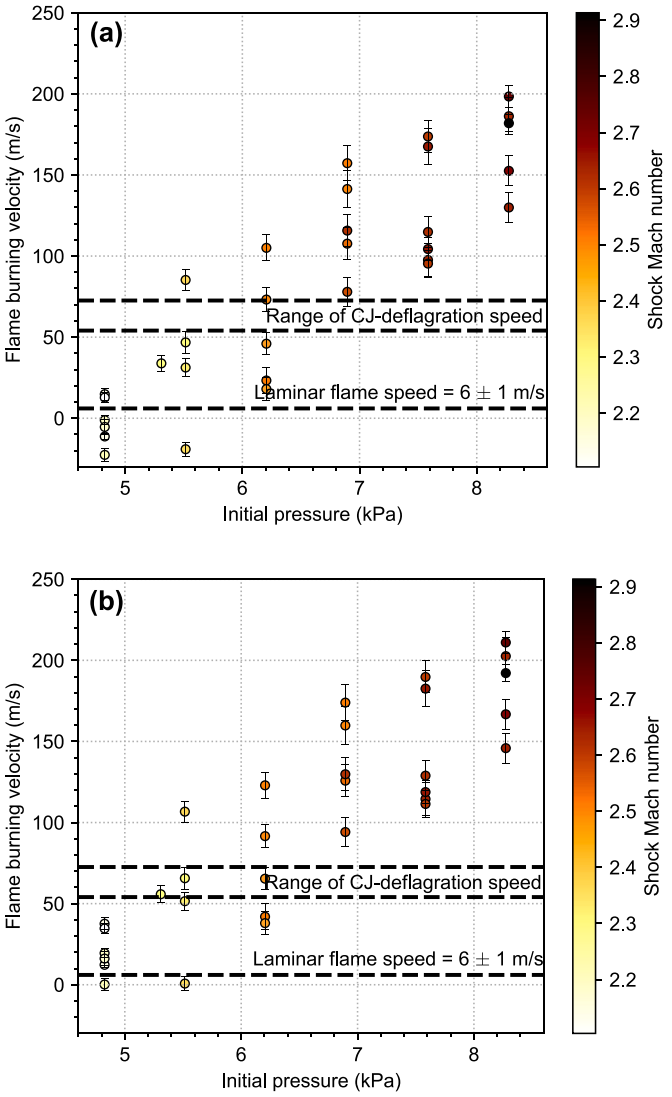

Fig. 2. Flame burning velocity and shock Mach number resulting from the decoupling of a detonation through a perforated plate, as a function of the initial pressure. (a) is using Fay's model for turbulent boundary layer (Fay, 1959). (b) is using Mirel's model for laminar boundary layer (Mirels, 1956).

speed variation. We start with the shock pressure evolution in time derived by Fickett and Davis (2000), in the laboratory frame of reference:

$$\left(\frac{dp}{dt}\right)_S = -K_1\left(\dot{\sigma_A} + \frac{\eta}{\rho_0 D}\frac{\partial p}{\partial x}\right)$$
$$K_1 = \frac{\rho c^2}{1 + (1-\eta)^{-1}\rho_0 D\left(\frac{du}{dp}\right)_H} \quad (1)$$

where the pressure p, density ρ, sound speed c and velocity u are evaluated at the post-shock state in the laboratory frame of reference, ρ_0 is the initial density, $\eta = 1 - (D-u)^2/c^2$ is the sonic parameter, and $\dot{\sigma_A} = (D-u)/A(dA/dx)$ a source term to account for geometrical flow divergence in the post-shock flow, $A(x)$ being the cross section area varying with the distance x from and downstream of the shock. Derivative with subscript H is taken along the shock Hugoniot, and derivative with subscript S is taken at the post-shock state, along the shock trajectory:

$$\left(\frac{dp}{dt}\right)_S = \frac{\partial p}{\partial t} + D\frac{\partial p}{\partial x} \quad (2)$$

The combination of energy and mass conservation equations:

$$\frac{\partial p}{\partial t} + u\frac{\partial p}{\partial x} + \rho c^2\frac{\partial u}{\partial x} = -\rho c^2\dot{\sigma_A} \quad (3)$$

is used to substitute the term $(\partial p/\partial x)$ in equation (2). Equation (2) is then used to replace $(dp/dt)_S$ in equation (1), to get an expression of the velocity gradient behind the shock $(\partial u/\partial x)$ in terms of the time derivative of pressure $(\partial p/\partial t)$ at a fixed location:

$$\frac{\partial u}{\partial x} = -\frac{1}{\rho c^2}\left\{\frac{\partial p}{\partial t} - uK_2\left[K_1\dot{\sigma_A} + \frac{\partial p}{\partial t}\right] + \rho c^2\dot{\sigma_A}\right\}$$
$$K_2 = \left[D + \frac{K_1\eta}{\rho_0 D}\right]^{-1} \quad (4)$$

Finally, the flame burning velocity u_f is estimated at the distance x_f downstream of the shock as:

$$u_f = u + \frac{\partial u}{\partial x}x_f \quad (5)$$

The terms in equation (4) were estimated through a series of experiments in which the shock-flame complex propagated in the tube with no obstruction. The term $(\partial p/\partial t)$ was estimated from the pressure signals provided by sensors P1 and P5, the latter being located 101.6 mm before P1 (see video frames below). It was taken as the slope of the straight line fitted simultaneously to the pressure signals provided by both sensors P1 and P5, using the least square method, in the time interval bounded by the passage of the shock and the passage of the flame. An example of measured pressure profiles and the fitted line is given in Fig. 3. Note the relatively large pressure fluctuations in the unburned gas separating the shock and the flame.

The velocity of the shock D was measured on the schlieren videos. It was taken as the average shock speed, deduced by the time it takes for the shock to cross the camera field of view from one side to the other, the camera looking at the location where the obstacle would be located. The shock Mach number could thus be deduced as $M = D/c_0$, where c_0 is the initial sound speed, that depends on the shock-tube filling conditions. The post-shock state was determined numerically in the ideal gas approximation using temperature dependent specific heats (Browne et al., 2015), with the help of the software Cantera (Goodwin et al., 2018) for thermochemical calculations. The derivatives along the shock Hugoniot were evaluated numerically by perturbing the shock-jump calculations by 1% in the shock speed. All the thermodynamic calculations were performed using the San Diego thermochemical database, relevant for propane-oxygen mixtures (Williams, 2014).

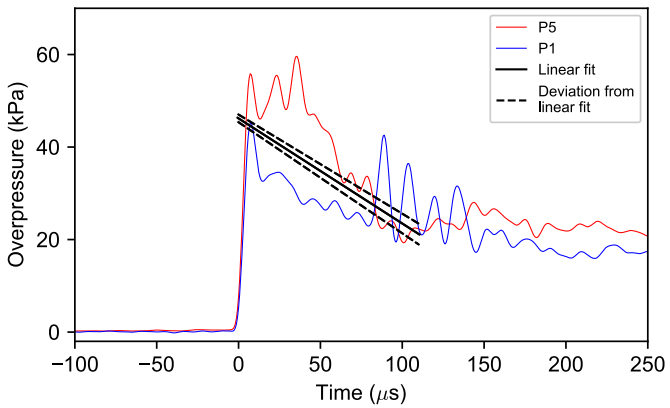

Fig. 3. Pressure signals from sensors P1 and P5 for an experiment at initial pressure 6.2 kPa. Signals are collapsed and fitted simultaneously to a straight line, between the time passage of the shock and the flame. Its slope is the term $(\partial p/\partial t)$ in equation (4) used to estimate the velocity gradient behind the shock $(\partial u/\partial x)$.

The term $\dot{\sigma_A}$ was used to account for the viscous losses due to the boundary layers in the tube width. They were modeled as a geometrical flow divergence downstream of the shock, with an expansion rate provided by the growth rate of the boundary layer displacement thickness $\delta^*(x)$, such that the cross section area at the distance x from and downstream of the shock is:

$$A(x) = hw + 2h\delta^*(x) \tag{6}$$

where $h = 203.2$ mm and $w = 19.05$ mm are respectively the height and the width of the tube. Approximating the area x-derivative at the flame position using:

$$\frac{dA}{dx} \simeq \frac{A(x_f) - hw}{x_f}$$

where x_f is the distance between the flame and the shock, and taking as an approximation for $1/A$ the constant value provided by the average cross section area between the shock and the flame such that:

$$A \simeq \frac{wh + A(x_f)}{2}$$

one could finally write:

$$\dot{\sigma_A} \simeq (D-u)\frac{2\delta^*(x_f)}{wx_f} \tag{7}$$

The boundary layer displacement thickness downstream of a shock could be found in the literature, for turbulent boundary layers using Fay's expression (Fay, 1959):

$$\delta^*(x) = 0.22x^{0.8}\left(\frac{\mu}{\rho_0 D}\right)$$

or for laminar boundary layers using Mirels's expression (Mirels, 1956):

$$\delta^*(x) = K\sqrt{\frac{\mu x}{\rho_0 D}}$$

where μ is the dynamic viscosity, constant, estimated at the post-shock state, and K is a constant equal to 2, relevant for our mixture (Xiao and Radulescu).

The flame burning velocities obtained by assuming either turbulent or laminar boundary layers are reported in Fig. 2. Error bars are representative of the deviation of the pressure signals from the linear pressure decay fitted after the passage of the shock, using the least square method (see Fig. 3). Despite some scatter, Fig. 2 shows a monotonically increasing trend of the flame burning velocity and the shock Mach number with increasing initial pressure. The flame burning velocity measured reaches up to 35 times the laminar flame burning velocity calculated with Cantera for initial conditions corresponding to the post-shock state, which is approximately equal to 6 ± 1 m/s for all experimental conditions tested.

One has to note however that the assumption of a linear flow velocity decay downstream of the shock as expressed by equation (5) makes this analysis local at the shock relevant in its close vicinity. Therefore, the error on the estimation of the flame burning velocity increases as the distance between the shock and the flame increases, i.e. when the initial pressure decreases. This error is difficult to quantify and is thus not included in the error bars of Fig. 2. The results of the present method are found in agreement with those obtained by using the lead shock deceleration directly (Rakotoarison et al., 2019). Future work should measure the flow velocity more accurately in order to further validate the method suggested here.

4. Experimental results

4.1. Cylindrical obstacle

Previous work (Rakotoarison et al., 2019) investigated in detail the mechanisms that promote transition to detonation from a supersonic shock-flame complex, interacting with a cylindrical obstacle. An example is shown in Fig. 4 for an initial pressure of 6.9 kPa. The frame at time 0 μs shows a turbulent deflagration with a shock wave ahead of it that starts interacting with the obstacle. For these conditions, the shock Mach number was approximately 2.57, measured from the videos, by taking the shock averaged velocity between the instant we see the shock entering the field of view, and the moment it starts to interact with the obstacle. The turbulent burning velocity was approximately 23 times the laminar value computed at the state behind the lead shock. The shock reflected on the obstacle is seen to interact with the flame at time 116.1 μs, giving rise to a reflected on flame shocks, denoted by arrows at time 232.2 μs These secondary shocks were found to be driven by the accelerating flame after the shock-flame interaction. The continuous amplification of these secondary shocks around the obstacle leads to the transition to detonation a few instants after time 348.3 μs, through their subsequent reflections behind the obstacle. It was found that at this moment, the flame burning velocity reached the speed of sound in the fresh gases just ahead of it (Rakotoarison et al., 2019). The forming detonation is seen at time 387.0 μs, and develops to become a cellular detonation as seen at time 425.7 μs At this initial condition, 8 experiments of 9 showed the ignition of the detonation in the wake of the obstacle.

Supplementary video related to this article can be found at https://doi.org/10.1016/j.jlp.2019.103963

For less sensitive mixtures at 4.8 kPa initial pressures (see Fig. 5), the overall evolution of the shock reflection and its interaction with a flame was similar, although both the turbulent burning velocity (18 times the laminar value) and the strength of the lead shock (Mach 2.23) were lower than above. The shock-flame interaction did not yield a sufficient acceleration of the flame, hence the secondary shocks, to affect DDT.

Supplementary video related to this article can be found at https://doi.org/10.1016/j.jlp.2019.103963

4.2. Square obstacle

Experiments were repeated using a square obstacle. Fig. 6 presents a set of frames obtained from an experiment performed at initial pressure 4.8 kPa, where the incident shock Mach number is 2.24. The configuration of shock-reflection on this experiment is similar to the case with the cylindrical obstacle at the same initial pressure. At later stages, no detonation occurred as shown on the pressure signals, where peaks are below the CJ detonation overpressure of 154 kPa, and the incident wave measured from time of arrival at sensors P3 and P4 is only 863.3 m/s, way below the calculated CJ detonation velocity of 2223 m/s.

Supplementary video related to this article can be found at https://doi.org/10.1016/j.jlp.2019.103963

As the initial pressure was increased, transition to detonation could be observed around the obstacle. Fig. 7 presents an experiment at initial pressure 7.6 kPa. The shock Mach number was 2.68. DDT was seen to occur at 225.8 μs on the top wall of the obstacle and the detonation is transmitted downstream of the obstacle, as shown on the overpressure signals that are above the CJ overpressure of 245.7 kPa, and by the incident wave velocity of 2170 m/s, that is 3.2% below the calculated CJ detonation speed, measured between sensors P3 and P4. At sufficiently high initial pressure, transition to detonation can be seen to occur on the leading edge of the obstacle. Fig. 8 shows an experiment done at initial pressure of 8.3 kPa where the incident shock Mach number is 2.74. Here, the interaction of the shock reflected on the obstacle with the flame front at 129.8 μs triggers the detonation. It is transmitted downstream of the obstacle, as can be seen on overpressure signals where peaks are above

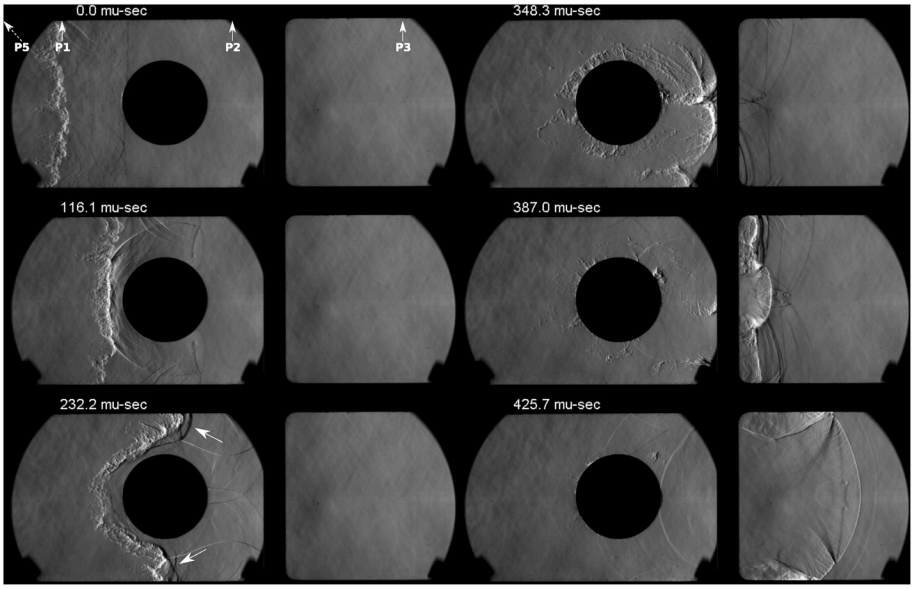

Fig. 4. Interaction of a C_3H_8+$5O_2$ mixture shock-flame complex with a cylindrical obstacle at 6.9 kPa initial pressure. The set of images was obtained by the splicing of 2 different experiments (Rakotoarison et al., 2019). Pressure sensors P1, P2, and P3 are localized on the first frame. Sensor P5 is out of the field of view, located 101.6 mm before P1. Full video is in supplemental material, file circle_6.9_kPa_77481_fps.mp4.

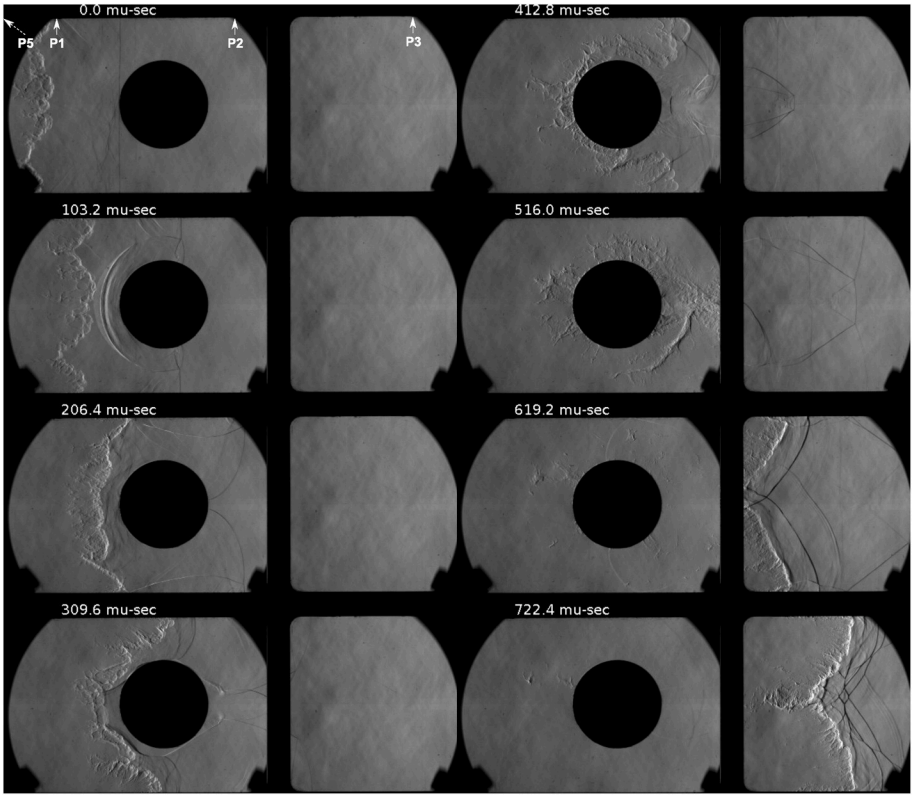

Fig. 5. Interaction of a C_3H_8+$5O_2$ mixture shock-flame complex with a cylindrical obstacle at 4.8 kPa initial pressure. The set of images was obtained by the splicing of 2 different experiments (Rakotoarison et al., 2019). Pressure sensors P1, P2 and P3 are localized on the first frame. Sensor P5 is out of the field of view, located 101.6 mm before P1. Full video is in supplemental material, file circle_4.8_kPa_77481_fps.mp4.

the CJ overpressure 268.9 kPa, and by the incident wave velocity of 2350 m/s, that is 4.6% above the calculated CJ detonation speed, measured between sensors P3 and P4.

Supplementary video related to this article can be found at https://doi.org/10.1016/j.jlp.2019.103963

4.3. Rectangular obstacle

Experiments using a rectangular obstacle are presented in this section. Fig. 9 shows one at initial pressure of 8.3 kPa, with an incident shock Mach number of 2.73. The detonation was ignited on the leading edge of the obstacle at the time the flame interacts with the shock

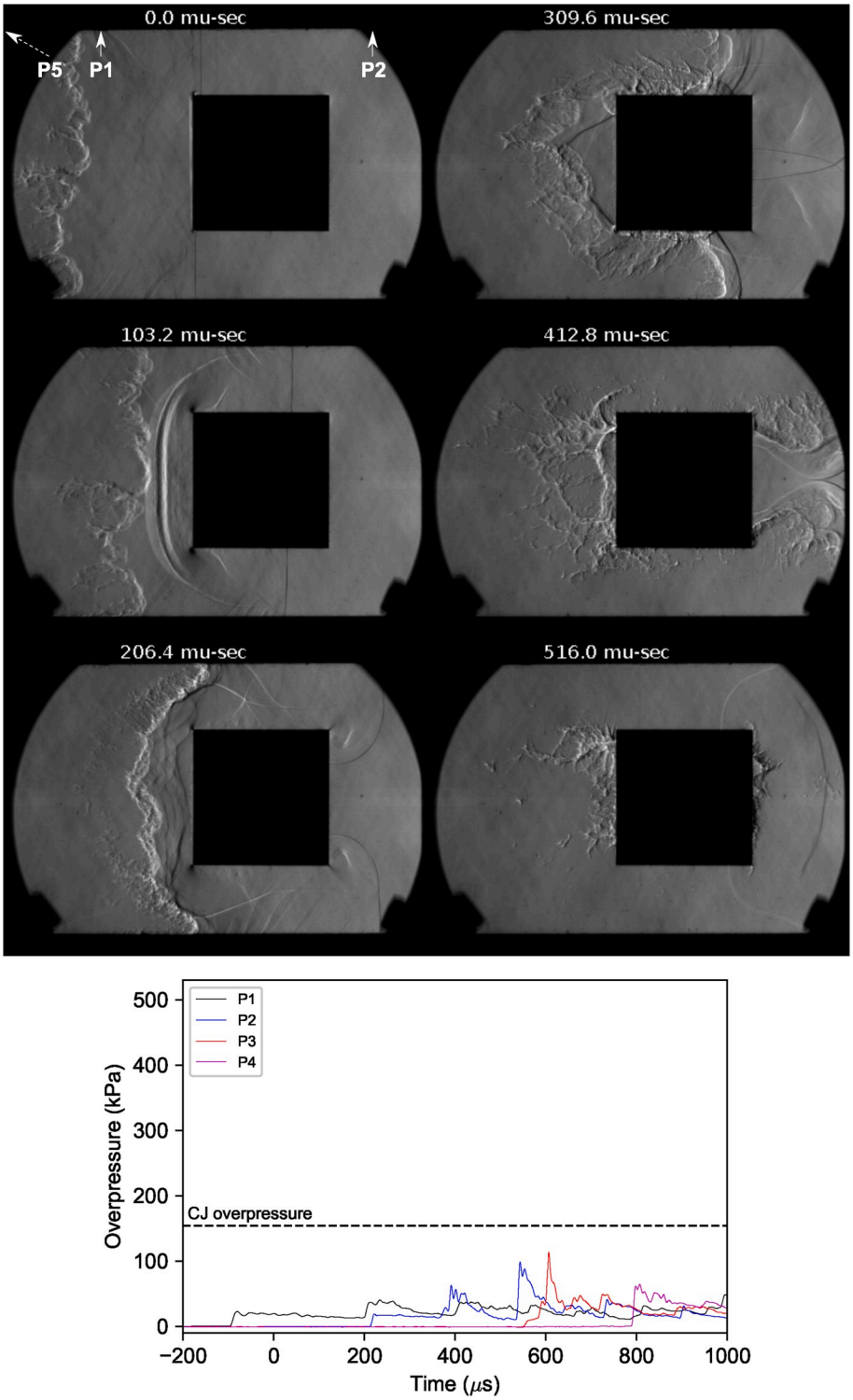

Fig. 6. Interaction of a $C_3H_8+5O_2$ mixture shock-flame complex with a square obstacle at 4.8 kPa initial pressure and overpressure signals associated. Pressure sensors P1 and P2 are localized on the first frame. Sensor P5 is out of the field of view, located 101.6 mm before P1. Full video is in supplemental material, file `square_4.8_kPa_77481_fps.mp4`.

reflected on the obstacle.

Supplementary video related to this article can be found at https://doi.org/10.1016/j.jlp.2019.103963

At lower initial pressure of 6.2 kPa, transmission of detonation after the obstacle was observed for 3 experiments out of 6, showing the proximity to the critical regime of transition of a detonation. An experiment at this initial pressure is shown in Fig. 10. The incident shock Mach number measured here is 2.43. Fig. 10 shows the assembly of 2 experiments. For one of them, a detonation was transmitted but not for the other. However, behavior of the shock-flame complex is similar before the transition to detonation, as shown on overpressure signals of P1, P2 and P3 for both experiments. Sensor P4 suggests that the detonation was ignited for one of them late after the passage of the obstacle, as the incident wave has an overpressure peak larger than the CJ

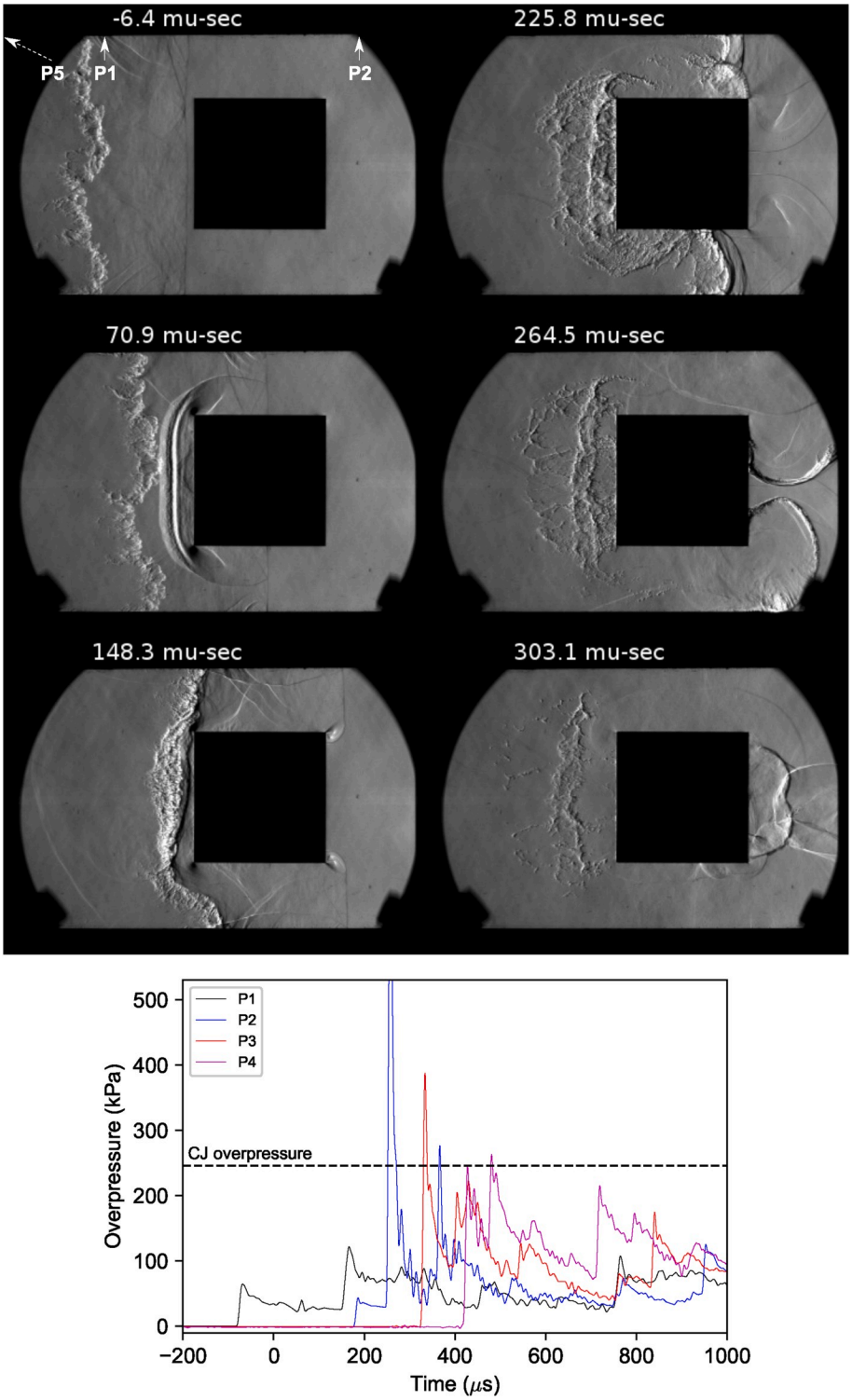

Fig. 7. Interaction of a C_3H_8+$5O_2$ mixture shock-flame complex with a square obstacle at 7.6 kPa initial pressure and overpressure signals associated. Pressure sensors P1 and P2 are localized on the first frame. Sensor P5 is out of the field of view, located 101.6 mm before P1. Full video is in supplemental material, file `square_7.6_kPa_77481_fps.mp4`.

overpressure 200 kPa. The formation of an apparently strongly coupled shock-flame complex can be seen at 445.1 μs Later, the shock is sufficiently amplified to ignite a detonation on the top and bottom walls of the channel, at reflection points of the weakly curve shaped shock.

Supplementary video related to this article can be found at https://doi.org/10.1016/j.jlp.2019.103963

4.4. C-shaped obstacle

Experiments involving a 180° rotated C-shaped obstacle were performed. Fig. 11 presents an experiment at initial pressure 7.6 kPa with an incident shock Mach number of 2.70, in which transmission of a detonation downstream of the obstacle was not observed. The incident shock was reflected on both branches of the obstacle. A part was

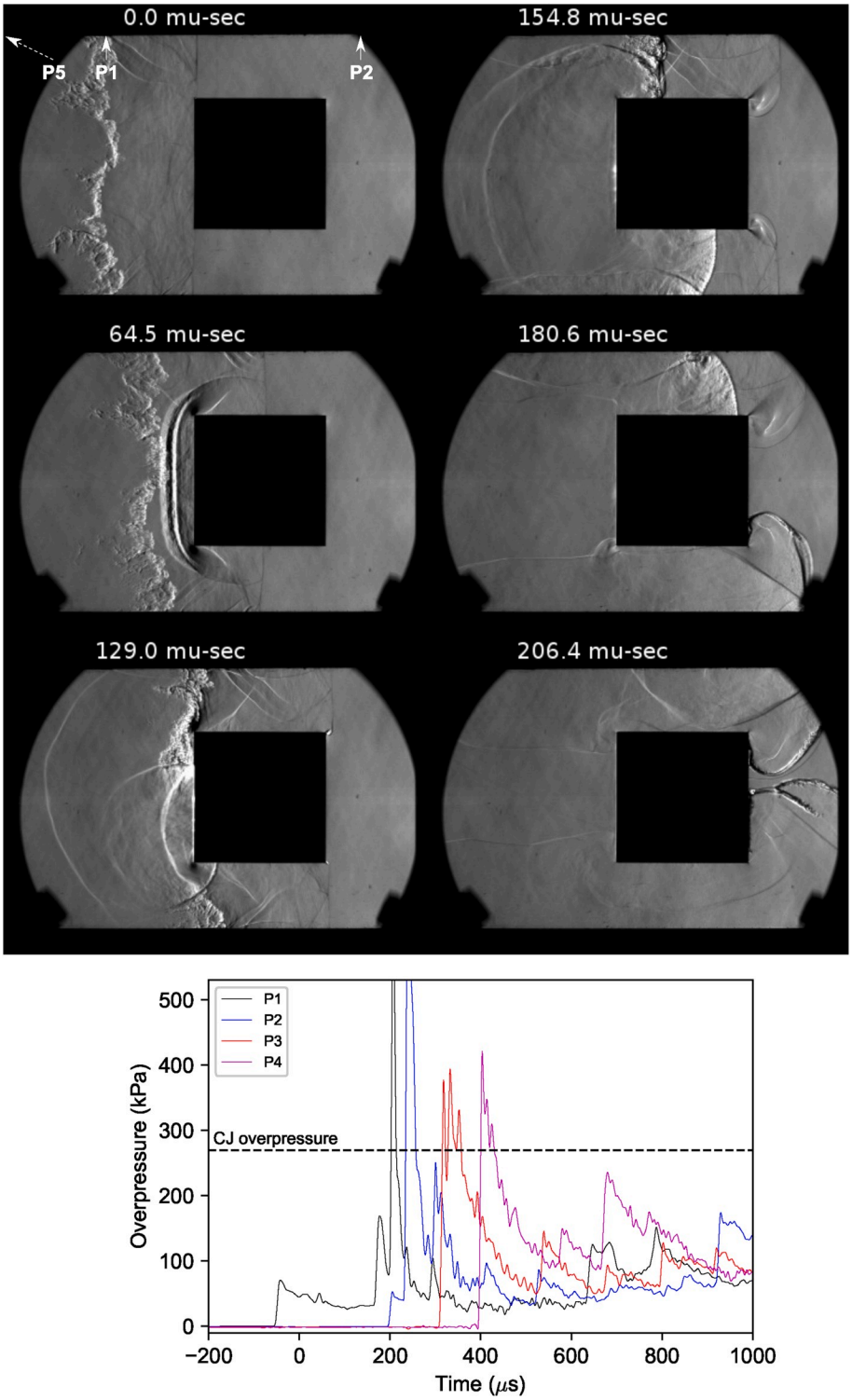

Fig. 8. Interaction of a C_3H_8+$5O_2$ mixture shock-flame complex with a square obstacle at 8.3 kPa initial pressure and overpressure signals associated. Pressure sensors P1 and P2 are localized on the first frame. Sensor P5 is out of the field of view, located 101.6 mm before P1. Full video is in supplemental material, file `square_8.3_kPa_77481_fps.mp4`.

transmitted in the cavity where an explosion is seen to occur at 245.1 μs The shock generated travels backward in the burnt gases and is not transmitted downstream of the obstacle. No detonation is ignited later in the channel, as shown by the overpressure signals associated to the experiment that are below the CJ detonation overpressure, and by the incident wave velocity of 813.9 m/s, way below the calculated CJ detonation velocity of 2242 m/s, measured between sensors P3 and P4.

As initial pressure was increased, the ignition and transmission of a detonation downstream of the obstacle was observed. Fig. 12 shows an experiment performed at initial pressure 9.7 kPa with an incident shock Mach number of 3.06. Ignition of a detonation could be observed on the leading edge of the lower branch of the obstacle at 96.8 μs, right after the shock-flame interaction. A second explosion occurred in the cavity due as well to the interaction of the reflected shock with the flame at 148.4

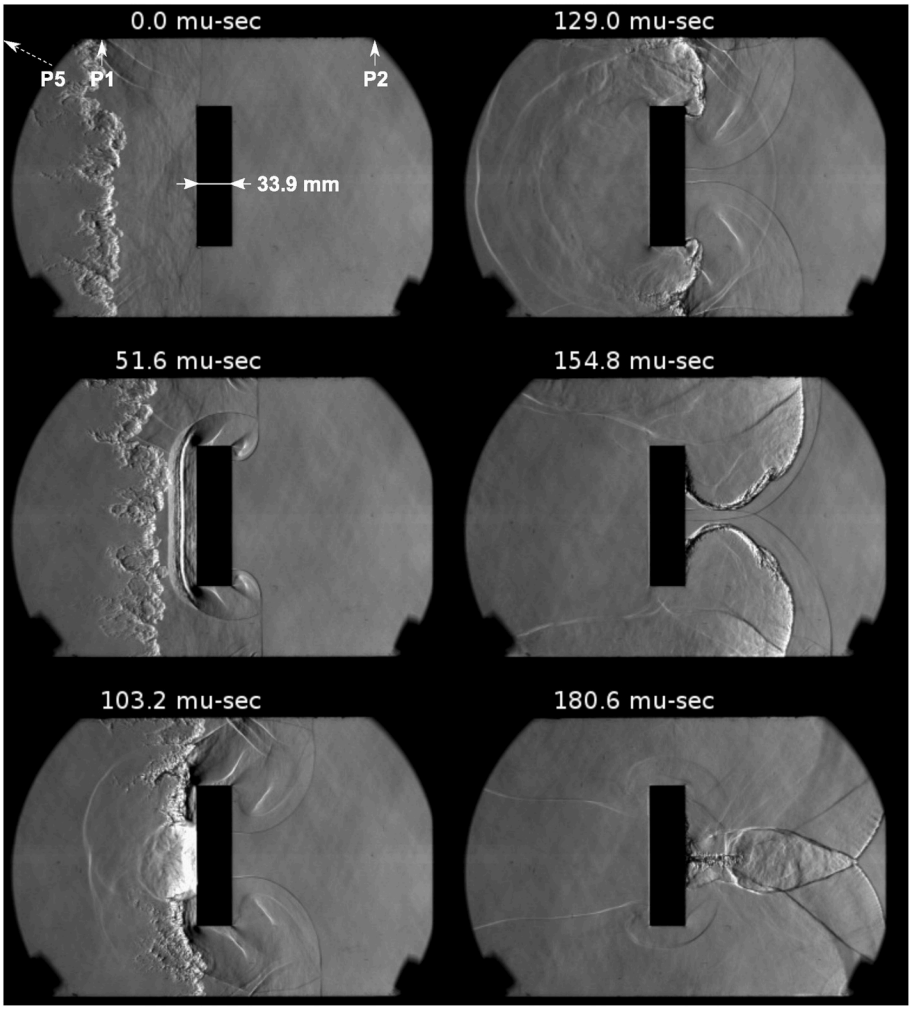

Fig. 9. Interaction of a C_3H_8+$5O_2$ mixture shock-flame complex with a rectangular obstacle at 8.3 kPa initial pressure. Pressure sensors P1 and P2 are localized on the first frame. Sensor P5 is out of the field of view, located 101.6 mm before P1. Full video is in supplemental material, file rod_8.3_kPa_77481_fps.mp4.

μs On the other side of the lower branch, the detonation propagated, as seen at time 135.4 μs It quenched while it was diffracted in the expanding section at 174.2 μs A subsequent re-ignition occurred as it met the transmitted shock-flame complex originating from the top side of the obstacle. A detonation was thus transmitted to the end of the channel, as shown by the overpressure signals associated where pressure peaks are above the CJ detonation overpressure, and by the incident wave corresponding to an overdriven detonation, propagating at a velocity of 2170 m/s that is 23.9% above the CJ detonation speed, measured between sensors P3 and P4. Experiments were repeated after rotating the C-shaped obstacle by an angle of 180°. Results are expressed in terms of transmission or not of a detonation downstream of the obstacle with the use of overpressure signals and are summarized in Fig. 14.

Supplementary video related to this article can be found at https://doi.org/10.1016/j.jlp.2019.103963

4.5. H-shaped obstacle

Experiments using an H-shaped obstacle were performed. At high enough initial pressure, the transmission of the detonation downstream of the obstacle could be observed, as presented in the experiment on Fig. 13. Initial pressure was 7.6 kPa and the incident shock Mach number was 2.74. The incident shock was reflected and diffracted twice on the branches of the obstacle, that are perpendicular to the direction of propagation of the incident shock-flame complex. After the first shock-flame interaction, the flame is seen at time 180.6 μs to drive a shock ahead of it. Shock-shock and shock-wall interactions in the cavity led to a first explosion at time 258 μs Similar shock-flame interaction could be observed at later times, leading to the ignition and transmission of a detonation downstream of the obstacle, at the intersection of flame-driven shocks seen at time 309.6 μs At initial pressures investigated below the critical regime of transition and transmission of the detonation, explosions could occur in the cavity following the same mechanism as previously described, but transmission of the detonation downstream of the obstacle could however not be observed.

Supplementary video related to this article can be found at https://doi.org/10.1016/j.jlp.2019.103963

5. Discussion

A summary of the occurrences of transition to detonation over the obstacles for all six geometries studied is shown in Fig. 14. Obstacles with no cavity facing the incident shock-flame complex such as the cylindrical, the square, the rectangular, the C-shaped and the H-shaped obstacles, show no significant differences regarding the critical regime of transition, which is approximately 6–7 kPa. This result is quite interesting, as it suggests that the shape of such obstacles does not play a sensible role in the detonation formation criterion.

This critical initial pressure corresponds on Fig. 2 to flames propagating with burning velocities of approximately the Chapman-Jouguet deflagrations burning velocities, ranging between 54 m/s and 73 m/s

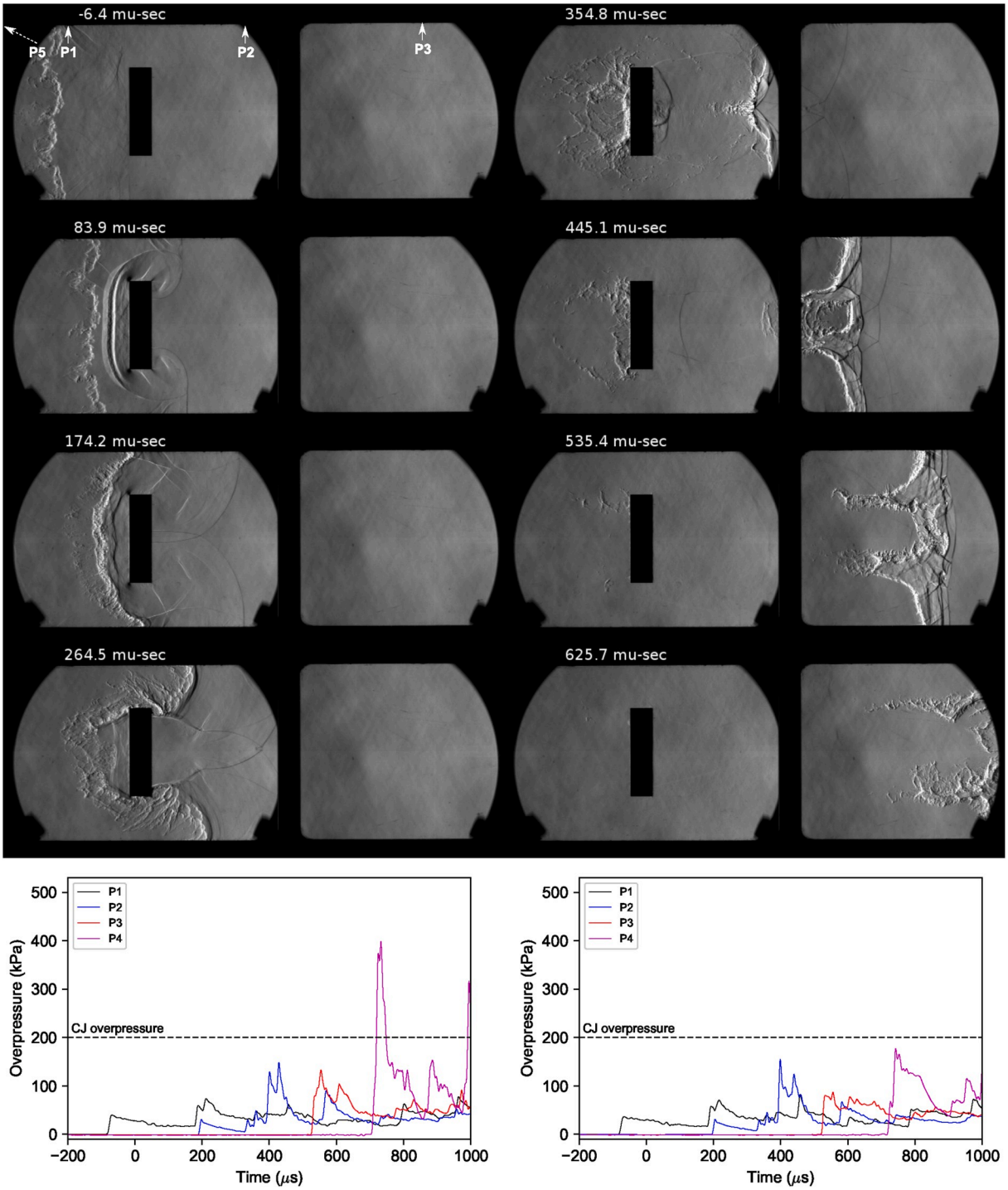

Fig. 10. Interaction of a C_3H_8+$5O_2$ mixture shock-flame complex with a rectangular obstacle at 6.2 kPa initial pressure and overpressure signals associated. The set of images was obtained by the splicing of 2 different experiments. Pressure sensors P1, P2 and P3 are localized on the first frame. Sensor P5 is out of the field of view, located 101.6 mm before P1. Full video is in supplemental material, file rod_6.2_kPa_77481_fps.mp4.

for all experiments, calculated numerically from the post-shock state, using methods derived from (Browne et al., 2015). Chapman-Jouguet (CJ) deflagrations are flames propagating with a flow in the burnt gases at sonic conditions in the frame attached to the flame, and their burning velocities are the maximum steady possible values a deflagration could propagate at.

The coincidence of the transition burning velocity with the CJ value can be misleading, in that the burning velocity of the flame increases when the reflected shock passes over the flame. It serves nevertheless to highlight the magnitude of the burning velocity relevant for transition, which is comparable with the speed of sound. Indeed, in our recent study analyzing the cylinder experiments (Rakotoarison et al., 2019), we estimated that the burning velocity after the interaction increases to approximately 400 m/s, which is closer to the sound speed ahead of the flame. Nevertheless, the flame burning velocity being comparable with the sound speed in either the burned gases (CJ deflagrations) or in the unburned gas ahead of the flame signifies that the flame is in phase with acoustic waves. This signifies the propensity of the flame to amplify

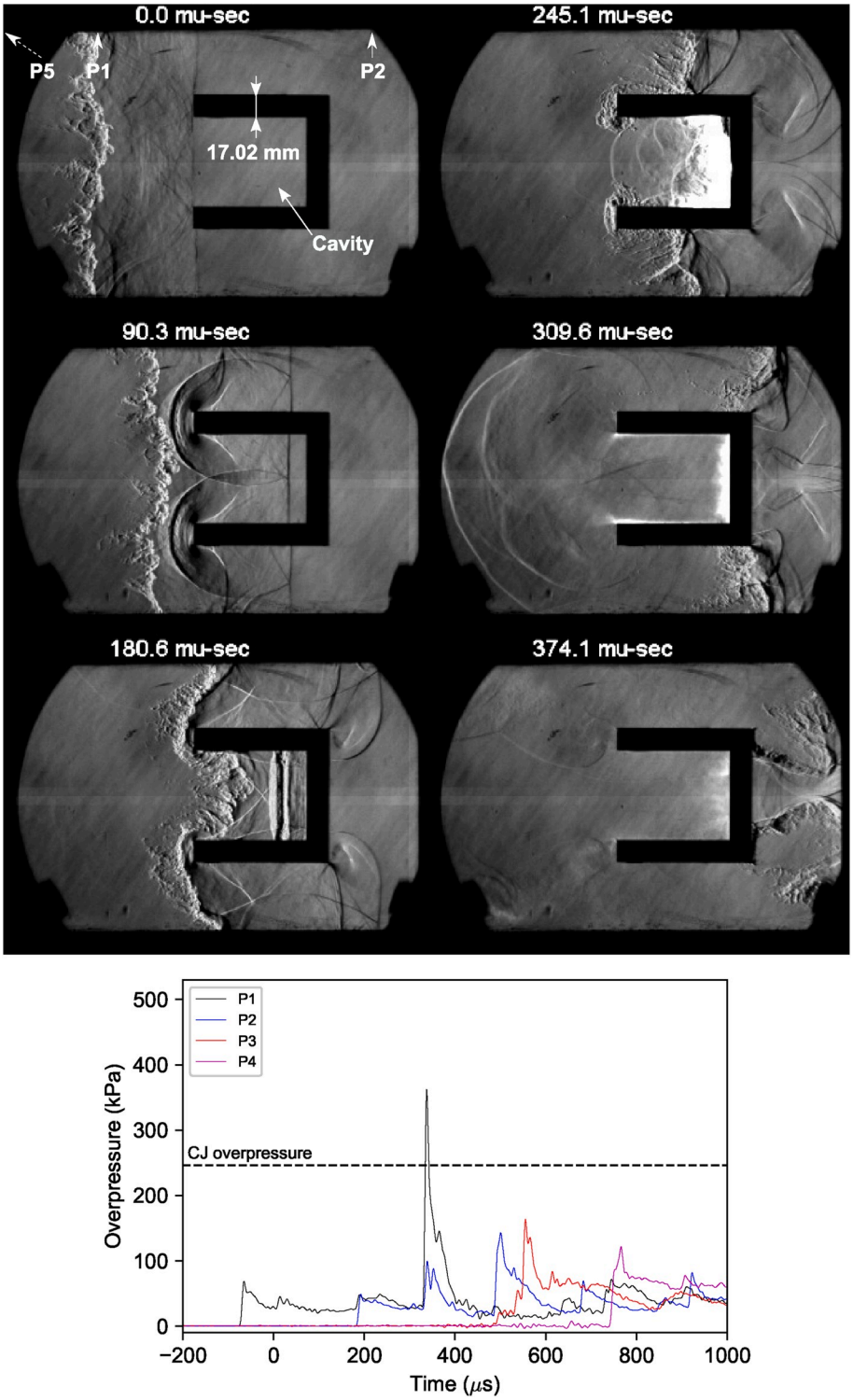

Fig. 11. Interaction of a C_3H_8+5O_2 mixture shock-flame complex with a 180° rotated C-shaped obstacle at 7.6 kPa initial pressure and overpressure signals associated. Pressure sensors P1 and P2 are localized on the first frame. Sensor P5 is out of the field of view, located 101.6 mm before P1. Full video is in supplemental material, file `revC_7.6_kPa_77481_fps.mp4`.

pressure waves (Travnikov et al., 1999; Saif et al., 2017; Poludnenko et al., 2011; Poludnenko, 2015; Rakotoarison et al., 2019) and effect transition, as also observed in the current study.

The mechanism of transition apparent for all geometries is the amplification of the burning rate by the reflected shock interaction with the flame. Since the strength of the reflected shock is expected to be very weakly affected by the shape of the obstacle, this explains the weak dependence found on the shape of the obstacle. It is to note that in our experiments, the reflected shock resulting from the first interaction of the incident shock with the obstacle was too weak to directly affect auto-ignition, as discussed by Rakotoarison et al. (2019).

Slight differences between the geometrical configurations were nevertheless observed. The experiments with the square showed that the detonation can form while the secondary shock flame complexes have

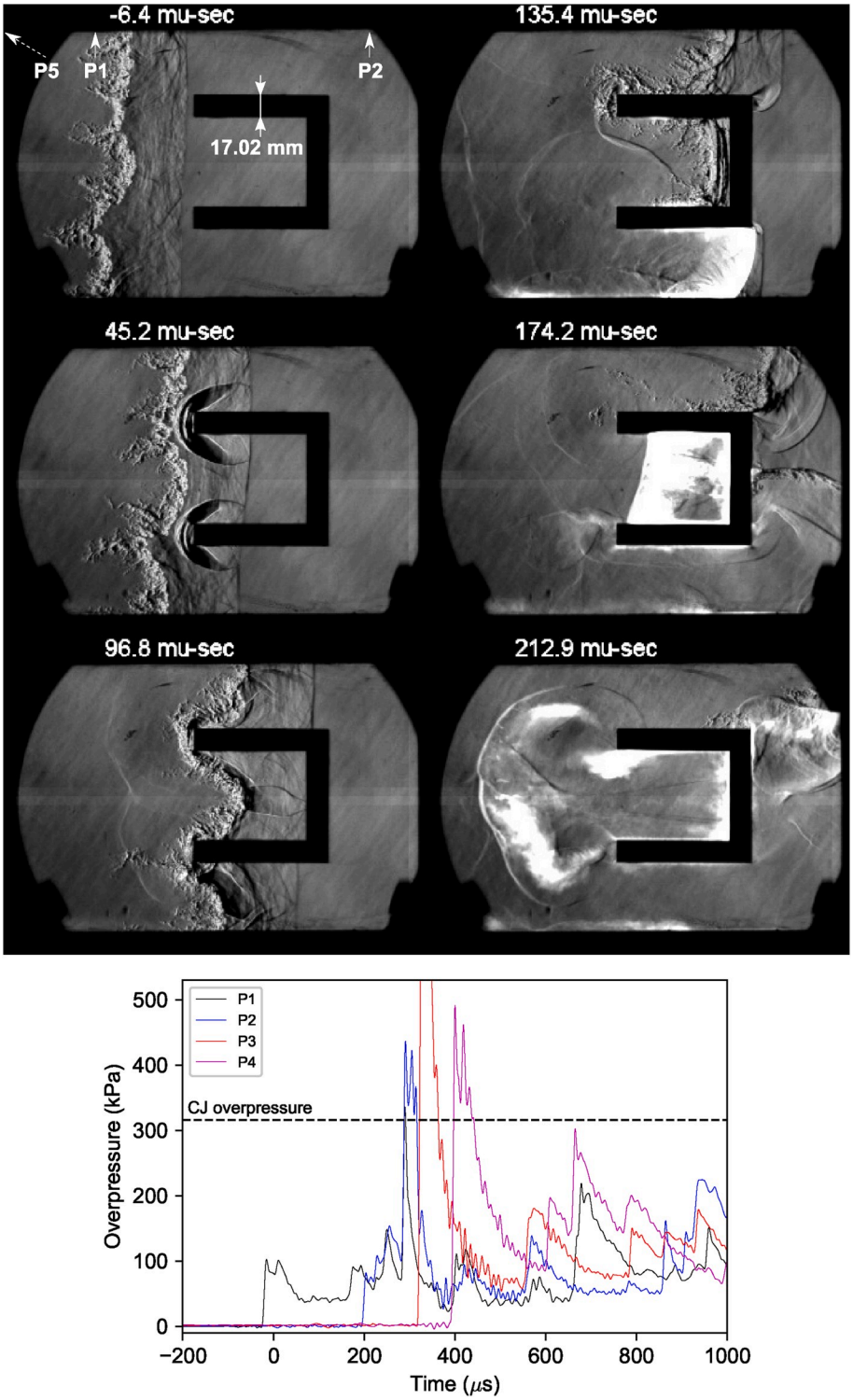

Fig. 12. Interaction of a $C_3H_8+5O_2$ mixture shock-flame complex with a 180° rotated C-shaped obstacle at 9.7 kPa initial pressure and lowerpressure signals associated. Pressure sensors P1 and P2 are localized on the first frame. Sensor P5 is out of the field of view, located 101.6 mm before P1. Full video is in supplemental material, file revC_9.7_kPa_77481_fps.mp4.

not yet diffracted behind the back side of the obstacle, while the experiments with the rectangle showed that the detonation formation can be delayed by the sudden expansion. This observation is consistent with the previous work (Rakotoarison et al., 2019), who suggested that the occurrence of DDT in the vicinity of the obstacle can be analyzed in terms of two competing processes: the amplification of the flame and the gas dynamic cooling as the flow expands as it passes over the obstacle. The geometrical shape of the object may provide some changes in the latter, at the back side of the obstacle, where the secondary shock-flame complex suddenly diffracts around the obstacle. While this geometric expansion is more intense for a square than for a rounded shape, the shock reflections following the diffraction is also more conducive to initiation. While these competing effects may change the local details of the re-initiation event, as was shown experimentally, the net result is to

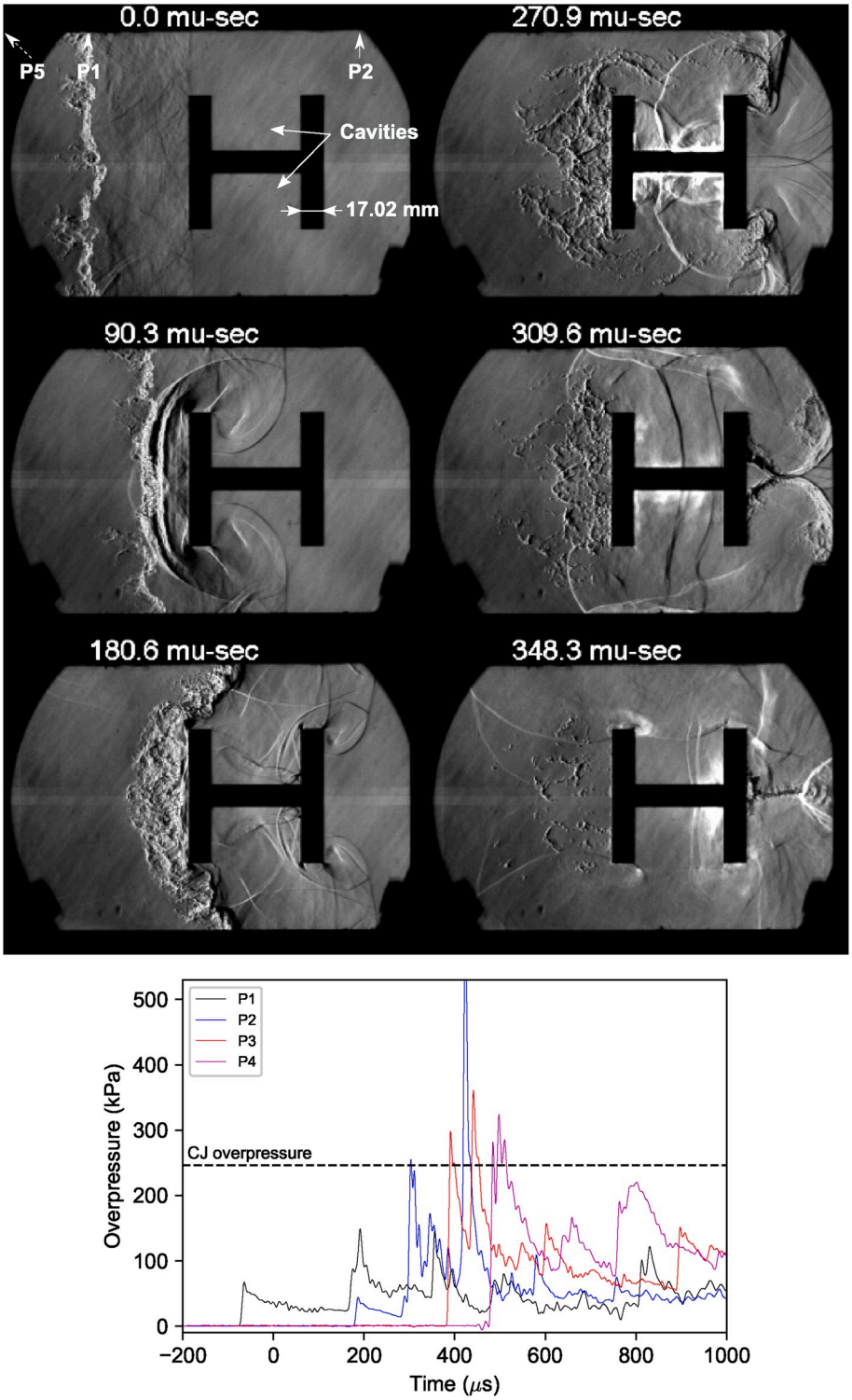

Fig. 13. Interaction of a $C_3H_8+5O_2$ mixture shock-flame complex with an H-shaped obstacle at 7.6 kPa initial pressure and overpressure signals associated. Pressure sensors P1 and P2 are localized on the first frame. Sensor P5 is out of the field of view, located 101.6 mm before P1. Full video is in supplemental material, file H_7.6_kPa_77481_fps.mp4.

not control sensitively the global condition for the transmission of a detonation downstream of the obstacle.

On the other hand, Fig. 14 shows that the critical regimes for obstacles with a cavity facing the incident shock-flame complex is larger than the others. It is in the range 8–10 kPa for the C-shaped obstacle. This could be explained in terms of the strength of the shocks reflected on the obstacle, that is smaller than for the square obstacle due to the reduced surface of reflection. Experiments at 7.6 kPa with the square obstacle (Fig. 7) showed that the shock reflected on the obstacle recorded by sensor P1 at 153 μshas a peak pressure of 125 kPa. At the same initial pressure, the same shock originating from the reflection on the top branch of the C-shaped obstacle (Fig. 11) recorded by the sensor P1 at the slightly later time 181 μs, has a peak pressure of 47 kPa. This difference of strength led to a weaker shock-flame interaction. The

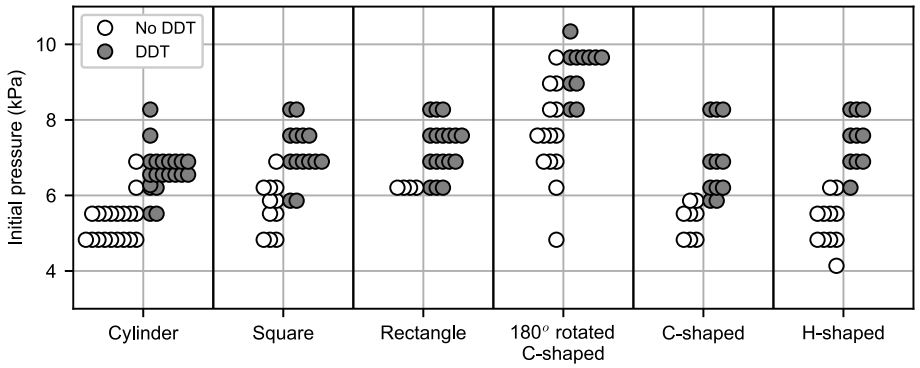

Fig. 14. Summary of occurrences of transmission of a detonation downstream of the obstacle, as a function of the initial pressure for a given obstacle.

subsequent flame acceleration around the obstacle is thus expected to be weaker and transition to detonation to be delayed, as the CJ-deflagration regime is less easy to reach. Although the explosion in the cavity of the C-shaped obstacle generated a strong shock propagating backward in the burnt gases (recorded by sensor P1 at 321 μs), it never reaches the flame front located near the trailing edge of the obstacle, and do not provide a supplementary mechanism for flame acceleration.

To summarize, the general result arising from these experiments is that the formation of a detonation downstream of the obstacle depends on the ability of the incident flame to reach sonic speeds in the vicinity of the obstacle, later leading to the formation of a detonation. All incident flames propagating with an initial burning velocity larger than the CJ-deflagration velocity transited very rapidly to detonations after their burning rate was further increased by the reflected shocks. Future tests should focus on establishing the scaling laws that control the amplification of a turbulent deflagration after the passage of a reflected shock wave and its run-away to a detonation wave.

6. Concluding remarks

Results of this study showed that the shapes of the obstacles investigated have an influence on the critical initial pressure necessary to observe the onset of the detonation, depending on the presence of a cavity facing the incident shock-flame complex. For obstacles with no cavity facing the incident shock, their shape was only found to play subtle effects on the locus of ignition of the detonation, occurring after the flame accelerated enough to drive shocks ahead of it. These flame-driven shocks could later ignite detonations at locations depending on the shape of the obstacle. The primary mechanism for flame acceleration was their interaction with shocks reflected on the obstacle, through the Richtmyer-Meshkov instability, which increases the burning rate of the flame.

A sufficient condition for DDT was found to be the flame reaching a burning velocity close the Chapman-Jouguet (CJ) deflagration burning velocity prior to its interaction with the obstacle. After the interaction with the reflected shocks, the burning velocity was closer to the sound speed ahead in the shocked gas ahead of the flame, resulting in efficient pressure wave amplification and rapid transition.

When comparing with other observations of DDT in channels with obstacles (e.g. (Oran and Gamezo, 2007),), it is not clear whether the flame reaching the sonic condition is also a necessary condition for all mixtures. While the global burning velocity is generally not reported, the mechanism of transition was found to be through auto-ignition from shock reflections on the obstacles. Care must be exercised when extrapolating results obtained for very sensitive mixtures with short ignition delays (like hydrogen) to mixtures that are much less sensitive to auto-ignition like in the present study.

In the presence of a cavity facing the incident shock, higher initial flame burning velocities were found to be required to allow the transmission of a detonation downstream of the obstacle. This is due to weaker flame acceleration, as the obstacle provided weaker reflected shocks owing to the smaller reflection surface, and also to isolation of the explosion in its cavity. This latter fact may be of interest in the design of detonation arrestors.

Declaration of competing interest

The authors ascertain there is no conflict of interest.

Acknowledgements

The authors wish to acknowledge financial support from Shell and from the Natural Sciences and Engineering Research Council of Canada (NSERC) through a Collaborative Research and Development Grant entitled “Quantitative assessment and modeling of the propensity for fast flames and transition to detonation in methane (CH4), ethane (C2H6), ethylene (C2H4) and propane (C3H8)”.

References

Breitung, W., Chan, C., Dorofeev, S., Eder, A., Gelfand, B., Heitsch, M., Klein, R., Malliakos, A., Shepherd, E., Studer, E., Thibault, P., 2007. Flame Acceleration and Deflagration-To-Detonation Transition in Nuclear Safety - State-Of-The-Art Report by a Group of Experts, Tech. Rep. NEA/CSNI/R(2000)7. Organisation for Economic Co-operation and Development, Nuclear Energy Agency, Committee on the Safety of Nuclear Installations.

Browne, S., Ziegler, J., Shepherd, J., 2015. Numerical Solution Methods for Shock and Detonation Jump Conditions. Mar.

Chao, J., Otsuka, T., Lee, J., 2005. An experimental investigation of the onset of detonation. Proc. Combust. Inst. 30 (2), 1889–1897. https://doi.org/10.1016/j.proci.2004.08.193.

Chue, R.S., Clarke, J.F., Lee, J.H., 1913. Chapman-jouguet deflagrations. Proc. Roy. Soc. Lond. Math. Phys. Sci. 441 (1993), 607–623. https://doi.org/10.1098/rspa.1993.0082.

Ciccarelli, G., Dorofeev, S., 2008. Flame acceleration and transition to detonation in ducts. Prog. Energy Combust. Sci. 34 (4), 499–550. https://doi.org/10.1016/j.pecs.2007.11.002.

Eder, A., Brehm, N., 2001. Analytical and experimental insights into fast deflagrations, detonations, and the deflagration-to-detonation transition process. Heat Mass Tran. 37 (6), 543–548. https://doi.org/10.1007/s002310100238.

Fay, J.A., 1959. Two–dimensional gaseous detonations: velocity deficit. Phys. Fluid. 2 (3), 283–289. https://doi.org/10.1063/1.1705924.

Fickett, W., Davis, W.C., 2000. Detonation: Theory and Experiment. Dover Publications.

Goodwin, D.G., Moffat, H.K., Speth, R.L., 2018. Cantera: an Object-Oriented Software Toolkit for Chemical Kinetics, Thermodynamics, and Transport Processes. Aug.

Grondin, J.S., Lee, J.H.S., 2010. Experimental observation of the onset of detonation downstream of a perforated plate. Shock Waves 20 (5), 381–386. https://doi.org/10.1007/s00193-010-0267-x.

Gubba, S.R., Ibrahim, S.S., Malalasekera, W., Masri, A.R., 2011. Measurements and LES calculations of turbulent premixed flame propagation past repeated obstacles. Combust. Flame 158 (12), 2465–2481. https://doi.org/10.1016/j.combustflame.2011.05.008.

Hall, R., Masri, A.R., Yaroshchyk, P., Ibrahim, S.S., 2009. Effects of position and frequency of obstacles on turbulent premixed propagating flames. Combust. Flame 156 (2), 439–446. https://doi.org/10.1016/j.combustflame.2008.08.002.

Lee, J.H.S., 2008. Deflagration-to-detonation Transition. Cambridge University Press, pp. 250–296. https://doi.org/10.1017/CBO9780511754708.009.

Lee, J.H.S., Moen, I.O., 1980. The mechanism of transition from deflagration to detonation in vapor cloud explosions. Prog. Energy Combust. Sci. 6 (4), 359–389.

Mirels, H., 1956. Boundary Layer behind Shock or Thin Expansion Wave Moving into Stationary Fluid. NACA Technical Note.
Oran, E.S., Gamezo, V.N., 2007. Origins of the deflagration-to-detonation transition in gas-phase combustion. Combust. Flame 148 (1), 4–47. https://doi.org/10.1016/j.combustflame.2006.07.010.
Park, D.J., Green, A.R., Lee, Y.S., Chen, Y.-C., 2007. Experimental studies on interactions between a freely propagating flame and single obstacles in a rectangular confinement. Combust. Flame 150 (1), 27–39. https://doi.org/10.1016/j.combustflame.2007.04.005.
Park, D.J., Lee, Y.S., Green, A.R., 2008. Experiments on the effects of multiple obstacles in vented explosion chambers. J. Hazard Mater. 153 (1), 340–350. https://doi.org/10.1016/j.jhazmat.2007.08.055.
Poludnenko, A.Y., 2015. Pulsating instability and self-acceleration of fast turbulent flames. Phys. Fluids 27 (1), 014106. https://doi.org/10.1063/1.4905298.
Poludnenko, A.Y., Gardiner, T.A., Oran, E.S., 2011. Spontaneous transition of turbulent flames to detonations in unconfined media. Phys. Rev. Lett. 107 (5), 054501 https://doi.org/10.1103/PhysRevLett.107.054501.
Rakotoarison, W., Maxwell, B., Pekalski, A., Radulescu, M.I., 2019. Mechanism of flame acceleration and detonation transition from the interaction of a supersonic turbulent flame with an obstruction: experiments in low pressure propane-oxygen mixtures. Proc. Combust. Inst. 37 (3), 3713–3721. https://doi.org/10.1016/j.proci.2018.08.050.
Saif, M., Wang, W., Pekalski, A., Levin, M., Radulescu, M.I., 2017. Chapman-Jouguet deflagrations and their transition to detonation. Proc. Combust. Inst. 36 (2), 2771–2779. https://doi.org/10.1016/j.proci.2016.07.122.
Travnikov, O.Y., Bychkov, V.V., Liberman, M.A., 1999. Influence of compressibility on propagation of curved flames. Phys. Fluids 11 (9), 2657–2666. https://doi.org/10.1063/1.870127.
Valiev, D.M., Bychkov, V., Akkerman, V., Eriksson, L.-E., 2009. Different stages of flame acceleration from slow burning to chapman-jouguet deflagration. Phys. Rev. E 80, 036317. https://doi.org/10.1103/PhysRevE.80.036317.
Williams, F.M., 2014. San Diego Mechanism, Tech. Rep. University of California San Diego.
Q. Xiao, M. Radulescu, Dynamics of Hydrogen-Hxygen-Argon Cellular Detonation with a Constant Mass Divergence, Submitted to Combustion and Flame.

Chapter 3

Model for Chapman-Jouguet deflagrations in open ended tubes with varying vent ratios

Deflagration to detonation transition (DDT) of flames propagating in tubes were extensively performed in experiments and numerical simulations. It is commonly admitted that DDT occurs when the flame reaches the speed of sound in the burned gases, as it is what is observed in most of the laboratory scale experiments. In these, the burned gases are confined by the walls of the tube, and are as a consequence at rest. A flame that reaches the speed of sound of the burned gases hence propagates with a sonic downstream flow, and thus is associated to Chapman-Jouguet (CJ) deflagrations. We propose in this paper a one-dimensional, quasi-steady model to predict the properties of CJ deflagrations, propagating in tubes where the burned gases can be vented to the atmosphere, through some opening with known surface area. This configuration aims to model the ones encountered in large scale DDT experiments, in which the burned gases are vented to the atmosphere through the obstacles used to promote flame acceleration. Results show that the properties of a CJ deflagration are strong functions of the exit section. Comparison with the terminal velocity of flames prior transition to detonation observed in large scale experiments suggests that, although they were smaller than the speed of sound in the burned gases, such flames are still CJ deflagrations.

This study is in preparation for publication in the journal Combustion and Flame. The current state of the article is attached to this thesis in the following pages. The author conducted the writing of the model, analysis and wrote the paper. The conceptual planning was performed with the Ph.D. supervisor Prof. M. I. Radulescu. Y. Vilende contributed to write the model during his stay as an intern. Dr. A. Pekalski participated in the discussions during the data reduction phase.

Model for Chapman-Jouguet deflagrations in open ended tubes with varying vent ratios

Willstrong Rakotoarison[a,*], Yohan Vilende[a], Andrzej Pekalski[b], Matei I. Radulescu[a]

[a] *Department of Mechanical Engineering, University of Ottawa, Ottawa ON Canada K1N6K5*
[b] *Shell Global Solutions, UK*

Abstract

Deflagration to detonation transition (DDT) of flames propagating in tubes were extensively performed in experiments and numerical simulations. It is commonly accepted that DDT is possible when flames reach the speed of sound in the burned gases, as observed in most of the laboratory scale experiments. In these, the burned gases are confined by the walls of the tube, and are as a consequence at rest. A flame that reaches the speed of sound of the burned gases hence propagates with a sonic downstream flow, and thus is associated to Chapman-Jouguet (CJ) deflagrations. We propose in this paper a one-dimensional, quasi-steady model to predict the properties of CJ deflagrations, propagating in tubes where the burned gases can be vented to the atmosphere, through some opening which section area is known. This configuration aims to model the ones encountered in large scale DDT experiments, in which the burned gases are vented to the atmosphere through the obstacles used to promote flame acceleration. Results show that the properties of a CJ deflagration are strong functions of the exit section. Comparison with the terminal velocity of flames prior transition to detonation observed in large scale experiments suggests that, although they were smaller than the speed of sound in the burned gases, such flames are still CJ deflagrations.

*Willstrong Rakotoarison
Email address: [redacted] (Willstrong Rakotoarison)

Keywords: Chapman-Jouguet deflagrations, Vented explosions

1. Introduction

The strongest, steady turbulent deflagrations propagating in closed-ended tubes filled with obstacles are known to propagate at a speed equal to the sound speed in the burned products, in the so-called *choking regime* [1]. This is the limiting regime before a quasi-detonation can be achieved in more sensitive mixtures or tubes with a larger characteristic porosity length scale [2].

In experimental and numerical studies of deflagration to detonation transition (DDT) of non-sensitive mixtures, the critical flame speed prior to rapid runaway to detonation waves was also found to be close to the speed of sound in the burned gases. In these experiments, flames were initiated in tubes with a closed rear end, forcing the burned gases to be at rest. A flame propagating at the speed of sound in the burned gases in such configuration thus has a downstream sonic flow in a frame attached to the flame, and is by definition associated to Chapman-Jouguet (CJ) deflagrations. Such flames propagate with a burning velocity, i.e. the flame velocity in a frame attached to the fresh gases just ahead of it, corresponding to the characteristic CJ deflagration burning velocity. The latter depends on the fresh gases initial conditions and composition and is the maximal steady burning velocity permissible for a subsonic flame [3, 4, 5, 6].

This statement made it commonly accepted that DDT is possible once flames reach the speed of sound in the burned gases. They are therefore CJ deflagrations. It however does not seem to hold anymore in DDT experiments at larger scales, as shown for example in the experiments reported by Pekalski et al. [7] and by Davis et al. [8], where the flame undergoes transition to detonation as it propagated in an array of obstacles, before it reached the speed of sound in the burned gases, that was approximately 900 to 1000 m/s. It is to note that in these experiments, the burned gases are not confined by walls but are vented to the atmosphere through the apertures provided by the obstacles, and thus have a certain velocity to account for when trying to determine a criteria for

DDT based on the *apparent flame speed*, i.e. its speed in the laboratory frame of reference. The question of whether in such configurations the flame could still be considered as a CJ deflagration prior transition to detonation arises.

As a starting point for the answer, some simple models could be developed to predict the properties of CJ deflagrations in a given configuration, and the results be compared to experiments. Such work was done by Chue et al. [9], for CJ deflagrations propagating in tubes with a closed rear end. Their model considered a quasi-steady, one-dimensional flow induced by the propagation of the flame following a precursor shock, that satisfies the zero flow velocity in the burned gases owing to the rear boundary condition. Hence, the CJ deflagration propagates with an apparent speed equal to the speed of sound in the combustion products. Different rear boundary conditions would give different absolute flame speeds and leading shock strengths. For example in the work of Saif et al., a similar model [10, 4] was used to characterize the quasi-steady, one-dimensional flow resulting from the decoupling of a detonation through a perforated plate, that became a shock followed by a CJ deflagration. The latter was supported by steady over-expanded jets of burned gases through the holes of the plate, leading to larger absolute flame speeds and stronger leading shocks than for the closed ended tube solution.

In the present study, we extend Chue's model to CJ deflagrations propagating in tubes with varying open area vent ratios. Other than finding direct application to fast flames propagating in tubes with open ends, the model is also expected to capture the fate of CJ deflagrations in different vented geometries, such as large scale tests of deflagrations propagating through an array of obstacles, where the sole confinement is provided by the congestion itself.

The present paper provides a gasdynamic model where the lead shock and the CJ deflagration are taken as discontinuities, where appropriate jump conditions may be applied, either using the perfect gas relations, or calculated numerically using equilibrium calculations and the ideal gas, i.e. temperature dependent, thermochemical properties of the mixture.

We formulate the problem of seeking the flame speed and lead shock strength

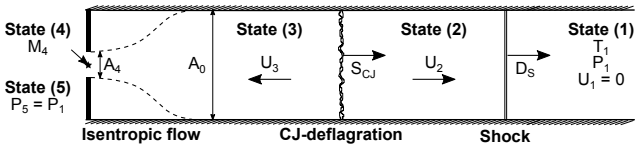

Figure 1: Schematic of the double discontinuity problem in a tube with rear venting.

of CJ deflagrations propagating in tubes with ends of varying open areas, ranging from the closed end boundary condition [9] to the fully open area, and extending it to geometries using diverging nozzles accommodating further expansion of the product gases behind the CJ deflagration.

2. Model

The model configuration is presented in Fig. 1. It consists in a tube of section area A_0, partially open at its back, providing an aperture with a section area A_4. The tube is filled with a gas at initial state (1). A shock propagating with a velocity D_s brings the flow to state (2), for which thermodynamic properties and flow velocity are calculated using the shock-jump equations.

The shock is followed by a CJ deflagration propagating at the velocity S_{CJ} in the laboratory frame of reference, that brings the flow to state (3), for which thermodynamic properties and flow velocity are calculated using the CJ deflagration jump conditions.

Due to the presence of the aperture downstream of the CJ deflagration, the flow is expanded isentropically to match the exit conditions at state (4), depending on the post-aperture state (5) where the pressure is fixed to match the initial pressure, i.e. $P_5 = P_1$.

2.1. Jump conditions in a perfect gas

The jump conditions across the shock and the flame could be derived in the perfect gas approximation with no changes of composition. The temperature and the speed of sound are thus related to the pressure p and density ρ by :

$$T = p/(\rho R_g) \quad ; \quad c = \sqrt{\gamma(p/\rho)} \tag{1}$$

where the specific heat capacity ratio γ and perfect gas constant R_g are assumed constant. Taking an arbitrary initial state (0) that moves at velocity u_0 in an absolute frame of reference, the pressure, density and velocity downstream of a shock propagating in it with an absolute velocity D_s, are given by the classical shock jump equations expressed in terms of the shock Mach number $M_s = (D_s - u_0)/c_0$:

$$p_s = p_0 \frac{2\gamma M_s^2 - \gamma + 1}{\gamma + 1} \tag{2}$$

$$\rho_s = \rho_0 \frac{\gamma + 1}{\gamma - 1 + \frac{2}{M_s^2}} \tag{3}$$

$$u_s = u_0 + \frac{2(M_s^2 - 1)}{(\gamma + 1)M_s}\, c_0 \tag{4}$$

Identically, the pressure, density and velocity downstream of a CJ deflagration propagating with an absolute velocity S_{CJ} are given by the CJ deflagration jump equations [11]:

$$p_{CJ} = p_0 \frac{\gamma M_{CJ}^2 + 1}{\gamma + 1} \tag{5}$$

$$\rho_{CJ} = \rho_0 \frac{M_{CJ}^2(\gamma + 1)}{\gamma M_{CJ}^2 + 1} \tag{6}$$

$$u_{CJ} = u_0 + M_{CJ}\left(1 - \frac{\rho_0}{\rho_{CJ}}\right) c_0 \tag{7}$$

where $M_{CJ} = (S_{CJ} - u_0)/c_0$ is the CJ deflagration Mach number expressed as :

$$M_{CJ}^2 = 1 + \frac{\gamma^2 - 1}{\gamma}\frac{Q}{p_0 v_0} - \sqrt{\left(\frac{\gamma^2 - 1}{\gamma}\frac{Q}{p_0 v_0} + 1\right)^2 - 1} \tag{8}$$

with Q the given gas specific heat of reaction, assumed constant.

The last useful relations are the ones in an isentropic flow in a channel with varying section. The flow Mach number at an arbitrary state (0) M_0 where the section area is A_0 is related to the section area A^* at the choked state (*), i.e. where $M^* = 1$ by :

$$\frac{A_0}{A^*} = \frac{1}{M_0}\left(\frac{2}{\gamma + 1} + \frac{\gamma - 1}{\gamma + 1} M_0^2\right)^{\frac{\gamma+1}{2(\gamma-1)}} \tag{9}$$

and their pressure by :

$$\frac{p_0}{p^*} = \left(1 + \frac{\gamma - 1}{2}\right)^{\frac{\gamma}{\gamma - 1}} \tag{10}$$

2.2. Jump conditions in ideal gases

Jump conditions across a shock and a CJ deflagration can also be calculated numerically, for realistic thermochemical properties of mixtures and allowing for either frozen or equilibrium compositions. Ideal gas properties, i.e. temperature dependent only, and equilibrium calculations were handled with the help of the software CANTERA [12]. Jump conditions accross a shock or a CJ deflagration were calculated using methods adapted from the Shock and Detonation Toolbox developed by Shepherd and co-workers [13].

Considering a gas at state (0) moving with an absolute velocity u_0, in which a generic discontinuity propagates with an absolute velocity D. Downstream of this discontinuity, the gas is brought to an equilibrium state (e). Defining $w_0 = D - u_0$ and $w_e = D - u_e$, respectively the velocities of the gas at state (0) and (e) in a frame attached to the discontinuity, the equations of conservation of mass, momentum and energy across it are :

$$\frac{w_0}{v_0} = \frac{w_e}{v_e} \tag{11}$$

$$p_0 + \frac{w_0^2}{v_0} = p_e + \frac{w_e^2}{v_e} \tag{12}$$

$$h_0 + \frac{1}{2}w_0^2 = h_e + \frac{1}{2}w_e^2 \tag{13}$$

where $v = 1/\rho$ is the gas specific volume. Using Eq. (11) to get an expression for w_e, Eq. (12) and (13) can be re-written as :

$$p_e(T_e, v_e) - p_0 + \frac{1}{v_0}\left(\frac{v_e}{v_0} - 1\right) w_0^2 = 0 \tag{14}$$

$$h_e(T_e, v_e) - h_0 + \frac{1}{2}\left(\frac{v_e^2}{v_0^2} - 1\right) w_0^2 = 0 \tag{15}$$

that constitute a set of two equations with the three unknowns T_e, v_e and w_0, used to determine the equilibrium state downstream of a discontinuity.

For an inert shock propagating with a given relative velocity w_0, its downstream equilibrium state is determined by finding the couple (T_e, v_e) that satisfies Eq. (14) and (15), assuming frozen chemistry. This was done numerically using a two-variables Newton-Raphson root finder algorithm applied to T_e and v_e [13], taking for initial guesses:

$$v_e^i = \frac{v_0}{5} \quad ; \quad T_2^i = T_0 \frac{p_0 v_0}{p_e^i v_e^i} \quad ; \quad p_e^i = p_0 + \frac{w_0^2}{v_0}\left(1 - \frac{v_e^i}{v_1}\right)$$

For a CJ deflagration, its burning velocity $w_0 = w_{CJ}$ must be determined first and should correspond to the maximum burning velocity a deflagration could propagate at, in the given initial state (0). The method used to find it was adapted from the *minimum wave speed algorithm* used in [13] to find the CJ detonation speed associated to state (0). It consists in finding the couple (w_0, T_e) that satisfies Eq. (14) and (15) for different values of v_e in a range that contains v_{CJ}, with equilibrium state at chemical equilibrium. The CJ deflagration state is then chosen as being the one that maximizes w_0.

Solving Eq. (14) and (15) for w_0 and T_e was done using a two-variables Newton-Raphson root finder algorithm. Initial guesses were chosen based on calculations in the perfect gas approximation, such that:

$$w_0^i = 1.5 \times w_{CJ,\text{perfect}} \quad ; \quad T_e^i = 0.8 \times T_{CJ,\text{perfect}}$$

The bounds of the range where to seek v_{CJ} were chosen as the specific volume of burned gases after a constant pressure combustion for the minimum, and twice the value of the specific volume of a CJ deflagration, calculated in the perfect gas approximation for the maximum. Such guesses were found appropriate for the mixtures and initial conditions presented in this paper.

The properties of a complex formed by a shock followed by a CJ deflagration as presented in Fig. 1 could then be calculated. Using the same notation, the CJ deflagration burning velocity w_{CJ} varying with the shock strength expressed in terms of shock overpressure $(p_2 - p_1)$ is plotted in Fig. 2, for different

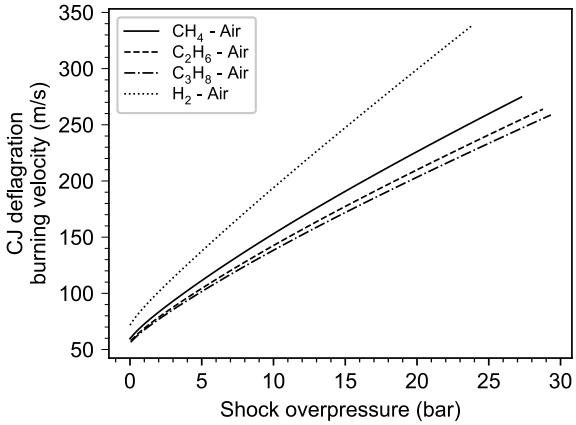

Figure 2: CJ deflagration burning velocity as a function of the leading shock overpressure for common fuel-air mixtures in stoichiometric proportions, using the San Diego chemical mechanism for the ideal gas properties. Initial pressure and temperature are 1 bar and 300 K.

stoichiometric fuel-air mixtures at initial pressure and temperature 1 bar and 300 K. As expected, the burning velocity of a CJ deflagration increases with the shock strength, owing to the fact that the temperature downstream of a shock increases with stronger shocks. This trend is easily shown in the perfect gas approximation using Eq. (8), that could be used with the relations (1) to show that the CJ deflagration burning velocity increases monotonously with an increasing upstream temperature, i.e. with an increasing shock strength.

2.3. General procedure to the solution of the double discontinuity problem

Finding the shock - CJ deflagration properties that satisfy the quasi-steady solution associated to the double discontinuity problem presented in Fig. 1 is done by finding the shock speed that satisfies the boundary condition at the aperture, using numerical, iterative methods. Three cases have to be considered. They are calculated in the following order:

1. From state (3), the flow reaches the choked state at the aperture, i.e. $M_4 = 1$ and is adapted to the atmosphere, i.e. $P_4 = P_5 = P_1$. In this

case, the gas exits the tube through the aperture as a perfectly expanded sonic jet (PEJ). This case is solved, first by iterating on the shock speed to satisfy the condition $P_4 = P_5$. It is done by calculating the state (3) for a given shock speed, then using the relation that links P_3 and P_4 in an isentropic flow where $M_4 = 1$ (Eq. (10) for a perfect gas). One could then deduce the associated aperture area section denoted A_4^* from the area - flow Mach number relation (Eq. (9) for a perfect gas), as A_0, M_3 and $M_4 = 1$ are known. A detailed algorithm for the perfectly expanded sonic jet solution using ideal gases properties is given in Appendix A, Fig. A.6.

2. Decreasing the area section of the aperture such that $A_4 < A_4^*$ keeps the flow choked at state (4), i.e., $M_4 = 1$, but increases the pressure P_4 such that $P_4 > P_5$. The gas is exiting the tube through the aperture as a choked, underexpanded jet. The entire flow is thus determined by iterating on the shock speed, to satisfy the sole condition $M_4 = 1$. It is done by calculating the state (3) for a given shock speed, then using the area - flow Mach number relation between state (3) and state (4) to calculate M_4, as A_4/A_0 and M_3 are known. A detailed algorithm for the choked, underexpanded sonic jet solution using ideal gases properties is given in Appendix A, Fig. A.7.
3. Increasing the section of the aperture such that $A_4 > A_4^*$ keeps the pressure at state (4) being $P_4 = P_5$, but the flow is now subsonic, i.e., $M_4 < 1$. The gas is exiting the tube through the aperture as a subsonic jet. The entire flow is thus determined by iterating on the shock speed, to satisfy the sole condition $P_4 = P_5$. It is done by calculating the state (3) for a given shock speed, then using the area - flow Mach number relation and the isentropic relations between state (3) and state (4) to calculate M_4 and P_4, as A_4/A_0, M_3 and P_3 are known. A detailed algorithm for the perfectly expanded subsonic jet solution using ideal gases properties is given in Appendix A, Fig. A.8.

3. Results

Results for the shock speed, shock overpressure and flame speed for a stoichiometric ethane - air mixture initially at 1 bar and 300 K are presented in Fig. 3, for both the perfect gas approximation (dashed lines) and using ideal gases thermochemical properties (solid lines). The various quantities are plotted in terms of the ratio of open area to tube area A_4/A_0 denoted as the *venting ratio*.

From a small to large venting ratio, the trends are as follow. The results for $A_4/A_0 = 0$ correspond to a tube with a closed rear end, and recover those of Chue et al. [9] for a closed end tube. The deflagration apparent speed, i.e. its speed in the laboratory frame of reference, is approximately 1000 m/s and drives the strongest shock with an overpressure of appoximately 9.2 bar calculated in the perfect gas approximation and 11.9 bar using ideal gases thermochemical properties.

As the venting ratio is increased, the shock strength decreases monotonously, as can be seen on the shock speed and overpressure plots. This is due to the fact that as the burned gases expand, they either drive a flow ahead of the flame, or in the presence of a rear venting, through the vented section to the atmosphere. A consequence is that the flow velocity of fresh gases just ahead of the flame decreases when the venting ratio increases. The shock is thus weaker for large venting ratios. This statement contributes to the fact that the apparent speed of the CJ deflagration decreases monotonously when the venting ratio increases, first because its advected component due to the flow of fresh gases ahead of it decreases, secondly because its burning velocity decreases as the shock strength decreases, as shown earlier using Eq. (8).

The particular venting ratio of approximately 0.785 corresponds, for this mixture at these initial conditions, to the perfectly expanded sonic jet solution. Below this value, the solution corresponds to the choked, underexpanded jet. Above, the solution corresponds to the perfectly expanded subsonic jet. In this latter range of venting ratio, the value $A_4/A_0 = 1$ corresponds to a tube open

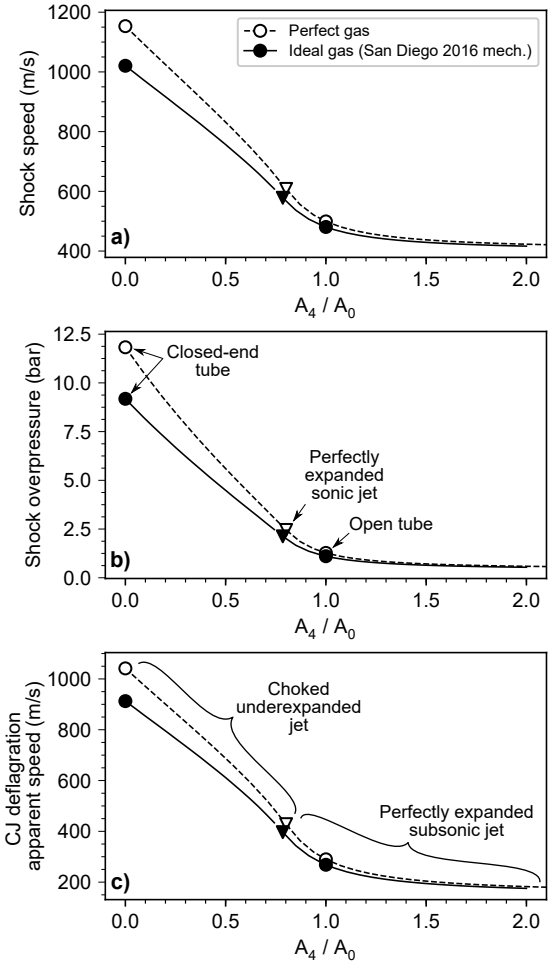

Figure 3: Shock speed, shock overpressure and CJ deflagration speed in a fixed frame of reference as a function of the venting ratio A_4/A_0, for stoichiometric ethane - air mixture at initial pressure and temperature 1 bar, 300 K. Dashed lines are results for the perfect gas approximation, solid lines are results for the ideal gas.

to the atmosphere with no changes of tube section. For venting ratios larger than 1, i.e. for tubes with exit sections larger than the tube section, the efficient venting of the products to the rear leads to CJ deflagrations propagating with an apparent speed ranging between approximately 200 and 300 m/s, and driving weak shocks with negligible overpressures.

Results for the shock speed and flame speed for methane - air mixtures initially at 1 bar and 300 K with equivalence ratio ϕ ranging between 0.2 and 10 are presented in Fig. 4, calculated using ideal gases thermochemical properties. The various quantities are plotted in terms of the venting ratio, and show the same trends as in Fig. 3.

An implication of the present results pertains to the speed of turbulent deflagrations that can be attained in vented large scale experiments, such as those compiled in references [14, 15, 16, 7, 8]. In such tests, deflagrations cannot be supported by a closed confinement, and their final apparent speed prior to transition to detonation was found to be lower than the speed of sound in the burned gases, the cause being that the burned gases are vented to the atmosphere and their motion is solely impeded by the congestion itself. As a reference, the apparent speed of CJ deflagrations as well as the shock overpressure predicted by the current model are plotted on Fig. 5, for a couple of mixtures found in the aforementioned references. A comparison can be made between these results and the velocity reached by the flame just prior transition to detonation, measured in the associated large scale experiments. Those are listed in Table 1.

These results are interesting in that, according to our model, the CJ deflagration apparent speeds one would observe in such configuration are comparable to the experimental speed of the flame observed prior transition to detonation. This is especially true for experiments involving hydrocarbon mixtures as those of Pekalski, Davis and Harris, suggesting that they could still be considered as CJ deflagrations. Other mixtures however, like the hydrogen ones from Sherman, and the acetylene ones from Moen show that transition to detonation occurs when the flame reaches a speed significantly smaller than the calculated CJ deflagration one. This difference may be anticipated by the high sensitivity

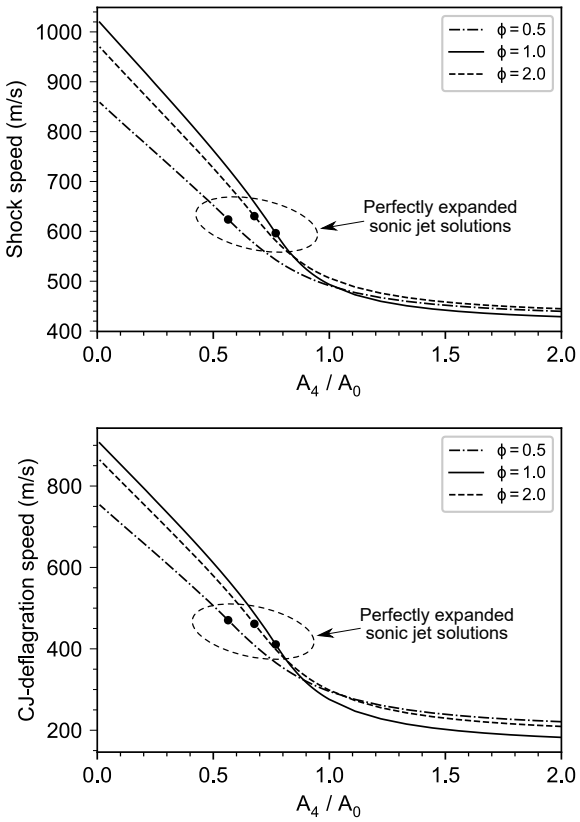

Figure 4: Shock-Mach number and CJ deflagration speed in a fixed frame of reference as a function of the venting ratio A_4/A_0 for methane - air mixtures with equivalence ratio ϕ ranging between 0.2 and 10, at initial pressure and temperature 1 bar, 300 K.

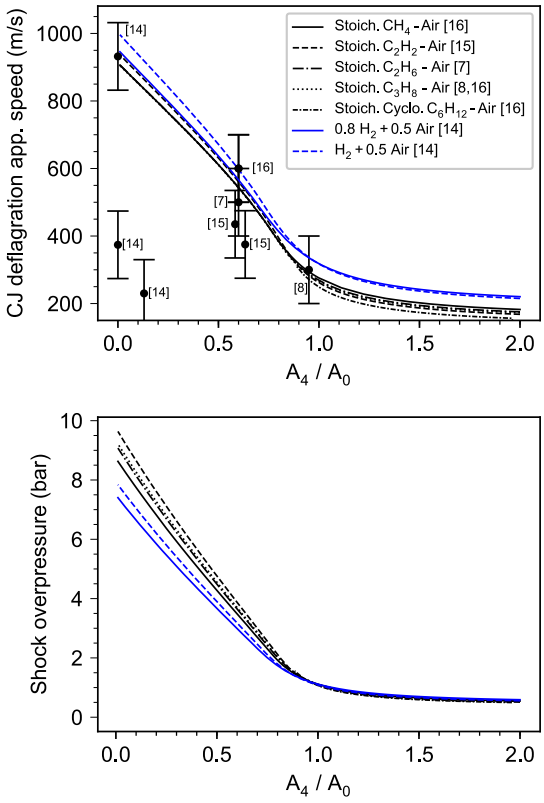

Figure 5: Apparent CJ deflagration speeds (measured in a fixed frame of reference) and shock overpressures, as a function of the venting ratio A_4/A_0, for common fuel-air mixtures found in the literature. Initial pressure and temperature are 1 bar, 300 K.

Table 1: Comparison of deflagration velocities just prior transition to detonation, with the CJ deflagration speeds obtained by the present model. Speeds referred here are the ones measured in the fixed frame of reference (apparent speeds).

Reference	Mixture	A_4/A_0	DDT speed (m/s)	CJ deflag. speed (m/s)
Moen, 1986 [15] Exp. 13	2 $C_2H_2 + 5$ Air	0.583	435	573
Moen, 1986 [15] Exp. 19	2 $C_2H_2 + 5$ Air	0.633	375	536
Harris, 1989 [16]	2 $C_6H_{12} + 9$ Air	0.6	500 - 700	567
Harris, 1989 [16]	$C_3H_8 + 5$ Air	0.6	600	543
Harris, 1989 [16]	$CH_4 + 2$ Air	0.6	-	544
Sherman, 1986 [14] Exp. F-12	0.78 $H_2 + 0.5$ Air	0	374	945
Sherman, 1986 [14] Exp. F-14	1.02 $H_2 + 0.5$ Air	0	932	1007
Sherman, 1986 [14] Exp. F-19	0.78 $H_2 + 0.5$ Air	0.13	230	865
Pekalski, 2015 [7]	$C_2H_6 + 3.5$ Air	0.6	500	543
Davis, 2019 [8]	$C_3H_8 + 5$ Air	0.95	300	284

of these mixtures to auto-ignition. In such cases, transition to detonation may be facilitated by the formation of hot spots where shocks reflect and interact, to cause self ignition of the gases, especially in the presence of obstructions. For less sensitive mixtures however, further flame acceleration is required to generate shocks strong enough to bring the gases to the conditions of ignition. Such conditions are expected to form rapidly when deflagrations reach conditions close to the CJ ones, as the release of chemical energy occurs in phase with the flow acoustics [17, 18].

A measure of this sensitivity can be inferred by a comparison of the characteristic time scales associated to the flame acceleration, with the one associated to the relevant conditions of auto-ignition. The latter is taken as the ignition time τ_i in the hot, unburned gases behind shock waves reflected over the obstacles. Using the proposed model, their state is calculated from constant volume ignition calculations behind a reflected shock, taking for incident shock the one

involved in the shock - CJ deflagration complex (see Fig. 1), which strength depends directly on the propagation medium geometry. On the other hand, a time scale characterizing the accelerating flame can be given by the rate of change of its burning velocity, assumed to be proportional to the rate of change of its front surface area. The latter is indeed expected to change as the flame deforms, while it propagates in the congested medium of known geometry. Hence, using the conservation of mass expressed as the production rate of burned gases:

$$\frac{d}{dt}(m_b) = \frac{d}{dt}(\rho_b A_f L_f) = \rho_u A_f S_f \tag{16}$$

where m_b is the mass of burned gases, ρ_b and ρ_u are respectively the burned and unburned gases densities, A_f the flame surface, S_f a relevant flame burning velocity and L_f a characteristic length scale of the propagation medium, typically its height, the growth rate of the flame burning velocity τ_f is given by the relation:

$$\tau_f^{-1} = \frac{1}{A_f}\frac{dA_f}{dt} = \frac{\rho_u}{\rho_b}\frac{S_f}{L_f} \tag{17}$$

Hence, for small values of the ratio τ_i/τ_f, ignition times are very short compared to the characteristic time of flame acceleration, such that the gases can easily ignite without requiring high flame acceleration, thus permitting transition to detonation at flame speeds below the CJ values. This is typically the case for hydrogen mixtures. For large values of the ratio τ_i/τ_f, ignition times are long compared to the increase rate of the flame speed, such that transition to detonation mostly relies on the formation of CJ deflagrations, conditions of propagation at which rapid flame acceleration and shocks formation occur, as commonly seen in hydrocarbon mixtures [4, 5]. Values of the ratio τ_i/τ_f are listed in Table 2, in which L_f was taken as the height of the propagation medium specific to each experiment, and S_f as either the laminar burning velocity, or the CJ deflagration burning velocity, both calculated in the state downstream of the shock of strength predicted by the proposed model.

High values of the ratio τ_i/τ_f correlate well with most experiments of Table 1, in which transition to detonation occurs when the flame reaches the apparent speed of CJ deflagrations predicted by our model. Exception is made on the

Table 2: Values of the ratio τ_i/τ_f for the selected set of experiments in Table 1. Burning velocities S_f were taken as the laminar or CJ ones, both taken in the shocked state predicted by the proposed model.

Reference	Mixture	A_4/A_0	τ_i/τ_f (S_f : laminar)	τ_i/τ_f (S_f : CJ)
Moen, 1986 [15] Exp. 13	2 $C_2H_2 + 5$ Air	0.583	250	2.0×10^4
Moen, 1986 [15] Exp. 19	2 $C_2H_2 + 5$ Air	0.633	1220	9.9×10^4
Harris, 1989 [16]	2 $C_6H_{12} + 9$ Air	0.6	229	27933
Harris, 1989 [16]	$C_3H_8 + 5$ Air	0.6	25	6702
Harris, 1989 [16]	$CH_4 + 2$ Air	0.6	$\gg 10$ ($\tau_i \gg 10$ s)	$\gg 10^4$ ($\tau_i \gg 10$ s)
Sherman, 1986 [14] Exp. F-12	0.78 $H_2 + 0.5$ Air	0	$5.1 \times 10{-}2$	4.6
Sherman, 1986 [14] Exp. F-14	1.02 $H_2 + 0.5$ Air	0	2.8×10^{-2}	1.7
Sherman, 1986 [14] Exp. F-19	0.78 $H_2 + 0.5$ Air	0.13	4.1×10^{-1}	36
Pekalski, 2015 [7]	$C_2H_6 + 3.5$ Air	0.6	25	6702
Davis, 2019 [8]	$C_3H_8 + 5$ Air	0.95	$\gg 10^2$ ($\tau_i \gg 10$ s)	$\gg 10^5$ ($\tau_i \gg 10$ s)

acetylene experiments of Moen, in which DDT occurs at speeds smaller than the CJ ones. This inconsistency is yet to be resolved, and may be due to the intrinsic nature of the fuel. Another cause may be the relative difficulty to set up the initial conditions in these large scale experiments, as well as collecting accurate and time resolved data. Hence, future work should be devoted to testing the predictions of the present model to turbulent flames propagating in vented mediums, with rear and side relief at the laboratory scale.

Finally, some limitations expected from this model can be commented. They are related to the assumptions done on the uniformity of state (2), the isentropic flow occurring between states (3) and (4), and the fact that the jump conditions across the flame is directly determined by the thermodynamics of flames propagating with burning velocities equal to the CJ deflagration ones, with no mention on how such velocities are reached. In practice, flames that reach the CJ deflagration regime are turbulent, and propagate in tubes with series of obstructions or rough walls. This would imply supplementary considerations on the shock propagation, that would be different than in the case of propagation in unobstructed channels with smooth walls, as well as including non-uniformities in state (2) and non-isentropic flow between states (3) and (4).

4. Conclusion

The present paper generalized the analysis of Chue et al. [9] for CJ deflagrations propagating in tubes, by allowing the tube end to assume different venting ratios. It was found that while the flame speed was given by the sound speed in the burned products for a closed end tube ($\sim$ 1000 m/s), this speed is a strong function of the venting ratio. For an open ended tube, the absolute flame speed drops to approximately 300 m/s and generates negligible overpressures. At intermediate venting ratios, a continuous range of flame speeds can be expected. The results obtained indicate that DDT criteria formulated in terms of a critical flame speed in vented explosions [7] are likely a very strong function of the amount of venting allowed by the congested geometry or other pressure

relief devices.

This model was applied to a selected set of large scale explosions experiments. The CJ deflagration apparent speed calculated was close to the terminal flame speeds prior DDT observed experimentally, suggesting that these flames could be associated to CJ deflagrations, especially for hydrocarbon - air mixtures. Other, more sensitive mixtures like the hydrogen - air ones, were found to allow transition to detonation at even smaller apparent flame speeds. This statement was justified by the fact that such mixtures have short ignition times when compared to the near CJ deflagration characteristic time for flame acceleration, hence permitting hot spots to rapidly explode and form detonations. Otherwise, in the case of less sensitive mixtures, rapid flame acceleration occurs when it reaches the CJ deflagration conditions, a propagation regime prone to the rapid formation and strengthening of shocks, thus playing in favor of the initiation of detonations.

Further experimental work shall however be performed to overcome the difficult comparisons with the model predictions, as seen with the acetylene - air experiments. Indeed, measurements on this kind of large scale set-up is difficult, as well as the control of the initial conditions, in a way that further understanding can be gained by performing experiments on turbulent flame propagating in vented mediums with rear and side relief, at the laboratory scale.

Acknowledgments

We acknowledge financial support provided by the Natural Sciences and Engineering Research Council of Canada (NSERC) through the Discovery Grant "Predictability of detonation wave dynamics in gases: experiment and model development" (grant number RGPIN-2017-04322).

References

[1] J. Lee, R. Knystautas, C. Chan, Turbulent flame propagation in obstacle-filled tubes, Symp. (Int.) Combust. 20 (1985) 1663–1672.

[2] S. Dorofeev, V. Sidorov, M. Kuznetsov, I. Matsukov, V. Alekseev, Effect of scale on the onset of detonations, Shock Waves 10 (2000) 137–149.

[3] A. Y. Poludnenko, Pulsating instability and self-acceleration of fast turbulent flames, Phys. Fluids 27 (2015) 014106.

[4] M. Saif, W. Wang, A. Pekalski, M. Levin, M. I. Radulescu, Chapman–Jouguet deflagrations and their transition to detonation, Proc. Combust. Inst 36 (2017) 2771–2779.

[5] W. Rakotoarison, B. Maxwell, A. Pekalski, M. I. Radulescu, Mechanism of flame acceleration and detonation transition from the interaction of a supersonic turbulent flame with an obstruction: Experiments in low pressure propane–oxygen mixtures, Proc. Combust. Inst 37 (2019) 3713–3721.

[6] W. Rakotoarison, A. Pekalski, M. I. Radulescu, Detonation transition criteria from the interaction of supersonic shock-flame complexes with different shaped obstacles, J. Loss Prevent. Proc. 64 (2020) 103963.

[7] A. Pekalski, J. Puttock, S. Chynoweth, Deflagration to detonation transition in a vapour cloud explosion in open but congested space: Large scale test, J. Loss Prevent. Proc. 36 (2015) 365–370.

[8] S. Davis, J. Pagliaro, D. Botwinick, T. DeBold, K. v. Wingerden, D. Allason, D. M. Johnson, Do not believe the hype: Using case studies and experimental evidence to show why the HSE is wrong about excluding deflagration-to-detonation transitions, Process Saf. Prog. 38 (2019).

[9] R. S. Chue, J. F. Clarke, J. Lee, Chapman-Jouguet Deflagrations, P. Roy. Soc. A-Math. Phy. 441 (1993) 607–623.

[10] M. Radulescu, W. Wang, M. Saif, L. Maley, M. Levin, A. Pekalski, On Chapman-Jouguet deflagrations, 25th International Colloquium on the Dynamics of Explosions and Reacting Systems (2015), paper 266.

[11] W. Fickett, W. C. Davis, Detonation, University of California Press, 1979.

[12] D. G. Goodwin, H. K. Moffat, R. L. Speth, Cantera: An Object-oriented Software Toolkit for Chemical Kinetics, Thermodynamics, and Transport Processes (Aug. 2018).

[13] S. Browne, J. Ziegler, J. Shepherd, Numerical Solution Methods for Shock and Detonation Jump Conditions (Mar. 2015).

[14] M. Sherman, S. Tieszen, W. Benedick, J. Fisk, M. Carcassi, The Effect of Transverse Venting on Flame Acceleration and Transition to Detonation in a Large Channel, Prog. Astronaut. Aero. (1986) 66–89.

[15] I. O. Moen, A. Sulmistras, B. H. Hjertager, J. R. Bakke, Turbulent flame propagation and transition to detonation in large fuel-air clouds, Symp. (Int.) Combust. 21 (1986) 1617–1627.

[16] R. Harris, M. Wickens, Understanding vapour cloud explosions - an experimental study, The Institution of Gas Engineers (1989), Communication 1408.

[17] A. Y. Poludnenko, T. A. Gardiner, E. S. Oran, Spontaneous Transition of Turbulent Flames to Detonations in Unconfined Media, Phys. Rev. Lett. 107 (2011) 054501.

[18] A. Y. Poludnenko, J. Chambers, K. Ahmed, V. N. Gamezo, B. D. Taylor, A unified mechanism for unconfined deflagration-to-detonation transition in terrestrial chemical systems and type Ia supernovae, Science 366 (2019).

Appendix A. Detailed algorithms

This section compiles detailed algorithms used for the calculations the perfectly expanded jet solution denoted *PEJ* (Fig. A.6), the choked, underexpanded jet solution (Fig. A.7) and the subsonic jet solution (Fig. A.8), using realistic thermochemical properties of mixtures (ideal gases).

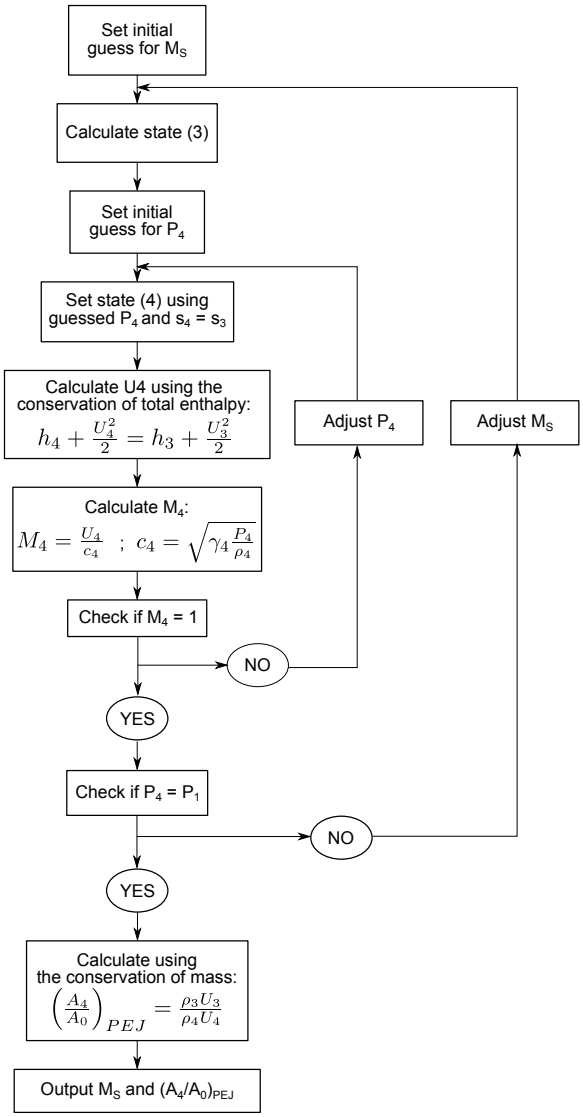

Figure A.6: Algorithm for the calculation of the perfectly expanded jet solution, using ideal gases properties.

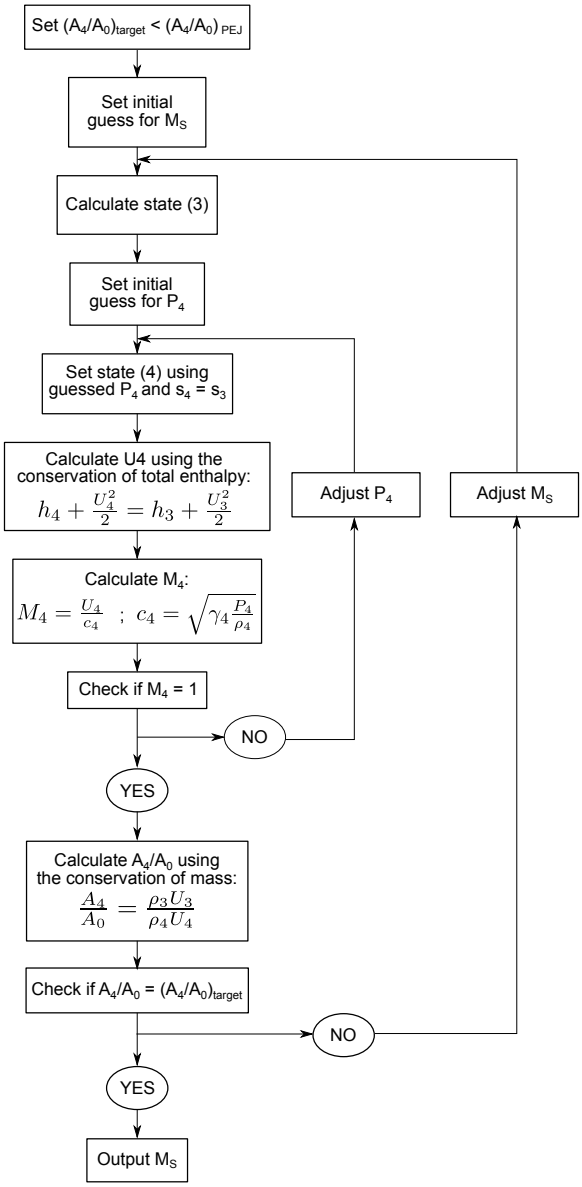

Figure A.7: Algorithm for the calculation of the choked, underexpanded sonic jet solution, using ideal gases properties.

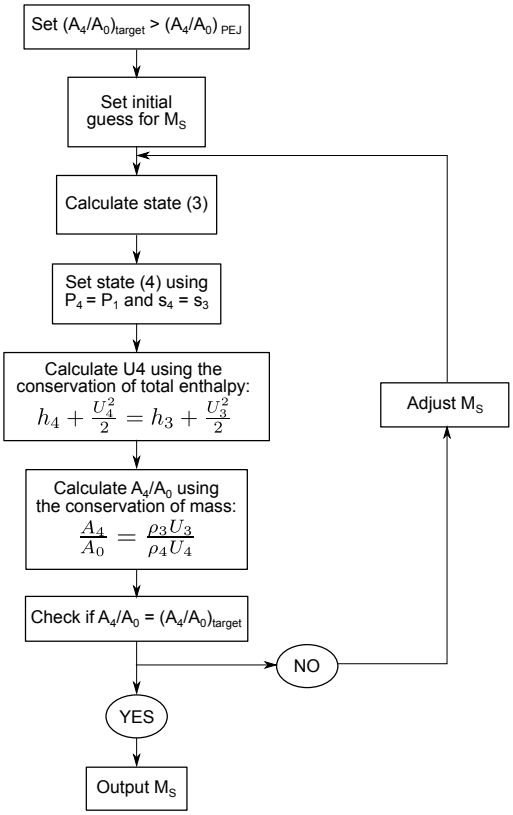

Figure A.8: Algorithm for the calculation of the subsonic jet solution, using ideal gases properties.

Chapter 4

A dynamical system approach for solving the steady structure of high speed deflagrations

High-speed deflagrations have burning velocities much higher than laminar ones, and are subject to significant compressible effects. In the present study, we investigate the structure of such high speed deflagrations in the thickened flame limit for a one-step Arrhenius rate law, whereby the transport coefficients are increased to give rise to buring velocities of finite Mach number. We study their steady structure and compare with the laminar low-Mach classical structure. The singular nature of both the fresh and burned gases conditions in the compressible regime, i.e. for large values of the flame propagation Mach number, which are both saddle points, precludes the application of simple shooting methods to obtain their structure. The steps leading to the flame structure borrow techniques used to treat mathematical features commonly found in the study of dynamical systems (phase portrait of the flame structure equations system, eigenvalue decomposition of its linearized version), that can also be used to further comment on the nature of high-speed flames. The method proposed permits to determine the structure of deflagrations propagating up to speeds of aproximately 0.95 of the CJ-deflagration burning velocity, for a wide range of gas parameters commonly found in the field of numerical simulation of accelerating flames and their transitions to detonations. We comment on how the increasing role of compressibility modifies the structure of the laminar flame.

This study was published in 2022 in the Proceedings of the Combustion Institute [46].The author conducted the writing of the method described, analysis and wrote the paper. The conceptual planning was performed with the Ph.D. supervisor Prof. M. I. Radulescu.

Available online at www.sciencedirect.com

ScienceDirect

Proceedings of the Combustion Institute 000 (2022) 1–11

Proceedings of the Combustion Institute

www.elsevier.com/locate/proci

A dynamical system approach for solving the steady structure of high speed deflagrations

Willstrong Rakotoarison*, Matei I. Radulescu

Department of Mechanical Engineering, University of Ottawa, Ottawa, Ontario, Canada

Received 5 January 2022; accepted 14 November 2022
Available online xxx

Abstract

High-speed deflagrations have burning velocities much higher than laminar ones, and compressible effects become important. In the present paper, we study the structure of such high speed deflagrations in the thickened flame limit for a one-step Arrhenius rate law, whereby the transport coefficients are increased to give rise to buring velocities of finite Mach number. We study their steady structure and compare with the laminar low-Mach classical structure. The singular nature of both the fresh and burned gases conditions in the compressible regime, i.e., for large values of flame propagation Mach number, which are both saddle points, precludes the application of simple shooting methods to obtain their structure. The steps leading to the flame structure borrow techniques used to treat mathematical features commonly found in the study of dynamical systems (phase portrait of the flame structure equations system, eigenvalue decomposition of its linearized version), that can also be used to further comment on the nature of high-speed flames. The method proposed permits to determine the structure of deflagrations propagating up to speeds of aproximately 0.95 of the CJ-deflagration burning velocity, for a wide range of gas parameters commonly found in the field of numerical simulation of accelerating flames and their transitions to detonations. We comment on how the increasing role of compressibility modifies the structure of the laminar flame.

Keywords: Flame structure; High-speed flames; Chapman–Jouguet deflagrations; Deflagration to detonation transition

1. Introduction

The properties of high speed deflagrations and their eventual transition to detonations are of relevance in the study of events like large scale explosions, and ignition in detonation based propulsion and power generation devices. Such high speed deflagrations appear at the late stages of flame acceleration and prior to the onset of detonations. They are in most cases turbulent and coupled with the gasdynamics of the flow. This makes them difficult to describe from experimental and numerical data. Typically, such turbulent deflagrations have turbulent burning velocities much larger than the laminar values, approaching the Chapman–Jouguet deflagration speed. Indeed, the Chapman–Jouguet burning velocity, associated with the so-called "choking regime" of propagation [1], has been used succesfully as a criterion for transition to detonation [2–4].

* Corresponding author.
E-mail address: [redacted] (W. Rakotoarison).

https://doi.org/10.1016/j.proci.2022.11.005

At these high burning velocities, compressible effects become important. While the dynamics of such high speed flames require detailed compressible simulations with accurate representation of the fluid-chemistry interactions [3], useful insights can be obtained from thickened flame models, where the burning velocity can be artificially augmented through modeling of the transport coefficients based on the turbulent intensity and adjustement of the reaction rate parameters.

In the present study, we adopt such a thickened-flame approach to study the structure of high-speed deflagrations, and how the compressible effects modify the classical one-dimensional structure of laminar flames. This is to serve as a first step for stability studies, both linear [5,6] and non-linear [7], which are currently under study in our laboratory [8]. To do so, we developped a simple numerical shooting method to determine the structure of high speed deflagrations. It is in that sense a strategy different from the commonly adopted finite differences or collocation methods used to determine the structure of low-speed deflagration [9] and viscous detonations [10], or those relying on non-steady numerical calculations, introducing start-up acoustic disturbances [8].

While for low-Mach flames, a shooting procedure is straightforward [11] and consists in integrating numerically the steady flame equations, starting from the burned gases for different values of the burning rate until the cold gas ignition conditions are met, the situation proved to be much more difficult for flames with finite Mach numbers. This can be anticipated by the nature of the fresh and burned gas points in phase space, which are known to both be saddle points [12]. This difficulty precludes shooting methods to be easily implemented unless special care is taken at the boundaries.

In the present work, we address the structure of compressible deflagrations by exploiting the singular structure of both so-called fixed points in the fresh and burned gases and investigating their eigenvalues and eigenvectors structure. We focus on the single step Arrhenius model flame. The method detailed in the present paper applies techniques commonly used to process singular points in dynamical systems, in order to construct steady flame profiles that are continuous from far in the fresh gases up to far in the burned gases. For clarity, the structure of the singular points under the low-Mach approximation will be treated first in a manner similar to the work of Clavin, Searby and Powers [13,14], from which extension to the case of arbitrary-Mach deflagrations will be done.

2. The flame steady state equations

One-dimensional deflagrations will be modeled using the reactive Navier–Stokes equations, with single-step, irreversible, first-order chemical reaction rate, expressed in the frame attached to the traveling wave:

$$\begin{aligned}
&\frac{\partial \rho}{\partial t}+\frac{\partial}{\partial x}(\rho u)=0\\
&\frac{\partial}{\partial t}(\rho u)+\frac{\partial}{\partial x}(\rho u^2+p)=\mathrm{Pr}\frac{4}{3}\frac{\partial^2 u}{\partial x^2}\\
&\frac{\partial E}{\partial t}+\frac{\partial}{\partial x}(Eu+pu)=\frac{\gamma}{\gamma-1}\frac{\partial^2 T}{\partial x^2}\\
&\qquad+\mathrm{Pr}\frac{4}{3}\frac{\partial}{\partial x}\left(u\frac{\partial u}{\partial x}\right)+Q\omega\\
&\frac{\partial}{\partial t}(\rho Y)+\frac{\partial}{\partial x}(\rho u Y)=\frac{1}{\mathrm{Le}}\frac{\partial^2 Y}{\partial x^2}\\
&\qquad-\Lambda\rho Y\exp\left(\frac{-\theta}{T}\right)\times H(T-T_i)
\end{aligned}\tag{1}$$

where $p=\rho T$, $E=\rho T/(\gamma-1)+\rho u^2/2$, H is the Heaviside function, and T_i an ignition temperature below which no chemical reactions occur. System (1) was non-dimensionalized using a scaling identical to Sharpe [11], so that:

$$\rho=\frac{\overline{\rho}}{\overline{\rho}_-}\quad u=\frac{\overline{u}}{\overline{u}_-}\quad x=\frac{\overline{u}_-}{\overline{\alpha}_-}\,\overline{x}$$
$$T=\frac{\overline{R_g}}{\overline{u}_-^2}\,\overline{T}\quad \theta=\frac{\overline{Ea}}{\overline{u}_-^2}\quad Q=\frac{\overline{Q}}{\overline{u}_-^2}$$

Variables ρ, u, T, Y, p, $M_f=u_-/c_-$ and $c=\sqrt{\gamma p/\rho}$ are respectively the gas density, flow velocity, temperature, mass fraction of fresh gases, pressure, flame burning Mach number and speed of sound. Variables denoted with an over bar relate to dimensional quantities, those with index $(-)$ to their value taken in the fresh gases located at $x\to-\infty$, and later introduced with index $(+)$ to their value in the burned state located at $x\to+\infty$.

The relevant dimensional gas properties are $\overline{\nu}_-$, $\overline{\alpha}_-$, $\overline{D}_-$, $\overline{R_g}$, $\overline{Q}$, $\overline{Ea}$ and $\overline{k}$, respectively the gas kinematic viscosity, thermal and molecular diffusivity coefficients, the specific perfect gas constant, heat of reaction, activation energy and reaction rate pre-exponential factor. They are used to define the non-dimensional gas parameters that are the Prandtl number $\mathrm{Pr}=\overline{\nu}_-/\overline{\alpha}_-$, the Lewis number $\mathrm{Le}=\overline{\alpha}_-/\overline{D}_-$, the dimensionless heat of reaction Q, activation temperature θ and reaction rate pre-exponential factor Λ, as well as the other commonly used and later useful non-dimensional energies:

$$\widetilde{Q}=\overline{Q}/\left(\overline{R_g}\,\overline{T}_-\right)\quad\text{and}\quad\widetilde{Ea}=\overline{Ea}/\left(\overline{R_g}\,\overline{T}_-\right)$$

The steady deflagration equations can be obtained from (1) in a manner identical to the work of Gasser [15], after dropping the unsteady terms and integrating once along the space coordinate x:

Please cite this article as: W. Rakotoarison and M.I. Radulescu, A dynamical system approach for solving the steady structure of high speed deflagrations, Proceedings of the Combustion Institute, https://doi.org/10.1016/j.proci.2022.11.005

$$\begin{aligned}
\frac{du}{dx} &= \frac{3u_-}{4\mathrm{Pr}}\left[(u-u_0)+\left(\frac{T}{u}-\frac{T_0}{u_0}\right)\right]\\
\frac{dT}{dx} &= \frac{\gamma-1}{\gamma}u_- \times \left[\frac{\gamma}{\gamma-1}(T-T_0)\right.\\
&\quad -u\left(\frac{T}{u}-\frac{T_0}{u_0}\right)+Q(Z-Z_0)\\
&\quad \left.-\frac{1}{2}(u-u_0)^2\right]\\
\frac{dY}{dx} &= \mathrm{Le}\,u_-(Y-Z)\\
\frac{dZ}{dx} &= -\Lambda\frac{Y}{u}\exp\left(-\frac{\theta}{T}\right)\times H(T-T_i)\\
\text{with}\quad Z &= Y-\frac{\overline{D}_-}{\overline{u}_-}\frac{dY}{d\bar{x}}
\end{aligned} \tag{2}$$

where quantities with index (0) are to be evaluated at a known state of the flow. The set of Eq. (5) is completed with the boundary conditions at the fresh and burned states:

$$\begin{aligned}
x\to-\infty &: (u,T,Y,Z)=(u_-,T_-,Y_-,Z_-)\\
x\to+\infty &: (u,T,Y,Z)=(u_+,T_+,Y_+,Z_+)
\end{aligned} \tag{3}$$

Both fresh and burned states are related by the Rankine–Hugoniot jump relations for a deflagration propagating at a known burning Mach number M_f [16]. Hence, the complete knowledge of one entirely defines the other. Finally, the extra condition $T_- < T_i$ is applied here, to ensure chemical reactions are not taking place far in the fresh gases, thus avoiding the cold boundary difficulty [12].

Getting the structure of deflagrations propagating at arbitrary speeds is thus done by solving the boundary value problem, defined by the relations (5) and boundary conditions (3). In this study, the state in the fresh gases, the flame parameters γ, Le, Pr, Q, θ, and the deflagration burning Mach number M_f are prescribed. In that respect, its structure is entirely determined once the remaining parameter Λ, also referred as the *burning rate eigenvalue* [12], is found. The following sections are meant to develop an original shooting method to determine the value of Λ, singular for a given, arbitrary value of M_f, as well as the associated flame profiles.

3. The flame structure

3.1. Low-Mach case with Le = 1 and Pr = 3/4

The simpler set of equations derived in this section for the low-Mach flame case, with Le = 1 and Pr = 3/4, permits to illustrate with convenience the mathematical features relevant for the later treatment of deflagrations propagating at arbitrary burning velocities.

In the case Le = 1 and Pr = 3/4, the progress variable is linearly related to the scaled gas stagnation enthalpy τ by Williams [12]:

$$\tau = \frac{\gamma}{\gamma-1}\frac{T-T_-}{Q}+\frac{u^2-u_-^2}{2Q}=\frac{Y-Y_-}{Y_+-Y_-} \tag{4}$$

Moreover under the low-Mach flame approximation, variations of pressure across the flame, represented by the term $(T/u - T_0/u_0)$ in system (2) can be neglected. The same applies to the gas kinetic energy, represented by the terms in $(u^2/2)$ in Eqs. (2) and (4), when compared to its enthalpy $\gamma T/(\gamma-1)$. These statements permit to re-write the system of Eq. (2) where integration constants were taken at $x\to-\infty$, as a single, second order ODE solving for T, that can be split to form a system of two first order ODEs solving for T and $w = dT/dx$:

$$\begin{aligned}
\frac{dT}{dx} &= w\\
\frac{dw}{dx} &= w-\Lambda Q\frac{\gamma-1}{\gamma}\\
&\quad\times\left[1-\frac{\gamma}{Q(\gamma-1)}(T-T_-)\right]\\
&\quad\times\frac{T_-}{T}\exp\left(-\frac{\theta}{T}\right)\times H(T-T_i)
\end{aligned} \tag{5}$$

with boundary conditions taken in the fresh state at $x\to-\infty : (T,w)\to(T_-,0)$, and in the burned state at $x\to+\infty : (T,w)\to(T_+,0)$, both related by the deflagration jump relations [16].

Handling the calculations and results was found to be easier using the set of variables τ and $\eta = d\tau/dx$ in place of T and w, for which two ODEs can easily be derived from Eqs. (4) and (5), with boundary conditions at $x\to-\infty : (\tau,\eta)\to(0,0)$ and $x\to+\infty : (\tau,\eta)\to(1,0)$. The solutions of the resulting system can be plotted as orbits, in the two dimensional phase space $(T-w)$ or $(\tau-\eta)$, as represented in Fig. 1 as arrowed lines, plotted for γ, $\widetilde{Q}$ and $\widetilde{Ea}$ arbitrarily chosen to provide a typical, qualitative representation of the solutions behavior, and different values of Λ (Fig. 1(a)–(c)), which determination method is discussed later. This representation highlights the singular nature of the two fresh and burned states, at coordinates $(T_-,0)$ and $(T_+,0)$ in the $(T-w)$ space respectively, where derivatives are 0. More specifically, the fresh state is an *unstable node* around which the region of positive τ and η leads towards the region of the burned state, whereas the region of negative η rapidly leads to states where the temperature is below the fresh gases temperature, that is not a physical solution for a flame. On the other hand, the burned state is at a *saddle*, around which the solution is expected to diverge when approaching it from the fresh gases, unless it is approached following the singular integral curve providing a finite slope when $x\to+\infty$.

Please cite this article as: W. Rakotoarison and M.I. Radulescu, A dynamical system approach for solving the steady structure of high speed deflagrations, Proceedings of the Combustion Institute, https://doi.org/10.1016/j.proci.2022.11.005

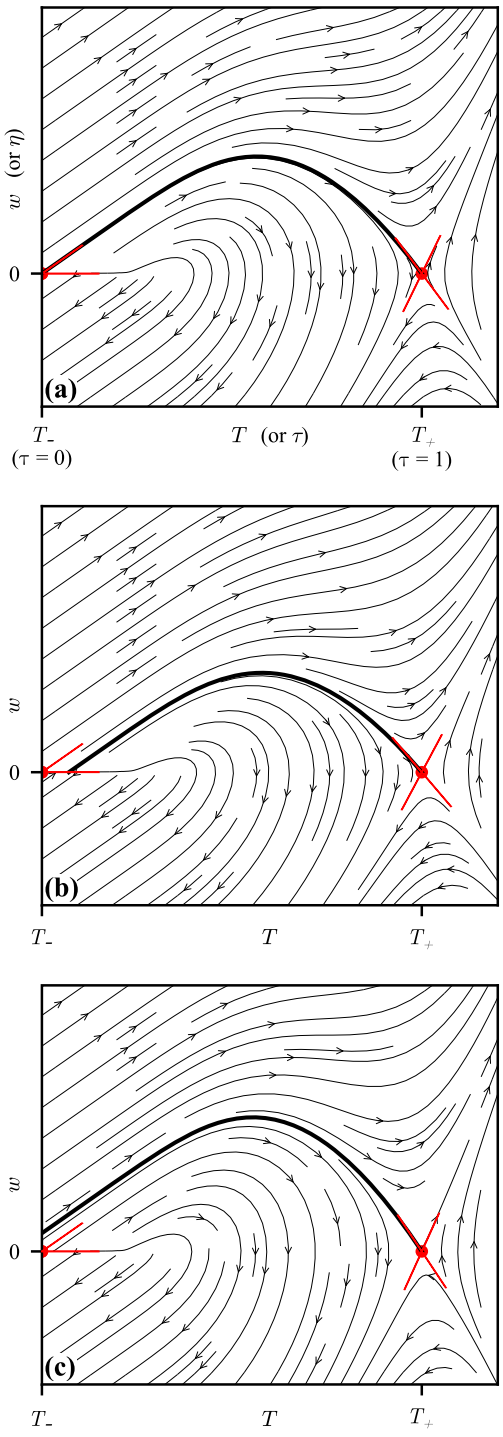

Fig. 1. Typical phase diagrams of equations system (5) given the parameters γ, $\widetilde{Q}$ and $\widetilde{Ea}$. The solid lines are the solutions integrated from the burned gases, for different values of Λ: (a) corresponds to the correct burning rate eigenvalue Λ that connects the fresh and burned state, and (b) and (c) underestimated and overestimated values of Λ, respectively.

The nature of the two equilibrium points is well documented in reference textbooks [12,17], in which the construction of approximate solutions near these singularities is described, generally integrated from the linearized version of Eq. (5), derived using first order Taylor series. The resulting system of $N = 2$ linear ODEs can be expressed in matrix form:

$$\frac{d}{dx'}\left[S'(x')\right] = [A]\left[S'(x')\right] + [B] \tag{6}$$

in which $x' = x - x_0$ is the deviation from the location x_0 where Taylor expansions are applied, $[S'(x')] = [T'(x'), w'(x')]^t$ the solution vector of the perturbed state near x_0, and for an arbitrary variable $\phi(x)$, one has $\phi'(x) = \phi(x) - \phi(x_0)$. The linear Eq. (6) are expressed around the fresh and burned state, where the N-components vector $[B]$ is naturally null in both cases owing to the zero gradient condition.

After elimination of high order terms, the $N \times N$ matrix $[A]$ is expressed near the fresh and burned states as:

$$[A]_- = \begin{bmatrix} 0 & 1 \\ 0 & 1 \end{bmatrix}$$

$$\text{and} \qquad [A]_+ = \begin{bmatrix} 0 & 1 \\ \Lambda \frac{T_-}{T_+} \exp\left(-\theta/T_+\right) & 1 \end{bmatrix} \tag{7}$$

Note that to write $[A]_-$, the condition $T_- < T_i$ was applied to ensure the reaction rate is equal to zero at the fresh state, a statement equivalent to having it to tend to zero when the temperature tends to T_- when x tends to $-\infty$ [12,18]. The solution $[S'(x')] = [T', w']^t$ to the system (6) thus takes the form of a series of N exponential functions:

$$\left[S'(x')\right] = \sum_{i=1}^{N} C_i [v_i] e^{\lambda_i x'} \tag{8}$$

where λ_i is the i^{th} eigenvalue of $[A]$, $[v_i]$ is the N-components eigenvector of $[A]$ associated to the eigenvalues λ_i (directions are plotted at the fresh and burned states in Fig. 1), and C_i is the integration constant associated to the i^{th} exponential term, to be determined at a known point in the physical domain x.

A few remarks can be drawn from the set of Eqs. (7) and (8). First, the exponential form of Eq. (8) can be used to determine, in the phase space $(\tau - \eta)$, the directions along which the solution is expected to converge or diverge near the singularities, based on the directions of $[v_i]$ and the sign of λ_i. The fact that the flame profiles converge towards the fresh state at $x \to -\infty$ and towards the burned state at $x \to +\infty$, suggests that the solution (8) should only include exponential terms with positive (resp. negative) eigenvalues, when willing to approximate the solution of system (5) near the fresh (resp. the burned) state. Later on, finding the

Please cite this article as: W. Rakotoarison and M.I. Radulescu, A dynamical system approach for solving the steady structure of high speed deflagrations, Proceedings of the Combustion Institute, https://doi.org/10.1016/j.proci.2022.11.005

eigenvector by which the orbit *escapes* the singularity will be useful to determine an initial perturbation of the equilibrium state where gradients are zero, from which numerical integration can be performed to construct the deflagration profiles. Secondly, the simple form of $[A]_-$ gives one eigenvalue to be 0 associated to eigenvector $[0, 1]^t$, and the other to be 1 associated to eigenvector $[1, 1]^t$. These eigenvalues formally states the nodal nature of the singularity at the fresh gases, from which evolution of the solution in the phase space is possible only along the direction given by eigenvector $[1, 1]^t$, associated to the non-zero eigenvalue. On the other hand, the more complex form of matrix $[A]_+$ was such that its eigenvalues and eigenvectors were conveniently determined numerically. The eigenvalues were found to consistently be of opposite sign, stating that the singularity at the burned state is a saddle.

The nature of both singularities is such that, accurate and stable solutions can be calculated by *backward* numerical integration of the system (5), i.e., from the saddle at the burned state at $x \to +\infty$, towards the node at the fresh state, stable when heading towards $x \to -\infty$. To ensure integration is not started from the zero-gradients point at the burned state, initial conditions for T and w must be taken slightly different from T_+ and w_+, and chosen along the eigenvector aiming towards the fresh state (see Fig. 1). With given values of γ, $\widetilde{Q}$ and $\widetilde{Ea}$, the low-Mach deflagration structure can thus be entirely calculated once the burning rate eigenvalue Λ is found.

The latter can be conveniently determined by means of a *shooting method*, in which backward numerical integration is performed multiple times for different values of Λ, until the calculated integral curve is found to tend towards the fresh state when $x \to -\infty$. Typically, narrowing down the correct burning rate eigenvalue Λ is done by bisection. This method is illustrated in the phase diagrams in Fig. 1(a)–(c), in which orbits and solutions integrated from the burned state were plotted for different values of Λ: the phase diagram (a) corresponding to the actual burning rate eigenvalue associated to given parameters γ, $\widetilde{Q}$ and $\widetilde{Ea}$, and phase diagrams (b) and (c) are underestimated and overestimated values, respectively.

Unfortunately, the use of an identical shooting method is precluded in the more general case of arbitrary-Mach deflagrations with $Le = 1$ and $Pr = 3/4$, as both equilibrium points are now saddles [12], inherently causing forward and backward numerical integration to fail at providing converging deflagration profiles. In that respect, the following section aims to propose a similar shooting method applied to deflagrations propagating at arbitrary velocities, in which the solution near the equilibrium points are treated specifically, so that converging and continuous profiles can be found.

3.2. Arbitrary M_f with $Le = 1$ and $Pr = 3/4$

In the more general case of arbitrary-Mach deflagrations, the kinetic energy and pressure gradients are not assumed negligible anymore. As a result, the system of Eq. (2) can only be reduced to a set of three ODEs solving for T, w and u:

$$\begin{aligned}
\frac{dT}{dx} &= w \\
\frac{dw}{dx} &= w - \Lambda Q \frac{\gamma-1}{\gamma}\frac{1}{u} \times \\
&\quad \left[1 - \frac{\gamma}{Q(\gamma-1)}(T - T_-) - \frac{1}{2Q}(u^2 - u_-^2)\right] \\
&\quad \times \exp\left(-\frac{\theta}{T}\right) \times H(T - T_i) \\
&\quad + \frac{\gamma-1}{\gamma} \times \left[(T - w) - (T_- + 1)\left(u - \frac{du}{dx}\right)\right. \\
&\quad \left. + \left(u^2 - 2u\frac{du}{dx}\right)\right] \\
\frac{du}{dx} &= u_-\left[(u - u_-) + \left(\frac{T}{u} - \frac{T_-}{u_-}\right)\right]
\end{aligned} \tag{9}$$

that can be linearized near the fresh and burned states to form a system of $N = 3$ ODEs, that takes a form identical to (6), with a solution of a form identical to Eq. (8).

This system has saddles at both equilibrium points, making forward and backward numerical integration unable to provide converging solutions at $x \to \pm\infty$, without special treatment of the solution at the boundaries. It was however found *a posteriori* that forward numerical integration from the fresh to the burned state is the most practical. The reason is that the fresh state has only one eigenvector providing a diverging solution when heading towards the burned state, hence one obvious direction in the phase space along which an initial perturbation of the solution shall be applied, from which numerical integration can be started. The latter will have the form $[S'] = \epsilon[v_0]_-$, where $[v_0]_-$ is the fresh state eigenvector associated to eigenvalue λ_0 of positive sign. In practice, this perturbation is scaled such that the perturbed temperature is equal to the ignition temperature T_i. On the other hand, the burned state has two eigenvenvectors providing a diverging solution when heading towards the fresh state, making it difficult to determine an initial perturbation from which numerical integration can be started, as one would need to seek for it in the plane formed by the two appropriate eigenvectors. This result was found to be true over the quasi-totality of burning rates, up to near CJ-deflagrations, over the whole range of gas parameters investigated, and was inferred by the sign of associated eigenvalues (see Fig. 6).

Please cite this article as: W. Rakotoarison and M.I. Radulescu, A dynamical system approach for solving the steady structure of high speed deflagrations, Proceedings of the Combustion Institute, https://doi.org/10.1016/j.proci.2022.11.005

From these statements, a three-steps procedure is proposed to construct the flame profiles, defined everywhere from $x \to -\infty$ up to $x \to +\infty$:

1. Integrating numerically the system (9) for multiple values of Λ from the fresh state, using bisection to narrow down the one allowing the integrated solution to get as close as possible to the burned state. Numerical integration should be done from an initial state perturbed by a small amount ϵ in the phase space's direction $[S']_- = \epsilon[v_0]_-$, as described earlier.
2. By bisecting on Λ, two close solutions, one overshooting and one undershooting the burned state temperature can be found. From those, one can assume the flame profiles to be accurate enough, as long as the norm defined in the three-dimensional phase space $(T - w - u)$ by:

$$\{[T_o(x) - T_u(x)]^2 + [w_o(x) - w_u(x)]^2 + [u_o(x) - u_u(x)]^2\}^{1/2}$$

where ϕ_o and ϕ_u are respectively the overshot and undershot solution of the arbitrary variable ϕ, is small enough. The point where this distance exceeds a defined small value, marks the *separation* of the overshot and undershot solutions in the physical space x, at the coordinate denoted x_{sep} where T, w and u are respectively equal to T_{sep}, w_{sep} and u_{sep}, as shown schematically in Fig. 2(a) for quantities T and w, and in Fig. 2(b), in a projection of the solution in the reference plane $(T - w)$ near the burned state.
3. For the profiles to be defined from $x \to -\infty$ to $x \to +\infty$, the numerical solution integrated from the fresh gases in step 1 is *cropped* at x_{sep}, then matched to the analytical solution (8) near the burned gases. Matching is done by determining the values of the constants C_{i+}. Those have to be 0 when associated to positive eigenvalues λ_{i+}, to ensure the solution is converging towards $x \to +\infty$. The remaining ones associated to negative eigenvalues are determined by matching the solution (8), to the numerical solution found in step 1 at coordinate x_{sep}. Assuming the latter is close enough to the burned state solution, i.e.:

$$x' = x_{sep} - x_+ \to 0 \quad \text{so that} \quad e^{\lambda_{i+}x'} \to 1 \quad \text{as} \quad \left[S(x_{sep})\right] - [S]_+ \to [0, 0, 0]^t \tag{10}$$

the remaining constants C_{i+} can be found using the simplified relation derived from (8):

$$\left[S'_{sep}\right] = \left[S(x_{sep})\right] - [S]_+ = \sum_{i=1}^{N=3} C_{i+}[v_i]_+ \tag{11}$$

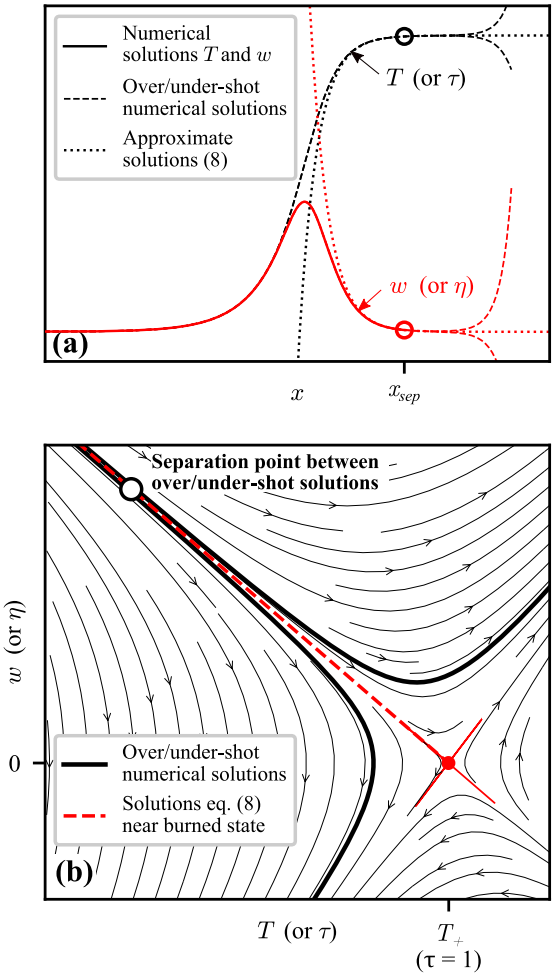

Fig. 2. Typical representation of the solution in (a) the physical space and (b) the phase space, projected in the reference plane $(T - w)$. Hollow markers show the separation point at x_{sep} between the temperature overshot and undershot solutions.

that constitutes a set of at most $N = 3$ algebraic equations with unknowns C_{i+} (defined at $x \to +\infty$), and less if it appears that some eigenvalues λ_{i+} are positive. In the latter case, the integration constants can be found from a subset of system (11), containing as many equations as the number of remaining integration constants.

Applying this procedure permitted to consistently solve the structures of flames propagating at various burning Mach numbers. Numerical integration was done using implicit, variable step, variable order backward differentiation formula for derivatives approximation [19], that provided consistent results with no special requirement on tolerances or maximum space step. The scaled flame profiles of progress variable, temperature, pressure, flow Mach number $M = u/c$, enthalpy $\widetilde{h} = \gamma/[Q(\gamma - 1)]\ T$, kinetic energy $\widetilde{k} = u^2/(2Q)$ and stagnation enthalpy $\widetilde{h}_0 = \widetilde{h} + \widetilde{k}$ are plotted in

Please cite this article as: W. Rakotoarison and M.I. Radulescu, A dynamical system approach for solving the steady structure of high speed deflagrations, Proceedings of the Combustion Institute, https://doi.org/10.1016/j.proci.2022.11.005

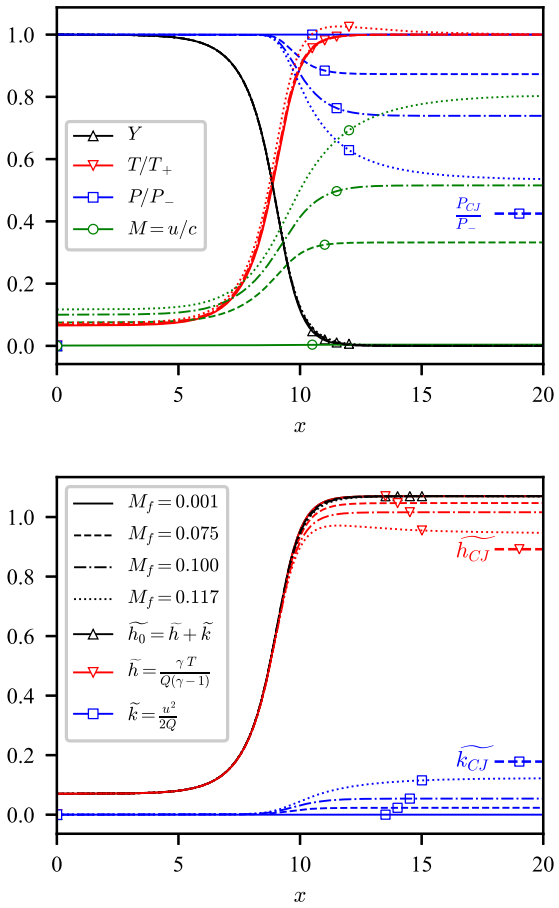

Fig. 3. Flame profiles for different flames propagating at Mach numbers 0.001, 0.075, 0.1 and 0.117. Gas properties are $\gamma = 1.4$, $\widetilde{Q} = 50$ and $\widetilde{Ea} = 50$.

Fig. 3, for $M_f = 0.001,\ 0.075,\ 0.1,\ 0.117$ and parameters γ, $\widetilde{Q}$ and $\widetilde{Ea}$, arbitrarily chosen to be 1.4, 50 and 50 respectively. These values were aimed to be of the order of what is commonly used in numerical studies of flame acceleration, deflagration to detonation transition (DDT) and detonations. It is to note that other sets of parameters give identical trends of the solution, so that the results plotted here are illustrating its typical behavior.

The lowest value of $M_f = 0.001$ was chosen to be one approximating the low-Mach flame case. The associated profiles of pressure and kinetic energy show negligible changes across the flame reaction zone, as expected for a low-Mach flame. The highest value of $M_f = 0.117$ corresponds closely to the CJ-deflagration burning Mach number $M_{f,CJ}$ here equal to 0.119, a function of the initial state and heat of reaction Q. The profiles calculated show features that differ from the low-Mach approximation, starting with the significant pressure drop that occurs across and beyond the reaction zone, and reaches about 50% of the initial pressure (about 40% for a CJ-deflagration). The variation of kinetic energy was also found non-negligible anymore, and increases up to about 11% of the stagnation enthalpy in the burned gases (about 17% for a CJ-deflagration), causing the gas enthalpy to drop accordingly. A feature worth noticing of high speed deflagrations is the fact that the enthalpy, hence the temperature, reaches a maximum before converging towards its value in the burned state. This is due to the expansion at high flow Mach number near the burned gases (about $M = 0.8$, and $M = 1$ for CJ deflagrations), that is still occurring after almost all the gas has reacted and heat has been released.

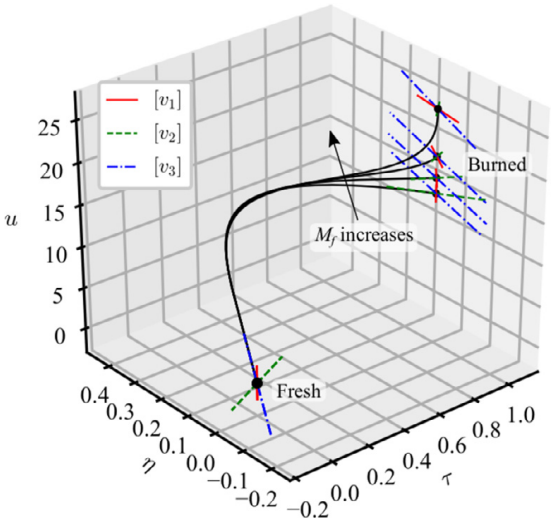

Fig. 4. Trajectories in the three-dimensional phase space $(\tau - \eta - u)$ of four flames propagating at a burning Mach number M_f equal to 0.001, 0.075, 0.1 and 0.117. Stylized lines at the fresh and burned states represent directions of the eigenvectors of matrix $[A]_\pm$. Gas properties are $\gamma = 1.4$, $\widetilde{Q} = 50$ and $\widetilde{Ea} = 50$.

The solutions to the flame structure can also be represented in the now three-dimensional phase space $(T - w - u)$, scaled as $(\tau - \eta - u)$, plotted in Fig. 4 and projected in the three reference planes $(\tau - \eta)$, $(\tau - u)$ and $(\eta - u)$, as shown in Fig. 5, for the same four flames propagating at M_f equal to 0.001, 0.075, 0.1 and 0.117. While the flame trajectories in the $(\tau - \eta)$ plane are similar to the low-Mach flame case, the contribution of the gas kinetic energy, hence its velocity, becomes obvious when the flames solutions are projected in the $(\tau - u)$ and $(\eta - u)$ planes. For low-Mach flames, the proportionality relation between the gas velocity and its stagnation enthalpy τ, i.e., its temperature in the low-Mach approximation, is recovered and shown as a straight line in the (τ, u) plane. At higher values of M_f, this linear relation still exists near the fresh state but degenerates close to the burned state, owing to the larger contribution of kinetic energy to the flow.

The directions given by eigenvectors $[v_i]_+$ in the phase space at the burned state, as well as their projections in the reference planes are also plotted

Please cite this article as: W. Rakotoarison and M.I. Radulescu, A dynamical system approach for solving the steady structure of high speed deflagrations, Proceedings of the Combustion Institute, https://doi.org/10.1016/j.proci.2022.11.005

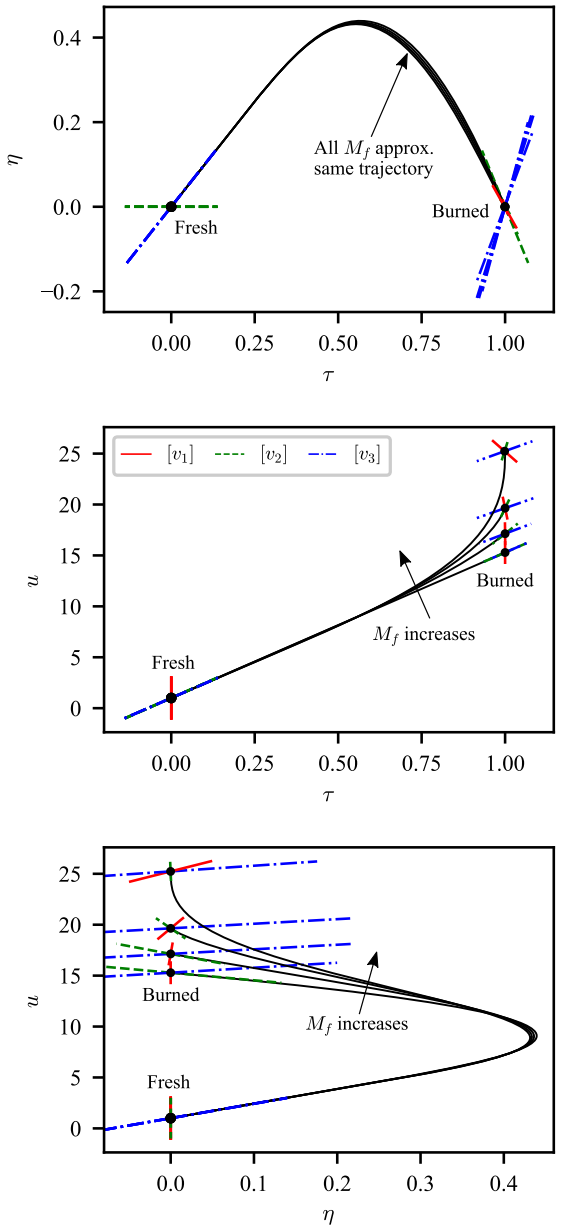

Fig. 5. Projections in the three reference planes of the phase space $(\tau - \eta)$, $(\tau - u)$ and $(\eta - u)$ of the flame trajectories shown in Fig. 4. Stylized lines at the fresh and burned states represent projected directions of the eigenvectors of matrix $[A]_{\pm}$. Gas properties are $\gamma = 1.4$, $\widetilde{Q} = 50$ and $\widetilde{Ea} = 50$.

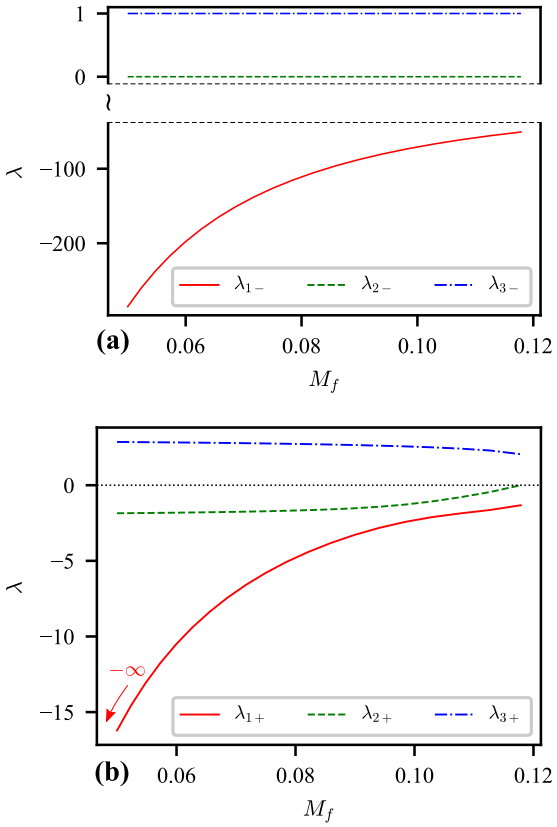

Fig. 6. Eigenvalues of matrices: (a) $[A]_-$ at the fresh state and (b) $[A]_+$ at the burned state, for different values of M_f. Gas properties are $\gamma = 1.4$, $\widetilde{Q} = 50$ and $\widetilde{Ea} = 50$.

in Figs. 4 and 5. The associated eigenvalues λ_{i+}, sorted by increasing algebraic value with increasing index i, are plotted in Fig. 6(b), for high values of M_f up to close to $M_{f,CJ}$. They are found to vary monotonously over the whole range of burning Mach numbers, and both λ_{1+} and λ_{2+} remain negative up to values close to $M_{f,CJ}$ (typically 0.98 $M_{f,CJ}$), where λ_{2+} becomes positive. A quick look at the phase space permits to identify $[v_2]_+$ to be the direction along which the flame trajectories reach the burned state from the fresh state. On the other hand, $[v_3]_+$ is associated to the only positive eigenvalue, along which the flame trajectories are expected to diverge. The fact that λ_{2+} and λ_{3+} are of opposite sign but their absolute values are of identical order of magnitude, suggests that near the burned state, the flame profiles in the physical space x are expected to converge from the region $x < x_{sep}$, at the same rate as they diverge towards regions $x > x_{sep}$.

Applying the same kind of argument when comparing the sign and absolute value of λ_{1+} to those of λ_{2+} and λ_{3+}, permits to tell that, over the wide range of low M_f, any orbit approaching the burned state by the direction $[v_1]_+$ from regions of $x < x_{sep}$, is expected to converge very quickly, before diverging in the direction given by $[v_3]_+$ when reaching regions of $x > x_{sep}$. In fact, for very low values of M_f, the exponential term associated to λ_{1+} in solution (8) can be assumed to be 0, such that one only needs to deal with the other two, like in the case of the low-Mach approximation.

Approaching the CJ-deflagration propagation regime is however more complicated, as all eigenvalues are now comparable in absolute values, causing the three-dimensional saddle at the burned state to be less stable, and making the approach from the fresh state difficult. Getting close enough to

Please cite this article as: W. Rakotoarison and M.I. Radulescu, A dynamical system approach for solving the steady structure of high speed deflagrations, Proceedings of the Combustion Institute, https://doi.org/10.1016/j.proci.2022.11.005

the burned state thus becomes impossible, in a way that matching at x_{sep} the numerical solution integrated from the fresh state, with solution (8) expressed at the burned state, fails at providing continuous and/or smooth flame profiles, because the condition $\left[S(x_{sep})\right] - [S]_+ \rightarrow [0, 0, 0]^t$ expressed in Eq. (10) is not satisfied anymore, making the determination of the integration constants C_{i+} inaccurate. Other than in these high velocity regimes, obtaining the flame structure up to burning Mach numbers typically of 95% $M_{f,CJ}$ was consistently successful.

Finally, a few comments can also be made on the solution behavior near the fresh state. As seen in Fig. 6(a), only λ_{3-} is positive, suggesting that profiles converging in the physical space towards $x \rightarrow -\infty$ should follow the direction given by $[v_3]_-$ in the phase space $(T - w - u)$, near the fresh state. Also, no evolution is expected in the phase direction given by $[v_2]_-$ as λ_{2-} is always 0. However, the fact that λ_{1-} is negative and has a large absolute value when compared to λ_{3-}, suggests that the solution is expected to diverge significantly faster along $[v_1]_-$ than it converges along $[v_3]_-$, when approaching the fresh state from the burned state. This result was another argument made for choosing to numerically integrate a solution from the fresh state to the burned state (as opposed to what is generally done when solving the structure of low-Mach flames), as it is significantly easier to get close to the burned state than to the fresh state, following the discussion above.

4. Concluding remarks

The present article proposed a convenient and consistent method to solve the structure of deflagrations propagating at arbitrary burning Mach numbers. Restrictions were made on the gas properties, namely Le = 1, Pr = 3/4 and a first order reaction rate, that permitted to describe deflagration structures using a system of three ODEs, and use its three-dimensional phase space to construct continuous and smooth flame profiles from far in the fresh gases, up to far in the burned gases. Lifting the approximations Le = 1 and Pr = 3/4 leads to process the four ODEs system (2), that can a priori be solved in a similar manner.

The range of parameters investigated here were chosen to match those commonly found in the field of numerical simulations of deflagration to detonation transition (DDT), namely $\widetilde{Q}$ and $\widetilde{Ea}$ in the range 10–60. A sample of values of Λ are shown in Table 1.

Table 1
Values of Λ as a function of $\widetilde{Ea}$ and M_f. γ and $\widetilde{Q}$ are respectively 1.4 and 50.

		M_f			
		0.001	0.075	0.1	0.117
$\widetilde{Ea}$	20	53.21	55.18	56.81	58.25
	30	228.6	240.4	250.2	258.9
	40	766.3	815.9	856.0	893.5
	50	2259	2433	2578	2707
	60	6153	6704	7162	7572

It is relevant to note that, prior to transition to detonation, the flame often propagates with a shock ahead of it at a velocity that is dependent on the flame acceleration history and confinement [20,21]. As a result, the fresh state ahead of the flame has a temperature higher than the unshocked gases, causing the non-dimensional energies $\widetilde{Q}$ and $\widetilde{Ea}$ to have lower values. This statement should however not be an obstacle in the future.

It is relevant to relate the problem of deflagration structure to those of viscous shocks and detonations, which formalism is similar if not identical. Both are often reduced to simple discontinuities, eventually accounting for purely reactive processes in the case of ZND (Zeldovich - von Neuman - Doring) detonations. In the commonly made assumption of Pr = 3/4, analytical solutions to the structure of viscous shocks can be found [22]. The general structure of their equilibrium points can also be discussed in the more general case of arbitrary Prandtl numbers [23,24], to show that the undisturbed and shocked states are respectively at a node and a saddle, suggesting that simple shooting methods can be used to calculate their structure numerically. On the other hand, the proof of existence of solution to viscous detonations was also demonstrated [15,25,26], and analysis of the associated equilibrium points can be done to show that the hot boundary of a strong detonation is a saddle, whereas its cold boundary is a node [12]. These elements suggest that finding the structure of viscous detonations can also be done using simple numerical shooting methods. This has to be opposed to the case of deflagrations, that have saddles at both equilibrium states, so that specific methods as the one proposed in this article is required to obtain end-to-end profiles. In that sense, the approach proposed here was found to be convenient as a tool for future work and analysis of their properties.

Other work in progress consists in using the continuous and smooth profiles obtained as starting points to investigate the behavior and fate of high speed deflagrations. It is already known that those are unstable, coupled to the flow compressible features, and self-accelerating when propagating close to the CJ-deflagration regime, until their transition to detonations [3,27,28]. Multiple approaches to discuss the stability of high speed flames are considered as future work, and consist in investigating the coupling of the flames with the flow acoustics in one-dimensional geometries, and the growth of small perturbations applied to an initially planar, multidimensional, high-speed flame front in a man-

Please cite this article as: W. Rakotoarison and M.I. Radulescu, A dynamical system approach for solving the steady structure of high speed deflagrations, Proceedings of the Combustion Institute, https://doi.org/10.1016/j.proci.2022.11.005

ner similar to the work presented in Strehlow and Fernandes [29], and Arienti [30].

Declaration of Competing Interest

The authors declare that they have no known competing financial interests or personal relationships that could have appeared to influence the work reported in this paper

Acknowledgments

We acknowledge financial support provided by the Natural Sciences and Engineering Research Council of Canada (NSERC) (RGPIN-2017-04322) through the Discovery Grant "Predictability of detonation wave dynamics in gases: experiment and model development". Many thanks also go to Ramki Murugesan, friend and colleague, whose discussion and advice in developing the proposed methodology were very helpful.

References

[1] J. Lee, R. Knystautas, C. Chan, Turbulent flame propagation in obstacle-filled tubes, Symp. (Int.) Combust. 20 (1) (1985) 1663–1672, doi:10.1016/S0082-0784(85)80662-7.
[2] A. Eder, N. Brehm, Analytical and experimental insights into fast deflagrations, detonations, and the deflagration-to-detonation transition process, Heat Mass Transf. 37 (2001) 543–548.
[3] A.Y. Poludnenko, T.A. Gardiner, E.S. Oran, Spontaneous transition of turbulent flames to detonations in unconfined media, Phys. Rev. Lett. 107 (5) (2011) 054501, doi:10.1103/PhysRevLett.107.054501.
[4] M. Saif, W. Wang, A. Pekalski, M. Levin, M.I. Radulescu, Chapman–Jouguet deflagrations and their transition to detonation, Proc. Combust. Inst. 36 (2) (2017) 2771–2779, doi:10.1016/j.proci.2016.07.122.
[5] S. Kadowaki, Instability of a deflagration wave propagating with finite mach number, Phys. Fluids 7 (1) (1995) 220–222, doi:10.1063/1.868721.
[6] O.Y. Travnikov, M.A. Liberman, V.V. Bychkov, Stability of a planar flame front in a compressible flow, Phys. Fluids 9 (12) (1997) 3935–3937, doi:10.1063/1.869494.
[7] O.Y. Travnikov, V.V. Bychkov, M.A. Liberman, Influence of compressibility on propagation of curved flames, Phys. Fluids 11 (9) (1999) 2657–2666, doi:10.1063/1.870127.
[8] A. Fecteau, The Effects of Compressibility on the Propagation of Premixed Deflagration, University of Ottawa, 2019 Master thesis.
[9] M.D. Smooke, Solution of burner-stabilized premixed laminar flames by boundary value methods, J. Comput. Phys. 48 (1) (1982) 72–105, doi:10.1016/0021-9991(82)90036-5.
[10] B. Barker, J. Humpherys, G. Lyng, K. Zumbrun, Viscous hyperstabilization of detonation waves in one space dimension, SIAM J. Appl. Math. 75 (3) (2015) 885–906, doi:10.1137/140980223.
[11] G.J. Sharpe, Linear stability of planar premixed flames: reactive Navier–Stokes equations with finite activation energy and arbitrary Lewis number, Combust. Theor. Model. 7 (1) (2003) 45–65, doi:10.1088/1364-7830/7/1/303.
[12] F.A. Williams, Combustion Theory: The Fundamental Theory of Chemically Reacting flow Systems, Combustion Science and Engineering Series, second ed., Benjamin/Cummings Pub. Co, Menlo Park, Calif, 1985.
[13] P. Clavin, G. Searby, Combustion Waves and Fronts in Flows: Flames, Shocks, Detonations, Ablation Fronts and Explosion of Stars, Cambridge University Press, 2016, doi:10.1017/CBO9781316162453.
[14] J. Powers, Combustion Thermodynamics and Dynamics, Cambridge University Press, 2016.
[15] I. Gasser, P. Szmolyan, A geometric singular perturbation analysis of detonation and deflagration waves, SIAM J. Math. Anal. 24 (4) (1993) 968–986, doi:10.1137/0524058.
[16] W. Fickett, W.C. Davis, Detonation: Theory and Experiment, Dover Publications, 2000.
[17] P. Clavin, G. Searby, Combustion Waves and Fronts in Flows: Flames, Shocks, Detonations, Ablation Fronts and Explosion of Stars, Cambridge University Press, Cambridge, 2016, doi:10.1017/CBO9781316162453.
[18] D. Layzer, Theory of linear flame propagation. Part I. Existence, uniqueness, and stability of the steady state, J. Chem. Phys. 22 (2) (1954) 222–229, doi:10.1063/1.1740035. Publisher: American Institute of Physics
[19] L.F. Shampine, M.W. Reichelt, The MATLAB ODE suite, SIAM J. Sci. Comput. 18 (1) (1997) 1–22, doi:10.1137/S1064827594276424.
[20] R.S. Chue, J.F. Clarke, J. Lee, Chapman–Jouguet deflagrations, Proc. R. Soc. Lond. Ser. A 441 (1913) (1993) 607–623, doi:10.1098/rspa.1993.0082.
[21] W. Rakotoarison, Y. Vilende, M. Radulescu, Model for CJ deflagrations in open ended tubes with varying vent ratios, in: Proceedings of the 27th International Colloquium on the Dynamics of Explosions and Reactive Systems, Beijing, China, 2019.
[22] M. Morduchow, P.A. Libby, On a complete solution of the one-dimensional flow equations of a viscous, heat-conducting, compressible gas, J. Aeronaut. Sci. 16 (11) (1949) 674–684, doi:10.2514/8.11882.
[23] R. Becker, Impact waves and detonation. Part I, NACA Technical Memorandums, NACA-TM-505(1929).
[24] R. von Mises, On the thickness of a steady shock wave, J. Aeronaut. Sci. 17 (9) (1950) 551–554, doi:10.2514/8.1723.
[25] R.A. Gardner, On the detonation of a combustible gas, Trans. Am. Math. Soc. 277 (2) (1983) 431–468, doi:10.1090/S0002-9947-1983-0694370-1.
[26] M. Williams, Heteroclinic orbits with fast transitions: anew construction of detonation profiles, Indiana Univ. Math. J. 59 (3) (2010) 1145–1209.
[27] W. Rakotoarison, B. Maxwell, A. Pekalski, M.I. Radulescu, Mechanism of flame acceleration and detonation transition from the interaction of a supersonic turbulent flame with an obstruction: experiments in low pressure propane–oxygen mixtures, Proc. Combust. Inst. 37 (3) (2019) 3713–3721, doi:10.1016/j.proci.2018.08.050.
[28] A.Y. Poludnenko, J. Chambers, K. Ahmed,

V.N. Gamezo, B.D. Taylor, A unified mechanism for unconfined deflagration-to-detonation transition in terrestrial chemical systems and type Ia supernovae, Science 366 (6465) (2019), doi:10.1126/science.aau7365.

[29] R.A. Strehlow, F.D. Fernandes, Transverse waves in detonations, Combust. Flame 9 (2) (1965) 109–119, doi:10.1016/0010-2180(65)90057-X.

[30] M. Arienti, A Numerical and Analytical Study of Detonation Diffraction, California Institute of Technology, 2003 Ph.D. thesis. Pasadena

Please cite this article as: W. Rakotoarison and M.I. Radulescu, A dynamical system approach for solving the steady structure of high speed deflagrations, Proceedings of the Combustion Institute, https://doi.org/10.1016/j.proci.2022.11.005

Chapter 5

A one-dimensional model for CJ-deflagrations and their transition to detonations

In Chapter 4, the steady structure of flames propagating at arbitrary burning velocities was found. This work was originally intended as a first step for the work presented in this Chapter, that focuses on the study of the flow field generated by accelerating, one-dimensional flames and their transition to detonations.

In the study of accelerating deflagrations and their transition to detonations, the main mechanisms leading to an overall increase of the burning rate are multi-dimensional. They include flame stretching and folding mostly due to preferential convection in tubes, hydrodynamic and thermal-diffusive instabilities, or interaction with turbulence, shocks or boundary layers, as well as their interactions [4, 8, 9]. Despite the complexity of these events, it is observed in shock tube experiments and numerical simulations, that flames reach a quasi-steady propagation regime known as the *choking regime* [28], during which it forms, strenghtens and drives pressure waves and shocks ahead of itself [8, 24, 47]. Those eventually become strong enough to, later on, allow thermal initiation of a detonation by shock pre-heating or by the formation of hot-spots at shock reflection locations, in the presence of solid walls [14].

This general view of the sequence of events suggests that a simpler, one-dimensional problem can be formulated to study the overall flow field involved in flame acceleration problems, in which the deflagration transition to detonation is controlled only by simple gasdynamical processes. This statement is plausible in that the initiation of detonations mostly relies on the formation of shock waves, which generally originate from the presence of a confinement (see Chap. 3), or from events

like sudden flame acceleration. In both cases, the formation of shock waves does not require the description of the detailed structure of the multidimensional flame, if proper modeling is performed from simple conservation principles. The approach chosen in this chapter was to artificially control the flame burning rate, in order to trigger a response of the flow, typically the formation of compression waves in the fresh gases as the burning rate increases. Here, altering the flame burning rate is done by arbitrarily modulating the pre-exponential factor of the one-step, irreversible, Arrhenius type law used to describe the depletion rate of reactants. Doing so permits to generate flow-fields relevant in accelerating flame problems, and better investigate the nature of the interaction between the flame and the compressible features of the flow field. This method is comparable to the one proposed in the former work on one-dimensional, accelerating flames by Deshaies, Kagan, Gordon and co-workers [48–50], in which the enhancement of the flame burning rate was achieved by means of a folding factor, meant to model the multidimensional increase of flame surface area leading to flame acceleration. The configuration studied in this chapter however differs in that focus is brought on freely propagating flames, i.e. flames propagating in tubes that are infinite on both sides, so that compression and shock waves formation is expected to only occur due to the acceleration of the flame. Special attention will be addressed to the case of high speed deflagrations, propagating near the Chapman-Jouguet (CJ) deflagration conditions. Those are associated to choked flames in shock tube experiments [30] and are, by definition, deflagrations propagating with a sonic downstream flow, at the theoretical highest burning velocity a subsonic flame could propagate at.

5.1 Governing equations and numerical setup

One-dimensional deflagrations were modeled using the reactive Navier-Stokes equations, with single-step, irreversible, first-order chemical reaction rate. They were non-dimensionalized in a manner identical to the work of Sharpe [41]:

$$\frac{\partial \rho}{\partial t} + \frac{\partial}{\partial x}(\rho u) = 0 \tag{5.1}$$

$$\frac{\partial}{\partial t}(\rho u) + \frac{\partial}{\partial x}(\rho u^2 + p) = \mathrm{Pr}\frac{4}{3}\frac{\partial^2 u}{\partial x^2} \tag{5.2}$$

$$\frac{\partial E}{\partial t} + \frac{\partial}{\partial x}(Eu + pu) = \frac{\gamma}{\gamma - 1}\frac{\partial^2 T}{\partial x^2} + \mathrm{Pr}\frac{4}{3}\frac{\partial}{\partial x}\left(u\frac{\partial u}{\partial x}\right) + Q\omega \tag{5.3}$$

$$\frac{\partial}{\partial t}(\rho Y) + \frac{\partial}{\partial x}(\rho u Y) = \frac{1}{\mathrm{Le}}\frac{\partial^2 Y}{\partial x^2} - \omega \tag{5.4}$$

$$\omega = \Lambda \rho Y \exp\left(\frac{-\theta}{T}\right) \times H(T - T_i) \tag{5.5}$$

where $p = \rho T$, $E = \rho T/(\gamma - 1) + \rho u^2/2$, H is the Heaviside function and T_i an ignition temperature below which no chemical reactions occur and typically set slightly above the unburned, undisturbed gases temperature. The following reference scales were used:

$$\rho = \frac{\overline{\rho}}{\overline{\rho}_u} \quad , \quad u = \frac{\overline{u}}{\overline{S_f}} \quad , \quad x = \frac{\overline{u}_u}{\overline{\alpha}_u}\,\overline{x} \quad , \quad T = \frac{\overline{R_g}}{\overline{S_f}^2}\,\overline{T} \quad , \quad \theta = \frac{\overline{Ea}}{\overline{S_f}^2} \quad , \quad Q = \frac{\overline{Q}}{\overline{S_f}^2} \tag{5.6}$$

Variables ρ, u, T, Y, p, $M_f = u_u/c_u$ and $c = \sqrt{\gamma p/\rho}$ are respectively the gas density, flow velocity, temperature, mass fraction of fresh gases, pressure, flame burning Mach number and speed of sound. Variables denoted with an over bar relate to dimensional quantities, those with index (u) to their value taken in the unburned and undisturbed gases.

The relevant dimensional gas properties are $\overline{S_f}$, $\overline{\nu}_u$, $\overline{\alpha}_u$, $\overline{D}_u$, $\overline{R_g}$, $\overline{Q}$, $\overline{Ea}$ and $\overline{k}$, respectively the flame burning velocity, gas kinematic viscosity, thermal and molecular diffusivity coefficients, the specific perfect gas constant, heat of reaction, activation energy and reaction rate pre-exponential factor, also referred to as the *burning rate eigenvalue* [40]. They are used to define the dimensionless heat of reaction Q, activation temperature θ and burning rate eigenvalue Λ, as well as the other commonly used and later useful non-dimensional energies $\widetilde{Q} = \overline{Q}/(\overline{R_g}\ \overline{T_u})$ and $\widetilde{Ea} = \overline{Ea}/(\overline{R_g}\ \overline{T_u})$. Finally, the non-dimensional parameters $\mathrm{Pr} = \overline{\nu}_u/\overline{\alpha}_u$ and $\mathrm{Le} = \overline{\alpha}_u/\overline{D}_u$ are the Prandtl and Lewis numbers, respectively equal 3/4 and 1.

This scaling was chosen so that the flame can be treated similarly to thickened flames [51]. It however differs from the usual formulation of such model as here, distances are scaled by the flame thickness, in a way that the pre-exponential factor Λ directly controls the flame burning velocity, similarly to the work of Gamezo et *al.* [52]. In the present study, the value of Λ is increased over time from an initial value representing a steady flame propagating at a prescribed burning rate, to cause the flame to accelerate accordingly. The numerical simulations aimed to model flame acceleration are thus performed as follow. The profiles of a steady flame propagating at a given burning Mach number M_{f0} are found using the method described in the previous work [46], together with the matching burning rate eigenvalue Λ_0. The profiles were imported as initial conditions in a hydrodynamical solver. The flame was left to propagate steadily for some time, typically over 10 times the characteristic particle flame crossing time, to ensure it keeps its original structure and eventual numerical disturbances fade far from the reaction zone. The value of Λ was

then increased linearly over time from $t = t_0$, i.e.:

$$\Lambda(t) = \Lambda_0 + \left(\frac{d\Lambda}{dt}\right)_0 (t - t_0) \tag{5.7}$$

where Λ_0 corresponds to the initial burning rate eigenvalue calculated for the steady flame set as initial conditions, and $\left(\frac{d\Lambda}{dt}\right)_0$ its increase rate, typically equal to a fraction of Λ_0. This causes the flame to accelerate and generate disturbances upstream and downstream of the reaction zone, until it eventually transits to a detonation.

The simulations were performed on a numerical solver developed by Falle [53,54]. Convective terms were solved using a second order accurate Godunov scheme, and diffusion terms were solved explicitly in time, using second order central differences in space. Zero-gradients conditions were set at the boundaries of the domain to approximate an open tube. The domain was discretized to provide 1/4 of a cell per unit length (1 cell covers 4 unit lengths), and adaptive mesh refinement was used [55] to provide details in high gradients regions, typically the reaction zones and shocks, allowing for a maximum resolution of 16 cells per unit length, i.e. about 32 cells per thickness of the initial, non-disturbed flame.

5.2 Results and discussion

The parameters γ, $\widetilde{Ea}$ and $\widetilde{Q}$ were chosen to be 1.4, 50 and 50. The initial flame was set to propagate at a Mach number $M_{f0} = 0.11$. This value is close to the CJ deflagration Mach number for the chosen set of parameters, equal to $M_{CJ} = 0.119$. The associated burning rate eigenvalue was thus found to be $\Lambda_0 = 2.65 \times 10^3$.

The flame was set to accelerate from time $t_0 = 40$, by increasing the value of Λ following the relation (5.7), where $\left(\frac{d\Lambda}{dt}\right)_0 = 5.90$, that corresponds to $0.22\%\ \Lambda_0$. The resulting flow can be visualized in the space-time diagrams plotted in Figures 5.1, showing density in gray scale. Plot (a) shows the overall flame acceleration process. At the very early times, the flame is steady and thus does not drive compression waves in the fresh gases. When the flame starts to accelerate, it generates and amplifies a shock ahead of it, that can be seen clearly in Figure 5.1(a). Its strength is annotated on the same figure at different space-time coordinates. At later times, the density jump across the shock propagating at a Mach number of about 2.2 is obvious, as seen on Figure 5.1(b), behind which the density increases monotonously until it reaches a maximum just ahead of the reaction zone. This density gradient can be seen on the few first density profiles plotted in Figure 5.2. Around time 2730, the deflagration transits to a detonation due to an explosion occurring just

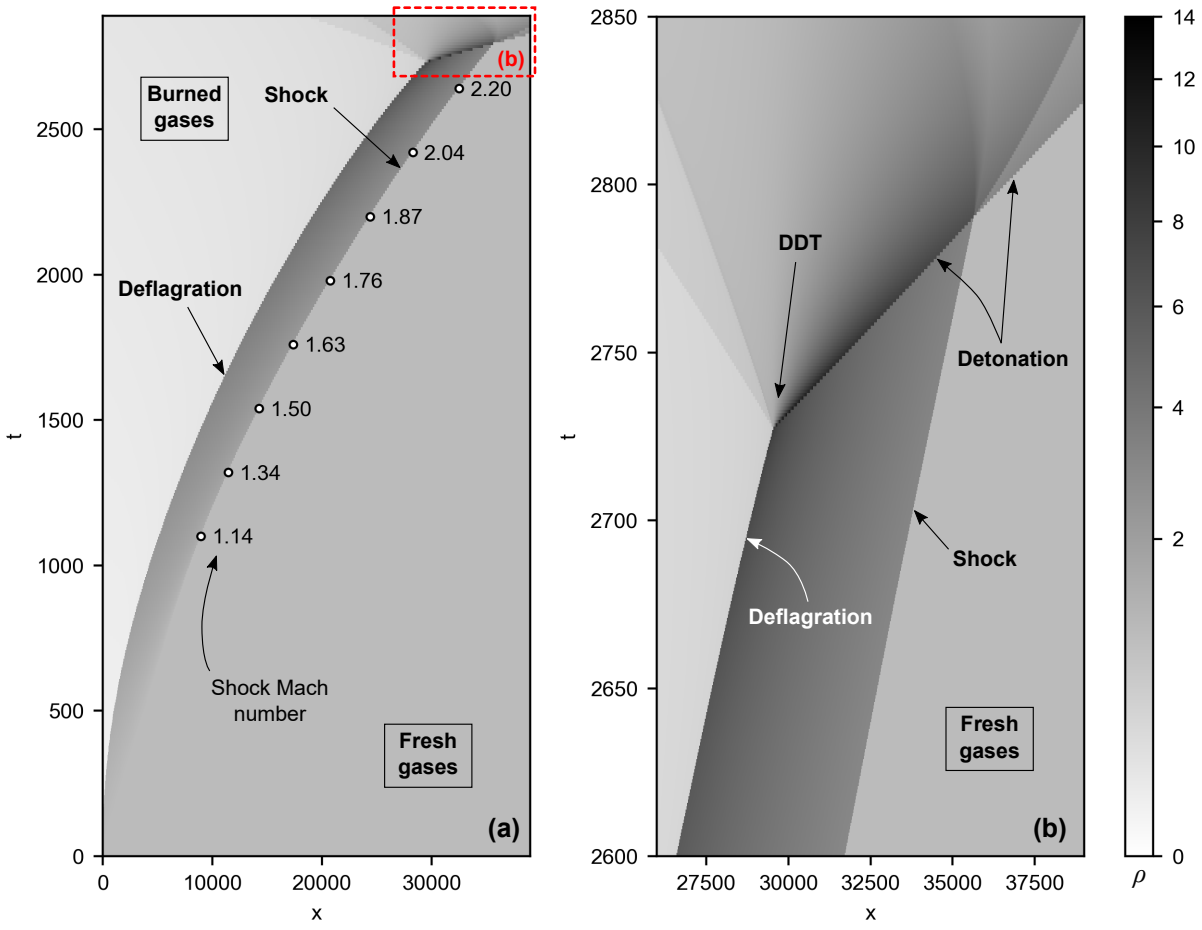

Figure 5.1: Space-time diagram plotted for density of the flame acceleration process. (a) shows the overall evolution of the flame and the shock, which strength is annotated along its trajectory. (b) shows the late stages of the flame acceleration process, where transition to detonation occurs.

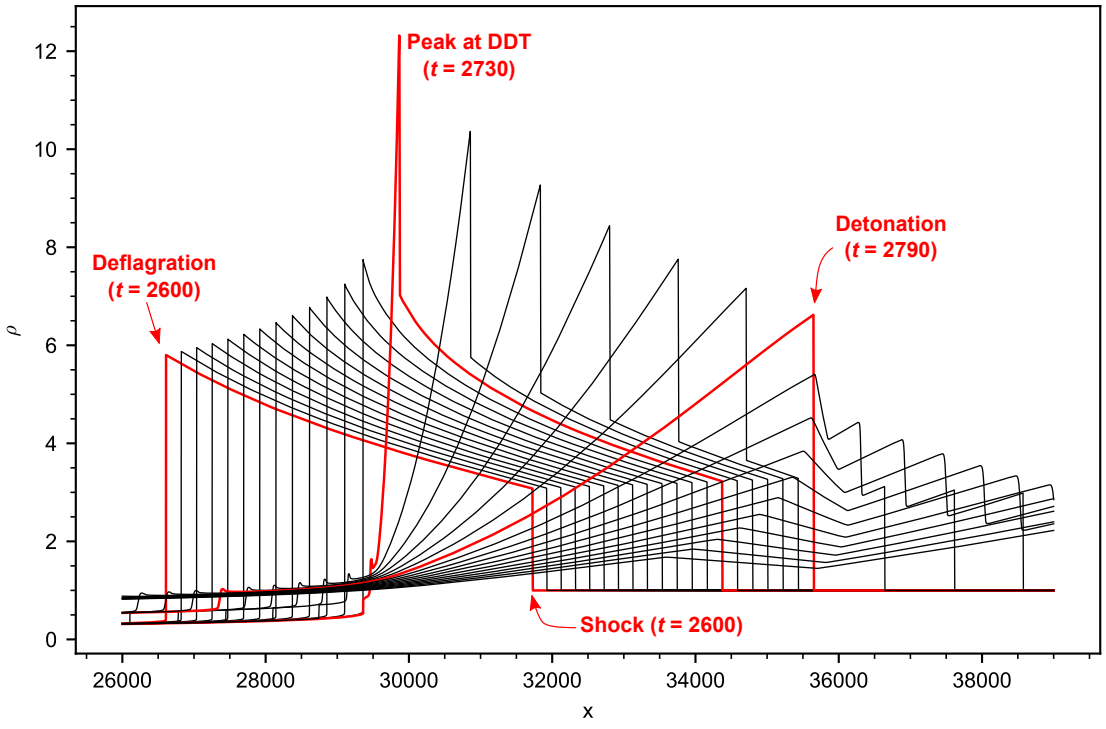

Figure 5.2: Series of density profiles plotted around the time of transition to detonation (see Figure 5.1(b)). Time interval between each plot is 10.

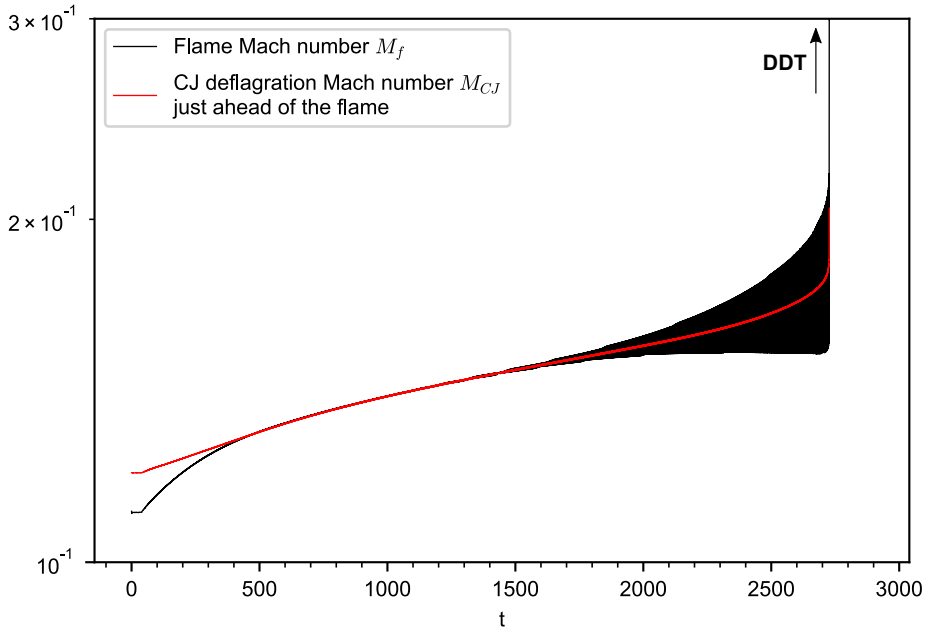

Figure 5.3: Evolution of the flame Mach number and the expected CJ deflagration Mach number over time.

ahead of the reaction zone. The detonation then travels in the shocked region until it catches up the shock wave around time 2790. The structure of the resulting wave was not studied, as the present study focuses on the flame acceleration process. It is however likely to be similar to viscous, weak detonation waves calculated by Gamezo et al. [52] at high values of the pre-exponential factor.

This sequence of events is typical of what was observed for other values of $\left(\frac{d\Lambda}{dt}\right)_0$, and differs only in the timing at which the shock forms and transition to detonation occurs. For high values of $\left(\frac{d\Lambda}{dt}\right)_0$, i.e. for highly accelerating flames, transition to detonation happens earlier than for low values. This result was anticipated, owing to the shock growing stronger more rapidly, thus providing the conditions required for thermal explosion more rapidly. Interestingly, this rapid shock formation occurs when the deflagration reaches a burning rate equal to the CJ conditions, here around time 500. This can be seen on Figure 5.3, where are plotted as a function of time the flame Mach number in black, and the CJ deflagration Mach number in red, both calculated taking as fresh gases conditions the state just ahead of the flame.

Later on and as seen in Figure 5.3 between times 500 and 1500, the flame remains in the CJ conditions despite the fact that its burning rate continuously increases. This is caused by the coupling between the shock and the flame: as the former gets continuously stronger and its downstream state hotter, the flame propagation conditions are changed such that larger CJ deflagration burning

velocities are allowed, thus permitting the flame to keep accelerating and strengthen the shock. As seen on Figure 5.3, this feedback mechanism goes on until time 1500, where the flame burning rate starts to oscillate around the CJ deflagration conditions. The amplitude of the oscillations increases until the deflagration transits to a detonation. This novel flame instability observed just prior to transition appears to be a gasdynamic pulsating instability characteristic of gasdynamic coupling, usually present in detonation waves. Such high frequency instabilities have been observed near detonation transition in accelerating flames in narrow tubes and re-initiation start of the galloping detonations [56]. However, although, our simulations reproducibly predicted such oscillations for all the acceleration rates investigated, numerical artifacts cannot be completely ruled out, and can actually be expected by the resolution of these simulations. As the flame accelerated, its thickness decreased accordingly. Prior to transition to detonations, the flame was about 10 times thinner than at its initial state, such that a maximum of only 4 cells could be fitted within the reaction zone. The difficulty here being to be able to properly resolve the flame structure at different stages, and especially at detonation initiation, detailed space and time resolution analysis is currently left for future work. At the present time, preliminary results at higher resolution in which the maximum resolution allowed was multiplied by two showed results comparable to the ones presented in this chapter, at least qualitatively.

These simulations were repeated starting with flames propagating at significantly lower values of the initial burning rate, far from the CJ conditions. In this case, the flame did not contribute to form shocks strong enough to allow the gases to ignite over a reasonably short time. This is consistent with the numerical work of Fecteau [22], in which the evolution of two-dimensional flames and their eventual transition to detonation was investigated. The burning rate of the initial flame was adjusted using the thickened flame model, and evolution to unsteadiness was favored by an initial deformation of the planar flame front. Under these conditions, the perturbation grows, thus increasing the flame surface area, providing the main cause of the global increase of the burning rate. Differences in the following events were found when the burning rate of the planar flame was changed. At low values, the flame eventually settles to propagate steadily. However at high values of the planar flame burning rate, a shock eventually forms in the fresh gases. When the planar flame burning rate was set to be close to the CJ conditions, transition to detonation occurred rapidly. This sequence of events is also consistent with experimental observations, where the increase of the burning rate is mostly provided by the deformation of the flame front, due to the presence of solid walls, to the interaction with the turbulence, or interaction with shocks and boundary layers. At the later stages of flame acceleration, strong shocks form rapidly when the flame eventually reaches conditions close to CJ deflagrations, i.e. the choking regime, supporting

the initiation of detonations [32–34, 44, 45].

The similarities of these results with the one-dimensional evolution of accelerating flames presented in this chapter suggests that a global description of DDT can be considered. Mostly, CJ deflagrations appear to be important, as they constitute a propagation regime that promotes the formation and growth of shocks strong enough to allow the onset of detonations. This is especially true in the present configuration, where the burned gases can expand freely due to the lack of rear confinement. As seen in the recent numerical work of Gordon, Kagan, Sivashinski and co-authors focusing on flame acceleration in semiconfined geometries [49, 50], transition to detonation was found to rely on the early formation of shock waves due to the rear confinement, causing the burned gases to expand forwards thus driving a flow ahead of the flame. This eventually permitted the unburned gases to sensitize as they are heated by shocks, such that detonation initiation could be achieved before the deflagration reached the CJ conditions [57]. Hence, the history of the flame acceleration becomes an important feature of the DDT phenomenon in that, various configurations like those involving some sort confinement (see Chap. 3), friction [24,58], or the presence of obstacles, can lead to various conditions just ahead of the flame that can affect transition to detonations differently.

In the present study, the closeness to the CJ deflagration conditions and the coupling identified between the shock and the flame is the main mechanism of flame acceleration and shock amplification, that lead to transition to detonation.

The fact that the flame remains in the CJ conditions while its burning rate is continuously increased, opens the path to models meant to describe in a simple way the resulting flow field. For example, in a manner similar to the two-discontinuities models describing the pseudo-steady flow field involving a shock followed by a CJ deflagration [30, 59], a simple model describing the evolution of an accelerating shock-flame complex can be developed, in which the flame, which burning rate grows but remains in the CJ conditions, causes the strengthening of its precursor shock accordingly. Such a model is currently left as a work in progress.

5.3 Concluding remarks

The relative simplicity of the simulations presented here made it easy to implement and generate results. The method described in this study to model accelerating flames was found to reproduce well the coupling that exists between the flame and the flow field, from the shock formation to the initiation of the detonation. This makes it a convenient tool to reproduce and better understand the overall conditions required for deflagrations to transit to detonations.

A very interesting result here is the role of the shock heating, allowing the deflagration to remain choked over some time, before the fresh gases located just ahead of it are thermally ignited to form a detonation. In this case, the coupling between the deflagration and the shock is such that, the latter's strength increases rapidly under the influence of the following CJ deflagration. With it, the deflagration remains in the CJ conditions even if its burning rate increases, owing to the continuously changing conditions in the shocked state. This result was expected as deflagrations propagating near the CJ conditions are prone to generate compression waves rapidly in the fresh gases, thus providing the main mechanism for flame acceleration in the proposed unconfined medium. While the propensity of CJ deflagrations to generate pressure waves is relatively accepted [25–27], the present results show that the deflagration does so in order to remain a CJ deflagration in relation to newly compressed gas just ahead of itself. This self-organization of CJ deflagrations into stronger CJ deflagrations is the first main finding of the present work.

Without discarding the possibility of numerical artifact, a second finding is the onset of the detonation being associated with a pulsating instability, akin to the gasdynamic coupling in detonation waves where reaction zones and flames are in phase with each other and yield very rapid amplification [60]. This instability may generate local hot-spots beyond what the lead shock is capable of. In the case such instability is confirmed to have a physical origin, further work should focus on this unique feature of accelerating flames.

Chapter 6

Conclusion

6.1 Summary

In this thesis, different aspects of Chapman-Jouguet deflagrations and their involvement in the deflagration to detonation transition were discussed.

In Chapter 2, series of experiments were performed, of a shock-flame complexes propagating in a shock-tube, and its interaction with a single obstacle. These experiments were designed to investigate the details of the flame interaction with the obstacle, at the last stages of their acceleration, prior to their transition to detonation, as found in similar experiments involving series of obstacles. The presence of the obstacle expectedly permitted the acceleration of the flames. The latter indeed, sees its burning rate increase as it interacted with shocks reflected on the obstacle. In some instances, transition to detonation was observed, and was found to depend on the initial conditions of flame propagation, set by adjusting the initial pressure in the tube, that sets the shock strength and the flame burning velocity of the shock-flame complex. It permitted to identify the critical initial pressure, hence the initial flame burning velocity, at which deflagration to detonation transition occurs. For the experiments presented, done in a low pressure, stoichiometric propane-oxygen mixture, this critical initial flame burning velocity correlated well with the CJ-deflagration burning velocity. This feature was attributed to the fact that CJ-deflagrations have a sonic downstream flow, that allows the formation and significant amplification of compression waves within the flame brush, as the chemical energy is released on a time scale comparable to the acoustic wave flame crossing time [27]. The acceleration of the flame was found to proceed until it approaches the sonic conditions in the fresh gases, conditions at which it is in phase with pressure waves and prone to drive strong shocks capable of initiating detonations.

Chapter 3 presented a model for predicting CJ-deflagrations apparent velocities, i.e. observed in a fixed frame of reference, in a configuration of large scale, vented deflagration to detonation transition. The goal was to discuss whether fast flames achieving transition to detonation in such configurations are CJ-deflagrations. It is indeed the case in shock tube experiments, where the gases are confined and flames transit to detonations when they reach an apparent velocity of about the speed in sound of the burned gases. The model is similar to the double-discontinuity model of Chue [30], involving a shock followed by a CJ-deflagration treated as discontinuities, and differs in that it accounts for the fact that the burned gases can be vented, i.e. expanded isentropically, to the atmosphere through an aperture of known dimensions. The flow induced ahead of the flame thus drives a weaker shock, downstream of which the flow velocity and temperature are lower than in a confined geometry. The apparent velocity of the CJ-deflagration is consequently smaller than in a closed ended tube. This statement was used to justify why transition to detonation occurs in vented DDT experiments when the flames reach an apparent velocity smaller than the speed of sound in the burned gases, while remaining CJ-deflagrations. Comparison with a selected set of experiments found in the literature showed good correlation between the apparent speed of the flame measured just before the initiation, and the one calculated by the proposed model, suggesting that such flames are indeed CJ-deflagrations.

Chapter 4 was dedicated to solving the structure of flames propagating at arbitrary burning velocities, for which a novel solving method was proposed. A shooting method was used to solve the boundary value problem posed by the the one-dimensional, steady state, reactive Navier-Stokes equations with a one-step, irreversible, Arrhenius type reaction rate, together with boundary conditions at the fresh and burned state, connected by the deflagration jump relations. Focus was made on the reduced set of 3 ordinary differential equations, derived under the assumptions of unity Lewis number and a Prandtl number equal to $3/4$. Because the shooting method relies on numerical integration performed multiple times to ensure the integral curve connects both the fresh and burned states, special treatment of the boundary conditions was needed to handle their saddle nature. This difficulty was addressed using techniques issued from dynamical systems analysis. Linearization of the flame equations upon the fresh and burned states was done, from which eigenvalues and eigenvectors could be calculated. Those were conveniently used to determine a perturbation of the initial state at equilibrium to start numerical integration, as well as to provide accurate, analytical solutions close to the saddles, where numerical solutions are aimed to fail at providing converging profiles. The method was found to consistently work at providing end-to-end, continuous and converging profiles of arbitrary speed deflagrations, from the low-Mach case up to burning velocities of about 95% the CJ-deflagration burning velocity, over a wide range of

gas parameters (ratio of specific heats, heat release and activation energy) commonly found in the literature on deflagration to detonation transition simulations.

Finally Chapter 5 proposed a novel approach for modeling one dimensional, high-speed deflagrations. The primary goal was to investigate the flow field involving a shock wave followed by a high speed, near CJ deflagration. This configuration is what is commonly found just prior transition to detonation. To generate such a flow, the burning rate of the one-dimensional flame was modeled using a one-step, irreversible, Arrhenius type law, in which the pre-exponential factor varied arbitrarily over time. Doing so permitted to control the flame acceleration. The main finding was that, as accelerating flames propagated near the CJ deflagration conditions, they generate and strengthen a shock in the fresh gases. The continuously accelerating flame could thus remain a CJ deflagration over some time as the shock modifies the state ahead of the flames. After enough shock amplification, thermal initiation of a detonation could occur just ahead of the flame reaction zone. The flow features preceding the initiation of detonations in this simple, one-dimensional model resemble those found in multi-dimensional configurations, as in experiments and numerical simulations. This suggests that a more global description of the conditions required for DDT to occur can be developed, in which CJ deflagrations play an important role.

6.2 Contributions of the work

An interesting conclusion of this thesis pertains to the requirement and sufficiency of CJ deflagrations to achieve transition to detonations, and how it is related to the conditions in which high-speed flames are allowed to propagate. As seen all along, deflagration to detonation transition highly relies on the presence of shock waves. They serve as a mean for pre-heating the unburned gas before the passage of the flame, provide further heating by friction in rough channels as they set into motion the fresh gases behind them, form nucleus for local explosions when they reflect with solid walls, or enhance turbulent mixing when interacting with the flame front or boundary layers. Their origin and strength can be of different kind. In most experiments done in shock tubes like those performed in Chapter 2, the closed nature of the rear end (where the flame is initiated) impedes the burned gases to expand freely, thus causing the flame to act as a porous piston pushing a flow, hence a shock ahead of it. As seen in Chapter 3, the strength of these shocks decreases when increasing amount of rear venting is allowed. Finally, Chapter 5 showed that in the case of freely propagating flames (i.e. totally unconfined), shock waves form naturally when flames are brought near the CJ deflagration regime.

Discussing whether DDT is likely to occur is thus discussing whether shocks strong enough

can form to allow thermal initiation of the reactive mixture. Because shock waves can have origins different than those formed when deflagrations approach the CJ regime, it can be concluded that CJ deflagrations do not constitute a necessary step to detonation initiation. However, the proximity of deflagrations to the CJ regime provides a strong mechanism for shock formation and amplification, making them an important step to achieve DDT in unfavorable conditions, such as in unconfined geometries or in insensitive mixtures. This statement seems especially true for the mixture investigated in Chapter 2, for some experimental results listed in the literature and presented in Chapter 3, as well as in the case of flame propagation in unconfined medium studied in Chapter 5.

As a result, being able to predict the conditions under which deflagration to detonation transition may occur can be done relatively easily using simple models, as the one presented in Chapter 3. This model, being simple to implement, constitutes a convenient way to characterize the critical conditions of detonation initiations in a given confinement, to be used in the field of industrial safety and others. At this stage of the research however, it would be of great interest to test and validate these critical conditions in laboratory scale DDT experiments, in order to overcome the difficulties inherent to the large scale ones, commonly found in the literature of vented explosions.

Overall, it appears occurrences of DDT events can be predicted from global flow properties, without the requirement to deal with the details of the flow local to the flame, like turbulence or shock reflection. In that sense, one dimensional flames propagating at high burning rates, modeled as thickened flames as presented in Chapter 4 and 5, can become a very useful and convenient tool to investigate the critical conditions for transition to detonation. In the thickened flame limit, tuning the burning rate can be done easily to match different events that may cause the flame to accelerate. The steady structure of deflagrations calculated in Chapter 4 thus constitutes the first step for further analysis of the behavior of high speed deflagrations. They can afterwards be imported in unsteady, hydrodynamics solvers like done in Chapter 5 as a preliminary study, to test their stability and ability to transit to detonations.

Bibliography

[1] D. Michael Johnson. The potential for vapour cloud explosions – Lessons from the Buncefield accident. *Journal of Loss Prevention in the Process Industries*, 23(6):921–927, 2010.

[2] V. N. Gamezo. Thermonuclear Supernovae: Simulations of the Deflagration Stage and Their Implications. *Science*, 299(5603):77–81, 2003.

[3] J.H.S. Lee and I.O. Moen. The mechanism of transition from deflagration to detonation in vapor cloud explosions. *Progress in Energy and Combustion Science*, 6(4):359–389, 1980.

[4] G. Ciccarelli and S. Dorofeev. Flame acceleration and transition to detonation in ducts. *Progress in Energy and Combustion Science*, 34(4):499–550, 2008.

[5] Elaine S. Oran and Vadim N. Gamezo. Origins of the deflagration-to-detonation transition in gas-phase combustion. *Combustion and Flame*, 148(1-2):4–47, 2007.

[6] M. Kellenberger and G. Ciccarelli. Propagation mechanisms of supersonic combustion waves. *Proceedings of the Combustion Institute*, 35(2):2109–2116, 2015.

[7] A. Eder. Brennverhalten schallnaher und überschall-schneller Wasserstoff-Luft Flammen. *PhD Thesis, Technischen Universität München*, 2001.

[8] H. Yang and M. I. Radulescu. Enhanced DDT mechanism from shock-flame interactions in thin channels. *Proceedings of the Combustion Institute*, 38(3):3481–3495, 2021.

[9] G. Thomas, R. Bambrey, and C. Brown. Experimental observations of flame acceleration and transition to detonation following shock-flame interaction. *Combustion Theory and Modelling*, 5(4):573–594, 2001.

[10] J. Chao, T. Otsuka, and J.H.S. Lee. An experimental investigation of the onset of detonation. *Proceedings of the Combustion Institute*, 30(2):1889–1897, 2005.

[11] M. Kellenberger and G. Ciccarelli. Advancements on the propagation mechanism of a detonation wave in an obstructed channel. *Combustion and Flame*, 191:195–209, 2018.

[12] Ya. B. Zel'dovich, V. B. Librovich, G. M. Makhviladze, and G. I. Sivashinskil. On the onset of detonation in a nonuniformly heated gas. *Journal of Applied Mechanics and Technical Physics*, 11(2):264–270, 1972.

[13] W.R. Chapman and R.V. Wheeler. The Propagation of Flame in Mixtures of Methane and Air. *Journal of the Chemical Society (Resumed)*, 129:2139–2417, 1926.

[14] P. A. Urtiew and A. K. Oppenheim. Experimental Observations of the Transition to Detonation in an Explosive Gas. *Proceedings of the Royal Society A: Mathematical, Physical and Engineering Sciences*, 295(1440):13–28, 1966.

[15] I. O. Moen, M. Donato, R. Knystautas, and J. H. Lee. Flame acceleration due to turbulence produced by obstacles. *Combustion and Flame*, 39(1):21–32, 1980.

[16] C. Chan, I. O. Moen, and J. H. S. Lee. Influence of confinement on flame acceleration due to repeated obstacles. *Combustion and Flame*, 49(1):27–39, 1983.

[17] C.J. Brown and G.O. Thomas. Experimental studies of ignition and transition to detonation induced by the reflection and diffraction of shock waves. *Shock Waves*, 10(1):23–32, 2000.

[18] O. Yu. Travnikov, M. A. Liberman, and V. V. Bychkov. Stability of a planar flame front in a compressible flow. *Physics of Fluids*, 9(12):3935–3937, 1997.

[19] O. Yu. Travnikov, V. V. Bychkov, and M. A. Liberman. Influence of compressibility on propagation of curved flames. *Physics of Fluids*, 11(9):2657–2666, 1999.

[20] L. He. Analysis of compressibility effects on Darrieus-Landau instability of deflagration wave. *Europhysics Letters*, 49(5):576, 2000. Publisher: IOP Publishing.

[21] V. Bychkov, M. Modestov, and M. Marklund. The Darrieus–Landau instability in fast deflagration and laser ablation. *Physics of Plasmas*, 15(3):032702, 2008.

[22] A. Fecteau. *The Effects of Compressibility on the Propagation of Premixed Deflagration*. PhD thesis, University of Ottawa, Ottawa, ON - Canada, 2019.

[23] A. Fecteau, J. McDonald, A. Sow, and M. I. Radulescu. The Effects of Compressibility on the Propagation of Premixed Deflagration. 2019.

[24] D. M. Valiev, V. Bychkov, Vya. Akkerman, and L.-E. Eriksson. Different stages of flame acceleration from slow burning to Chapman-Jouguet deflagration. *Physical Review E*, 80(3):036317, 2009.

[25] A. Y. Poludnenko, J. Chambers, K. Ahmed, V. N. Gamezo, and B. D. Taylor. A unified mechanism for unconfined deflagration-to-detonation transition in terrestrial chemical systems and type Ia supernovae. *Science*, 366(6465), 2019.

[26] A. Y. Poludnenko. Pulsating instability and self-acceleration of fast turbulent flames. *Physics of Fluids*, 27(1):014106, 2015.

[27] A. Y. Poludnenko, T. A. Gardiner, and Elaine S. Oran. Spontaneous Transition of Turbulent Flames to Detonations in Unconfined Media. *Physical Review Letters*, 107(5):054501, 2011.

[28] J.H.S. Lee, R. Knystautas, and C.K. Chan. Turbulent flame propagation in obstacle-filled tubes. *Symposium (International) on Combustion*, 20(1):1663–1672, 1985.

[29] S.B. Dorofeev, V.P. Sidorov, M.S. Kuznetsov, I.D. Matsukov, and V.I. Alekseev. Effect of scale on the onset of detonations. *Shock Waves*, 10(2):137–149, 2000.

[30] R. S. Chue, J. F. Clarke, and J.H.S. Lee. Chapman-Jouguet Deflagrations. *Proceedings of the Royal Society London. Series A: Mathematical, Physical and Engineering Sciences*, 441(1913):607–623, 1993.

[31] M. I. Radulescu and B. M. Maxwell. The mechanism of detonation attenuation by a porous medium and its subsequent re-initiation. *Journal of Fluid Mechanics*, 667:96–134, 2011.

[32] M. Saif, W. Wang, A. Pekalski, M. Levin, and M. I. Radulescu. Chapman–Jouguet deflagrations and their transition to detonation. *Proceedings of the Combustion Institute*, 36(2):2771–2779, 2017.

[33] B. Maxwell, A. Pekalski, and M. I. Radulescu. Modelling of the transition of a turbulent shock-flame complex to detonation using the linear eddy model. *Combustion and Flame*, 192:340–357, 2018.

[34] T. Jaravel, O. Dounia, Q. Malé, and O. Vermorel. Deflagration to detonation transition in fast flames and tracking with chemical explosive mode analysis. *Proceedings of the Combustion Institute*, 38(3):3529–3536, 2021.

[35] A. Teodorczyk, J. H. S. Lee, and R. Knystautas. Propagation mechanism of quasi-detonations. *Symposium (International) on Combustion*, 22(1):1723–1731, 1989.

[36] Y.J. Zhu, J. Chao, and J.H.S. Lee. An experimental investigation of the propagation mechanism of critical deflagration waves that lead to the onset of detonation. *Proceedings of the Combustion Institute*, 31(2):2455–2462, 2007.

[37] S. Browne, J. Ziegler, and J.E. Shepherd. Numerical Solution Methods for Shock and Detonation Jump Conditions, 2015.

[38] A. Pekalski, J. Puttock, and S. Chynoweth. Deflagration to detonation transition in a vapour cloud explosion in open but congested space: Large scale test. *Journal of Loss Prevention in the Process Industries*, 36:365–370, 2015.

[39] S. Davis, J. Pagliaro, D. Botwinick, T. DeBold, K. van Wingerden, D. Allason, and D. M. Johnson. Do not believe the hype: Using case studies and experimental evidence to show why the HSE is wrong about excluding deflagration-to-detonation transitions. *Process Safety Progress*, 38(2):e11998, 2019.

[40] F. A. Williams. *Combustion theory: the fundamental theory of chemically reacting flow systems*. Combustion science and engineering series. Benjamin/Cummings Pub. Co, Menlo Park, Calif, 2nd ed edition, 1985.

[41] G. J. Sharpe. Linear stability of planar premixed flames: Reactive Navier–Stokes equations with finite activation energy and arbitrary Lewis number. *Combustion Theory and Modelling*, 7(1):45–65, 2003.

[42] G. J. Sharpe and S. A. E. G. Falle. Nonlinear cellular instabilities of planar premixed flames: numerical simulations of the Reactive Navier–Stokes equations. *Combustion Theory and Modelling*, 10(3):483–514, 2006.

[43] P. Clavin and G. Searby. *Combustion Waves and Fronts in Flows: Flames, shocks, detonations, ablation fronts and explosion of stars*. Cambridge University Press, Cambridge, 2016.

[44] W. Rakotoarison, B. Maxwell, A. Pekalski, and M. I. Radulescu. Mechanism of flame acceleration and detonation transition from the interaction of a supersonic turbulent flame with an obstruction: Experiments in low pressure propane–oxygen mixtures. *Proceedings of the Combustion Institute*, 37(3):3713–3721, 2019.

[45] W. Rakotoarison, A. Pekalski, and M. I. Radulescu. Detonation transition criteria from the interaction of supersonic shock-flame complexes with different shaped obstacles. *Journal of Loss Prevention in the Process Industries*, page 103963, 2020.

[46] W. Rakotoarison and M. I. Radulescu. A dynamical system approach for solving the steady structure of high speed deflagrations. *Proceedings of the Combustion Institute*, 2022.

[47] D. M. Valiev, V. Bychkov, V. Akkerman, L.-E. Eriksson, and C. K. Law. Quasi-steady stages in the process of premixed flame acceleration in narrow channels. *Physics of Fluids*, 25(9):096101, 2013.

[48] B. Deshaies and G. Joulin. Flame-speed sensitivity to temperature changes and the deflagration-to-detonation transition. *Combustion and Flame*, 77(2):201–212, 1989.

[49] Leonid Kagan and Gregory Sivashinsky. Parametric transition from deflagration to detonation: Runaway of fast flames. *Proceedings of the Combustion Institute*, 36(2):2709–2715, 2017.

[50] Peter V. Gordon, Leonid Kagan, and Gregory Sivashinsky. Parametric transition from deflagration to detonation revisited: Planar geometry. *Combustion and Flame*, 211:465–476, 2020.

[51] O. Colin, F. Ducros, D. Veynante, and T. Poinsot. A thickened flame model for large eddy simulations of turbulent premixed combustion. *Physics of Fluids*, 12(7):1843–1863, 2000.

[52] V.N. Gamezo, A.Y. Poludnenko, and E.S. Oran. One-dimensional evolution of fast flames. In *Proceedings of the 23rd International Colloquium on the Dynamics of Explosions and Reactive Systems*, page Paper 330, Irvine, CA - USA, 2011.

[53] S. A. E. G. Falle. Self-similar jets. *Monthly Notices of the Royal Astronomical Society*, 250(3):581–596, 1991.

[54] S. A. E. G. Falle and S. S. Komissarov. An upwind numerical scheme for relativistic hydrodynamics with a general equation of state. *Monthly Notices of the Royal Astronomical Society*, 278(2):586–602, 1996.

[55] S. A. E. G. Falle and J. R. Giddings. Body capturing using adaptive cartesian grids. In *Baines, M.J., Morton, K.W. (Eds.), Numerical Methods for Fluid Dynamics*. Oxford University Press, 1993.

[56] D. H. Edwards and J. M. Morgan. Instabilities in detonation waves near the limits of propagation. *Journal of Physics D: Applied Physics*, 10(17):2377, 1977.

[57] Peter V. Gordon, Leonid Kagan, and Gregory Sivashinsky. Parametric transition from deflagration to detonation in stellar medium. *Phys. Rev. E*, 103(3):033106, 2021. Publisher: American Physical Society.

[58] I. Brailovsky and G. Sivashinsky. Effects of momentum and heat losses on the multiplicity of detonation regimes. *Combustion and Flame*, 128(1-2):191–196, 2002.

[59] W Rakotoarison, Y Vilende, and M.I. Radulescu. Model for CJ deflagrations in open ended tubes with varying vent ratios. In *Proceedings of the 27th International Colloquium on the Dynamics of Explosions and Reactive Systems*, Beijing, China, 2019.

[60] M. I. Radulescu and J. Tang. Nonlinear Dynamics of Self-Sustained Supersonic Reaction Waves: Fickett's Detonation Analogue. *Physical Review Letters*, 107(16):164503, 2011. Publisher: American Physical Society.

Appendix A

Schlieren visualization of hydrogen-air flames in a spherical vessel

The work presented in this appendix was conducted in collaboration with the Canadian Nuclear Laboratories (CNL). It was aimed to design and assemble a high-speed, schlieren photography set-up for visualizing spherical, hydrogen-air flames in a combustion vessel. With that objective, the choice of the elements constituting the optical system, including the light source, lenses, vessel windows and camera, were justified to provide a simple and reliable experimental bench. Advises and software regarding post-processing of the footage were also included. Those mostly consisted in image enhancement techniques, like background removal and contrast adjustments.

The document presented in the following pages summarizes the design implemented, with details on the choices made.

Schlieren visualization of hydrogen-air flames in a spherical vessel

Willstrong Rakotoarison

[redacted]

Last updated on December 8, 2021

Contents

Introduction

Schlieren photography is a common optical technique in fluid mechanics, for visualizing regions where gas density varies, like the plume of hot air over a heat source, jets, shocks, combustion waves, etc.

This document is aimed to summarize the experimental technique used to visualize the combustion front of hydrogen-air flames in a spherical vessel.
The first section presents the basic principle of schlieren photography, to be used as a reference to justify the use of the different parts of the final optical bench.
The second section focuses on image acquisition and image processing to enhance and/or compensate for the inherent issues unsolved using the available hardware.
The third section proposes some directions for the amelioration of the setup, that may be relevant to implement in further experiments.

1 Experimental setup

1.1 Working principle of schlieren photography

The working principle of schlieren photography is presented in Figure 1. The light of a light source is captured by a condenser lens, that focuses it through a pinhole, downstream of which the spot of light transmitted is small enough to be considered as a *point light source*.
A first field lens is placed at a distance equal to its focal length away from the pinhole, causing the beam of light to become parallel.
As the light crosses the test region in which density gradients exist (schlieren object), part of the light is diffracted. As a result, only part of the light crosses the second field lens. The latter collects the remaining light, focusing it at a distance equal to its focal length where a *knife edge* is placed, which role is to block the diffracted light that has crossed the second field lens, done by partially masking the spot of light located at the focal point of the second field lens.
Finally, a screen or a camera can be placed downstream of the knife edge to visualize a schlieren image. With the set-up described above, bright regions of the image correspond to regions across which the light has not (or mildly) been diffracted by the density gradients in the test region, as opposed to darker regions, across which light has been diffracted in a way that it has either not crossed the second field lens, or has been blocked by the knife edge.

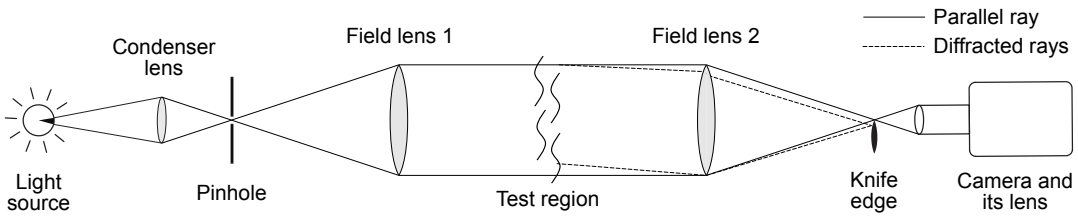

Figure 1: Schematic of a linear schlieren set-up.

Alternatively, a Z-type schlieren set-up can be used to produce the same images. It consists in using two parabolic mirrors instead of two lenses, to parallelize the beam of light transmitted through the pinhole and re-focus it towards the knife edge. The main advantage is to provide larger fields of view as large mirrors are generally cheaper than large lenses, and/or allow a more compact set-up in length owing to the *folded* optical path.
The choice of the linear schlieren set-up was made for the present project, based on the relatively small size of the field of view, limited by the 8 cm diameter view ports located on each side of the combustion vessel, that are 137 cm apart.

1.2 Light source

The assembly of light source, condenser lens and pinhole proposed in Figure 1 is the most common in schlieren setup. The use of a condenser lens and a pinhole can however be avoided if the physical size of the light source emitter is small enough, unlike incandescent light bulbs or flash tubes. On the other hand, high power point light sources like spark gaps do not permit long time or continuous illumination, making them unsuitable for videotaping laminar flames.
A good compromise can be found in LEDs. They were for a long time avoided owing to their low light power output, if not used as intermittent light sources [4, 5], but recent technological

progress made them suitable for schlieren visualization owing to the small size of their bulb and high power [1].

The LED chosen was the ThorLabs mounted, white LED, part # MCWHLP1 (discontinued at the date of December 7th, 2021). Its bulb size is 3.5 mm diameter, it has a nominal power output of 2700 mW and a view angle 125 degrees (full angle). The high power was chosen in prevision of its usage on self-luminous events, for which bright enough illumination must be reached to overcome light polluted schlieren images, as well as its potential use in larger schlieren set-up. Details on the effective illumination of a schlieren setup are developed in Section 1.3.
The LED is driven by the ThorLabs LED constant current (adjustable) driver part # LEDD1B coupled with its power supply ThorLabs part # KPS101. The current delivered to the LED by the current driver can be adjusted to set the brightness of the LED. It is a convenient feature to accommodate for the specific experimental conditions, determined by the field lens properties (focal length, diameter), camera sensor sensitivity, brightness of self-luminous events, and the use or not of neutral density filters.

1.3 Field lenses

The role of the first field lenses is to parallelize the beam of light emitted by the LED, and the role of the second one is to focus the light back to the knife edge. Although they do not need to be identical, they were chosen to be both the Edmund Optics condenser lens part # 27-503. They have a diameter of 10 cm, enough to cover the 8 cm diameter field of view, and a focal length of 40 cm, giving a focal length to aperture ratio (f-number) of f_n = 4, corresponding to the largest f-number available for a 10 cm diameter lens.

The choice of the lens was done based on the optical quality and the amount of light wanted to be captured.
The lens quality is generally satisfied by the quality of the glass provided by specialized manufacturers like Edmund Optics. However, images formed can be affected by optical aberrations introduced by the geometry of the optics. In the present case, the main concern may be *spherical aberrations* (case in which parallel rays intercepted on the outer sections of the lens do not focus at its focal length) and *chromatic aberrations* (case in which parallel rays of different wavelength do not focus at the same spot), both being generally corrected in devices involving lenses assembly (camera lenses, telescope refractor) [3]. In the case of a single lens set-up (as used here), spherical aberrations can be minimized when using lenses with a large f-number (small diameter, long focal length). Regarding chromatic aberrations, the small size of the optical system and the use of gray-scale cameras makes it negligible.

The fraction of light r captured by the first field lens relative to the total amount of light emitted by the LED, is the effective amount to be considered for illumination of the schlieren object. It can be determined geometrically by the lens diameter d, its focal length f, the light source viewing angle α and its light power, that are related by :

$$r = \frac{\beta}{\alpha} = \frac{\tan^{-1}(1/2f_n)}{\alpha} \tag{1}$$

where β is the angle of light emitted by the point light source intercepted by the lens. A schematic of the geometrical configuration, as well as a plot of the values of r for different values of α are presented in Figure 2.

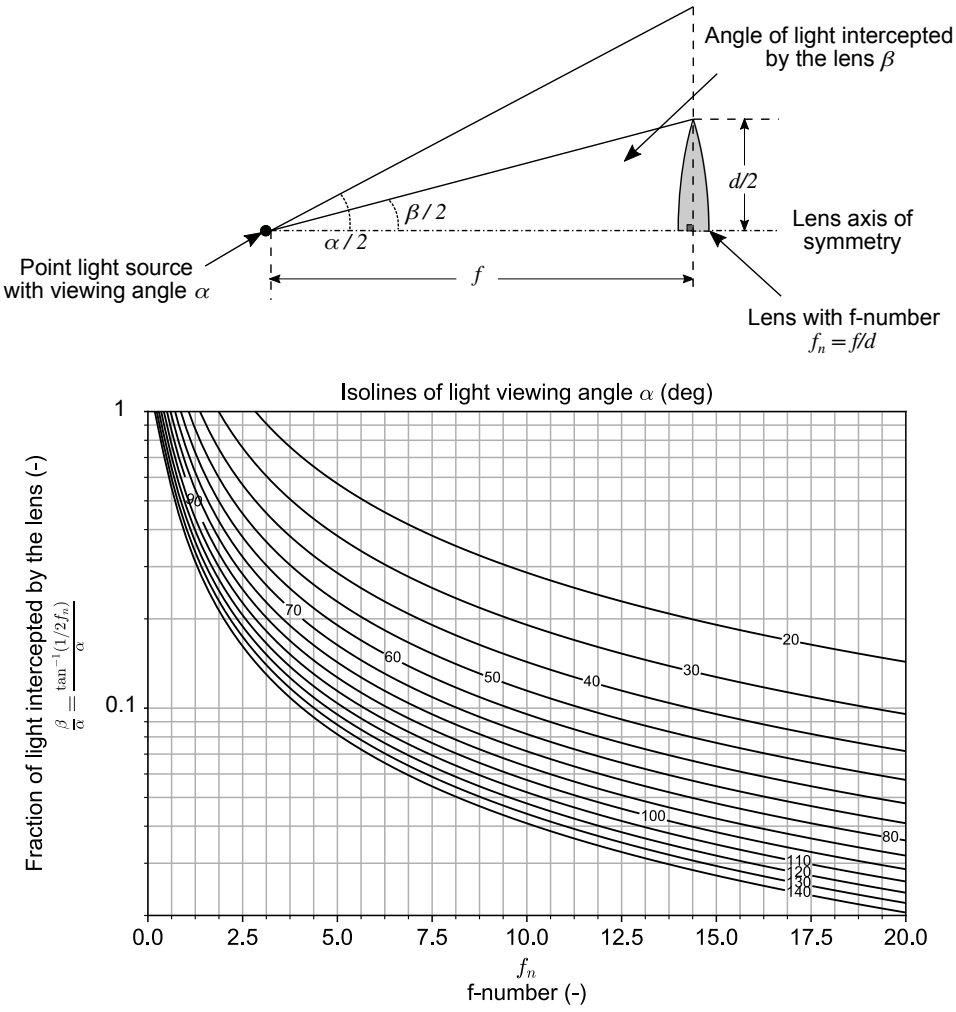

Figure 2: Fraction of light intercepted by the first field lens, for estimating the effective illumination of the schlieren set-up.

In the present configuration, one expects to capture about 10% of the light emitted by the LED, that should give images similar to the experiments presented in [1].

1.4 Vessel windows

The transparent windows of the combustion vessel must be chosen to satisfy resistance to pressure difference between the ambient air and the inner side of the sphere, as well as allowing good optical quality.

Because schlieren photography highlights density gradients through a transparent medium, the windows should be transparent and manufactured in a way that its mass is homogeneously distributed on its whole section. Hence, a material may look transparent to the naked eye, but the schlieren image may show variations in the local brightness of the resulting background image, owing to the variations of mass in the window's section.

For this reason, glass windows are generally recommended over transparent plastics like acrylic

or polycarbonate. Indeed, their manufacturing process relies on the formation of a crystalline structure, that is less subject to medium non-uniformity, compared to the polymerization process involved in the manufacture of plastics.
Glass windows are however not absolutely free from defects, the latter being enhanced when the windows thickness increases, making the design of the setup more complex as the window needs to be thick enough to support high pressure differences between the inner and outer sides of the combustion vessel. These defects can however be corrected via image processing as long as no regions of the field of view is completely opaque to light, as developped in Section 2.
It is also to be noticed that the windows have to be set perfectly normal to the parallel beam of light, in order to avoid extra light diffraction that may cause the resulting background image to be non-uniformly bright.
Final choice was made on approximately 2 cm thick borosilicate glass windows, that satisfies the glass resistance criteria to pressure differences and optical quality.

1.5 Knife edge

The role of the knife edge is to mask the light that has cross the second field lens but that has been diffracted when crossing the test region.
It is to be placed downstream of the second field lens where the light is focused to a spot of a size equal to the LED bulb size, such that it partially masks it. Its orientation, horizontal or vertical, will determine the direction of the gradients the schlieren set-up will highlight:

- a vertical knife edge will block light deflected horizontally, that allows to see horizontal gradients in the test region
- a horizontal knife edge will block light deflected vertically, that allows to see vertical gradients in the test region

A pinhole can also be used to mask the outer section of the light spot, to show gradients in all directions, and is what would be recommended to visualize the front of spherical flames.
In the ideal case, the edge of the knife-edge should be infinitely thin in order to mask the light at exactly the second field lens focusing point. In practice, a razor blade was chosen, assuming it is thin enough to serve this purpose when using a vertical or horizontal knife edge. In the case of circular pinholes, precision pinholes or irises can be used, and are available at specialized optomechanical components providers, like ThorLabs or Edmund Optics.

1.6 Image acquisition

The choice of a proper camera and lens must be done based on the interval of time during which the events of interest are occurring and their size.
For still photography of propagating flames, the exposure time should be long enough to allow enough light to reach the camera sensor for proper exposure, while being short enough to *freeze* the event and avoid motion blur.
The amount of light reaching the sensor depends on the whole schlieren set-up, including brightness of the light source, field lenses properties, amount of knife-edge cutoff, sensitivity of the sensor or the use or not of neutral density filters, and is generally set by trial and errors.

On the other hand, motion blur can be estimated by the speed at which events of interest occur. For freely propagating, unconfined laminar flames, the velocity of interest is generally the laminar flame speed s_l, that can be estimated using a computational code for thermochemical calculations like the commercially available code Ansys Chemkin-Pro, or the free, open-source software library for Python and C++ Cantera [2].
In the case of laminar spherical flames propagating in a combustion sphere, the apparent velocity of the flame $U_{l,sph}$ at the early stages can be estimated by the apparent velocity of laminar spherical flames propagating in an unconfined medium using the relation:

$$U_{l,sph} = \frac{\rho_f}{\rho_b} \times s_l \tag{2}$$

where ρ_f and ρ_b are respectively the density of the fresh and burned gases.
For schlieren videography of propagating flames, the recording time will mostly be based on the amount of time it takes for the flame front to cross the field of view, and the frame rate should be chosen according to the time resolution required for the analysis.

Spatial resolution of the images should be chosen according to the size of the smallest element involved in the events. It is set by choosing appropriately the camera and its sensor, and the camera lens. The role of the camera lens is to project and magnify the schlieren image formed through the optical arrangement on the camera sensor, longer focal lengths giving larger magnifications.
The resolution of the sensor itself can be chosen to allow image enlargement via cropping, with no loss of relevant details. However, in the case of high speed videography, high resolution may make frame acquisition difficult to perform. The consequence may be limitations in the frame rate (impossible to transfer sensor data to the camera memory fast enough), or in the total amount of frames acquirable (impossible to store so much data in the camera memory).
In the case of laminar flames, one can target a certain amount of pixels, generally 3-5, in the thickness of laminar flames δ_f, that can be estimated using a thermochemical computational code, by the relation:

$$\delta_f = \frac{T_b - T_f}{\left(\frac{dT}{dx}\right)_{max}} \tag{3}$$

where T_f and T_b are respectively the temperature in the fresh and burned gases, and $\left(\frac{dT}{dx}\right)_{max}$ is the maximum temperature gradient across the laminar flame temperature profile.

The values of s_l, U_l and δ_f for laminar, stoichiometric hydrogen-air flames were found to range between $s_l = 1.9$ m/s, $U_l = 10.1$ m/s, $\delta_f = 5.4$ m/s at initial pressure 10 kPa, and $s_l = 2.3$ m/s, $U_l = 16.0$ m/s, $\delta_f = 0.3$ m/s at initial pressure 1 bar, calculated using the attached Python script named `flame.py`.

2 Image processing

This section is aimed to summarize the different steps of image processing of schlieren videos, for applications that are shock waves, detonations, flames, plumes and jet visualization.
They are implemented in Python scripts available for both versions Python 2.xx and Python 3.xx, and requires the non standard libraries *NumPy* and *OpenCV*.

The reference image presented here is taken from a schlieren video showing a cellular detonation. Schlieren images permits to highlight the presence of longitudinal and transverse shocks, as well as shear layers, all connected at triple points as shown in Figure 3. Note that the images brightness in this sequence has been adjusted from the raw footage in a way that the features are easily visible.

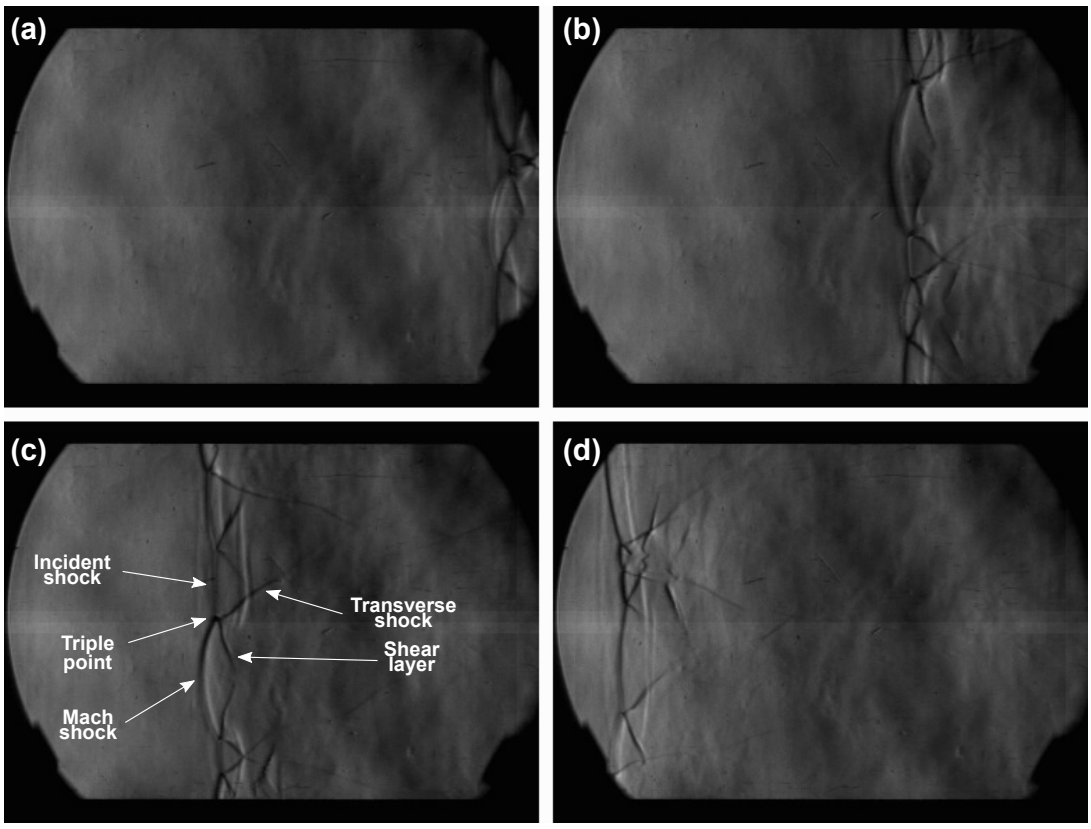

Figure 3: Sequence of images from (a) to (d) showing a cellular detonation propagating from right to left, using high speed schlieren photography.

The images were taken using a Phantom V1210 high speed camera, at a resolution of 384 by 288 pixels, on a field of view of approximately 31 cm from left to right limited by the circular, parabolic mirrors diameter, and bounded on top and bottom by the straight frame of the shock tube in which the detonation front propagates.
The resulting frames are grayscale coded on 8 bits, for which gray level has value 0 for pure black, 255 for pure white, and 128 for medium gray.

2.1 Background removal

Background removal applied to schlieren photography is aimed to remove persistent spots present on the frame. They can be due to the presence of dust on the camera sensor, dirt present along the optical path or defects on transparent elements of the optical setup.
It consists in taking a frame containing the event of interest, and subtracting to each pixel's value the value of the same pixel on a reference frame that contains the background (where

no event occur), then adding to each pixel's value the middle gray value (equal to 128 for an 8 bits image) to make the background be medium gray. The pixel value is then compared to the bounds of the range given by the input image bit depth, and overexposed or underexposed regions are clipped accordingly. The pixel operation transforming the input pixel p_{in} into the output pixel p_{out} is thus, for an 8 bits image:

$$p_{out} = \max[0,\ \min(255,\ p_{in} - p_{ref} + 128)] \tag{4}$$

where p_{ref} is the pixel value of the reference frame containing the background image. An example of the resulting image is shown in Figure 4b, based on the raw image in Figure 4a.

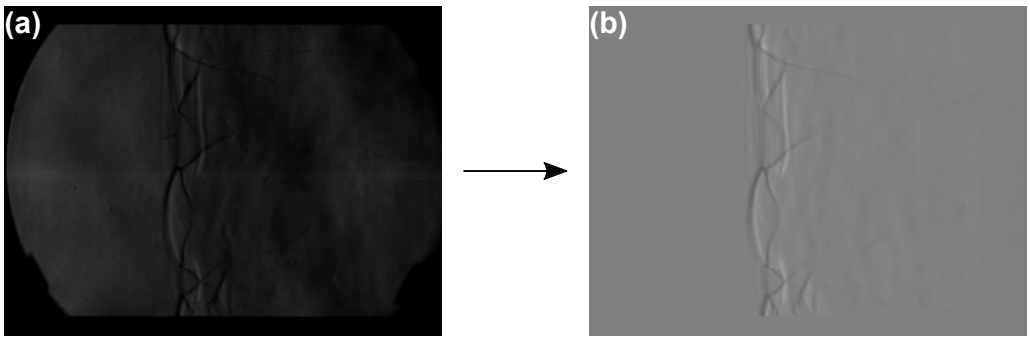

Figure 4: Rendering of the frames after background removal.

The operation (4) can also be applied using for reference frame an image that contains the continuation of the observed event at a few frames earlier or later. Doing so permits to enhance the features in the records of events occurring slowly or captured at high frame rates, where consecutive frames are not significantly different. As a consequence, the background of the frame processed is assumed to be what is contained in the few earlier or later frames of the video.
Proceeding this way is however not recommended when processing records of events occurring fast or captured at a slow frame rate, as the subtraction of two, significantly different consecutive frames may cause the appearance of *ghost* images. As a result, the reference frame containing the background used to generate Figure 4b is the first frame of the footage, in which the detonation front did not appear yet, a few frames before the one shown in Figure 3a.

Background removal also removes opaque elements in the field of view, in a way that masking is required to be done for convenience to identify objects like framing, object, posts, *etc*. Because no light passes through opaque elements, the pixels they are associated supposedly have value 0 or close. Identifying the regions to *mask* thus consist in identifying regions of the unprocessed current image where pixel values are smaller than a small value, generally 1.
Alternatively, if the opaque elements are fixed, processing time can be shortened by assuming all pixels to be masked can be found from a single frame. This latter choice was done to generate the final image shown in Figure 5b, where the pixels to be masked were taken from the first frame of the footage, a few instants before the one shown in Figure 3a.

2.2 Contrast enhancement

As seen in Figure 5, background removal can cause the features of interest to be faint, so that contrast enhancement may be required. This is typically done by applying an *S-shaped* tone

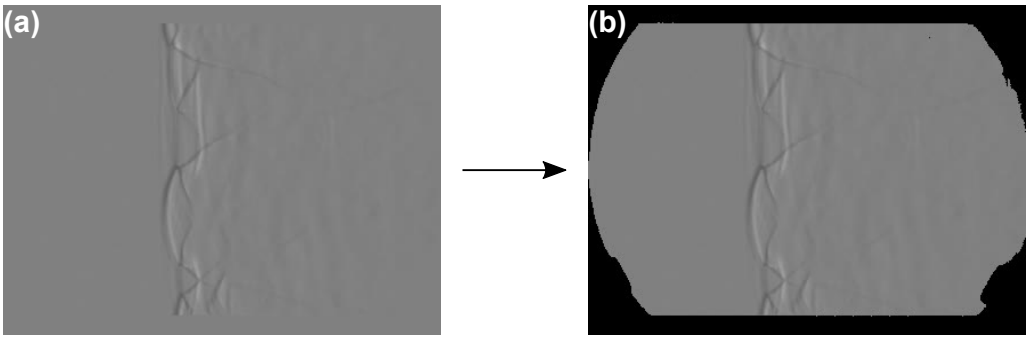

Figure 5: Rendering of the frames after masking.

curve to the image, that has for effect to darken the shadows and brighten the highlights while keeping neutral gray constant, and avoid clipping whites and blacks.
For an 8 bits image, a simple relation between the input pixel p_{in} of an image and the value it should be after contrast enhancement p_{out} is:

$$p_{out} = \frac{255}{1 + \exp(-\frac{p_{in}-128}{\sigma})} \tag{5}$$

in which σ is the parameter that controls the slope at the middle gray input pixel value $p_{in} = 128$. Examples of renderings for multiple values of σ are shown in Figure 6. Note that owing to the relation (5) cases where σ is too small or too large may cause losses of information in the shadows and highlights. For 8 bits images, keeping σ in the range 5 - 20 is recommended.

2.3 Using the Python scripts

The two Python scripts titled `remove-background-pythonX.py` associated to this document perform image processing as described above. They are different in that they are compatible for Python 2 and Python 3.
For them to work, they require libraries *NumPy* for basic mathematics and array handling, and *OpenCV* for image and video processing to be installed. Instructions for their installation can be found at their official links:

- *NumPy* : `https://numpy.org`
- *OpenCV* : `https://opencv.org`

The scripts can be edited in a regular text editor, then ran in a command line under Linux Shell, MacOS command line or Windows *cmd* through the command:

- `python remove-background-python2.py` for versions Python 2.xx
- `python3 remove-background-python3.py` for versions Python 3.xx

The first few lines of the scripts serve as the user interface, and is the only section required to be set to convenience. It contains definitions for the useful parameters, described in Table 1.

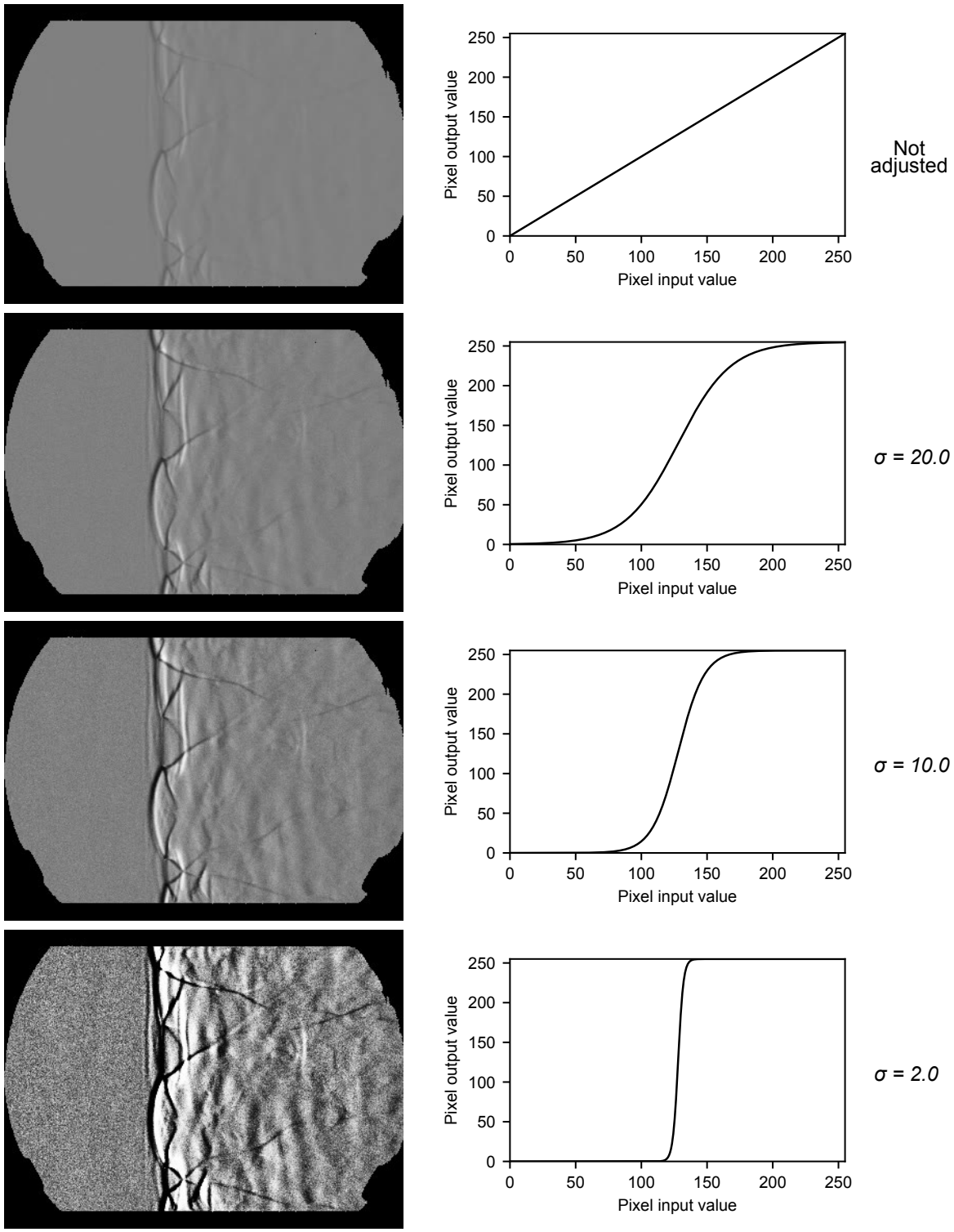

Figure 6: Rendering of the footage for different values of σ.

`in_video`	Name of the video to be processed.
`out_video`	Name of the processed video.
`firstframe`	Index of the first frame to be processed in the video.
`lastframe`	Index of the last frame to be processed in the video. Can be set to an integer to define any index for the last frame, or as the character string "last" to select the last frame. In the case the value chosen is larger than the number of frames in the video, the last frame is automatically chosen.
`output_framerate`	Frame rate of the output video.
`bginterframe`	Number of frames between the frame to process and the reference image containing the background at few instants later, for background removal. See Section 2.1 for details on how to chose this value. Can be set to any integer from 1 and above. To be set to value 0 to consider the first frame defined in variable `firstframe` to be the one and only containing the background.
`showframe`	Takes boolean values *True/False* to show/hide the current frame processed. Showing the current frame can make the process slow.
`mask_threshold`	For masking, set the pixel value in the reference frame below which a pixel should be masked (typically 1).
`maskfromfirst`	Set boolean value *True* if masking shall be done only based on the first frame. If set to *False*, masking is done based on the frame currently processed. Setting to *False* causes processing to be slow, but is relevant if opaque moving objects are present in the field of view.
`change_contrast`	Set boolean value to *True* to apply contrast adjustment.
`sigma`	Set any floating point number as value of σ in relation (5).

Table 1: Table of reference for the parameters called in the image processing Python scripts.

3 Further improvements

3.1 Use of a neutral density filter

Dealing with self-luminous events like a flame may require the light source to be powerful enough to overcome the brightness of the schlieren object. The consequence is that the camera may gather too much light in a way that the sensor is saturated.
To compensate for this, one may use a neutral density (ND) filter to dim the light reaching the camera sensor, to be placed after the knife edge. Finding the appropriate amount of light transmitted across the ND filter to properly expose the camera sensor can be done by:

1. setting the light source brightness in a way the camera sensor gives properly exposed images
2. measuring the amount of light reaching the camera lens (in *lux*) using an incident light meter
3. increasing the light source brightness to the required value and measuring it again
4. calculating the fraction of light to be collected for proper exposure, relative to the amount of light available when the light source brightness is at the desired value

Neutral density filters of various light transmission fraction can be found in optomechanical components shops like ThorLabs or Edmund Optics, generally available in the form of sheets or plates that can be mounted on an appropriate optical post for easy integration to the overall optical bench. Photography shops also provide ND filters in the form of camera lens filters. They are however less flexible than sheets as they must be chosen to fit the camera lens on which it will be mounted.

References

[1] GISKES, E., VERSCHOOF, R. A., SEGERINK, F. B., AND VENNER, C. H. Schlieren study of a sonic jet injected into a supersonic cross flow using high-current pulsed LEDs. *69th Annual Meeting of the APS Division of Fluid Dynamics - Gallery of Fluid Motion* (Nov. 2016). arXiv: 1606.06683.

[2] GOODWIN, D. G., MOFFAT, H. K., AND SPETH, R. L. Cantera: An Object-oriented Software Toolkit for Chemical Kinetics, Thermodynamics, and Transport Processes, Aug. 2018.

[3] SETTLES, G. S. *Schlieren and shadowgraph techniques: visualizing phenomena in transparent media*, softcover reprint of the hardcover 1st edition 2001 ed. Experimental fluid mechanics. Springer, Berlin Heidelberg, 2001. OCLC: 248149245.

[4] WILLERT, C. E., MITCHELL, D. M., AND SORIA, J. An assessment of high-power light-emitting diodes for high frame rate schlieren imaging. *Experiments in Fluids 53*, 2 (Aug. 2012), 413–421.

[5] WILSON, S., GUSTAFSON, G., LINCOLN, D., MURARI, K., AND JOHANSEN, C. Performance evaluation of an overdriven LED for high-speed schlieren imaging. *Journal of Visualization 18*, 1 (Feb. 2015), 35–45.

Appendix B

Jet visualization and analysis for the study of the influence of the Lombard effet on speech aerosol dispersion

The report attached in the following pages summarizes the experiments and analysis proposed for the study of jets formed at humans' mouth during speech, in order to investigate the influence of the Lombard effect, i.e. the way speech changes depending on the ambient noise in which it is performed, on speech aerosol dispersion.

An experimental procedure was designed to visualize human exhalation during speech, using high-speed schlieren videography. To investigate the influence of the Lombard effect, human participants were asked to recite four simple sentences, while background noise at different volume was played. Audio records, together with the schlieren videos, were then used to comment on the dispersion of aerosol originating from human speech.

Tools aimed to analyze the high-speed video footage were also developed, in order to extract relevant quantitative data. They relied mostly on jet detection algorithms, and the use of particle image velocimetry like methods. Those permitted to evaluate the evolution of the jet size, flow velocity field and volumetric flow rate of air exhaled. These data collected over the whole set of experiments were then compiled, and statistical analysis aimed to discuss how the ambient noise may affects aerosol dispersion from human speech was performed.

Jet visualization and analysis for the study of the influence of the Lombard effet on speech aerosol dispersion

Willstrong Rakotoarison, Farzane Zangene

Abstract

The following document summarizes the experiments and analysis proposed for the study of jets formed at humans' mouth during speech, in order to investigate the influence of the Lombard effect on speech aerosol dispersion.
An experimental procedure was designed to visualize human exhalation during speech, using high-speed schlieren videography. To investigate the influence of the Lombard effect, i.e. the way speech changes depending on the ambient noise in which it is performed, human participants were asked to recite four simple sentences, while background noise at different volume was played. Audio records, together with the schlieren videos, will later be used to comment on the dispersion of aerosol originating from human speech.
Tools aimed for the analysis of the high-speed video footage were also developed, in order to extract relevant quantitative data. They relied mostly on jet detection algorithms, and the use particle image velocimetry like methods. Those permitted to evaluate the evolution of the jet size, flow velocity field and volumetric flow rate of air exhaled. These data collected over the whole set of experiments could then be compiled, and statistical analysis aimed to discuss how the ambient noise may affects aerosol dispersion from human speech can be performed.

Contents

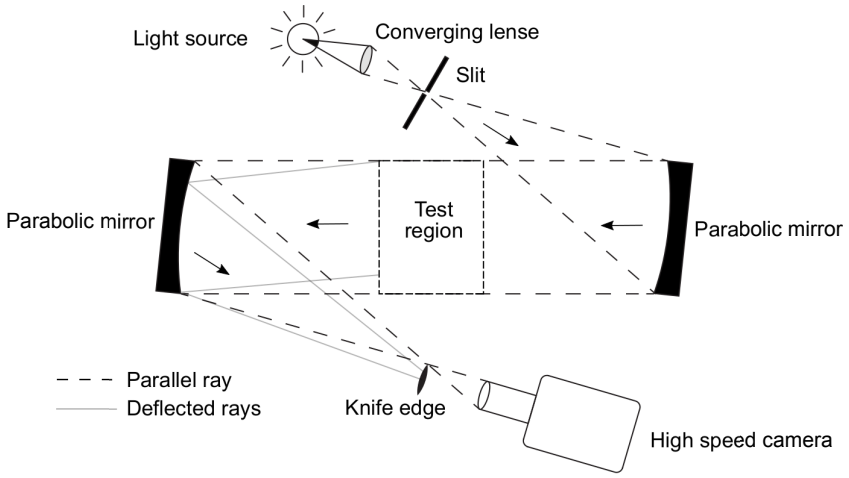

Figure 1: Raw schlieren image (left) and processed image to remove the background (right).

1 Experimental setup

1.1 Video

To perform flow visualization of exhalations coming out of the mouth of a person, a Z-type schlieren setup is used. This setup uses light refraction to visualize regions where gas density varies, like the plume of hot air over a heat source, or jets, shocks, combustion waves, etc.

The working principle is presented in Figure 1. A point light source is placed at the focal point of a parabolic mirror, to form a beam of parallel light. The flow subject is placed on the path of this parallel light beam. As the light crosses a *schlieren object*, i.e. a region where the gas density changes, the light rays are slightly deflected due to light refraction. Passed the schlieren object, the beam of parallel light is re-focused using a second parabolic mirror.
In the case where no light has been refracted, a point of light should be located at the focal point of the second parabolic mirror. If light was refracted a spot of light is observed instead. The spot is partially covered using a *knife edge*. This has for effect to block the rays deflected by the schlieren object. For visualization, a screen or a camera is placed behind the knife edge. The resulting schlieren image appears as a grayscale representation of the regions where the light has been deflected as it crossed the schlieren object.

The schlieren videos were recorded using a Phantom V1210 high speed camera. An example of the raw image is presented in Figure 2a. The sample videos presented here were recorded at a framerate of 400 frames per second, and with a resolution of 768 by 768 pixels, giving a resolution of approximately 2383 pixels per meter, determined using the circular section of the mirror that has a diameter of 317.50 mm. The resulting frames are grayscale coded on 8 bits, for which gray level has value 0 for pure black and 255 for pure white.

The videos were pre-processed to have them ready for data extraction. To get the focus on the jet, the background was removed. The method used to achieve it was to take the gray value of

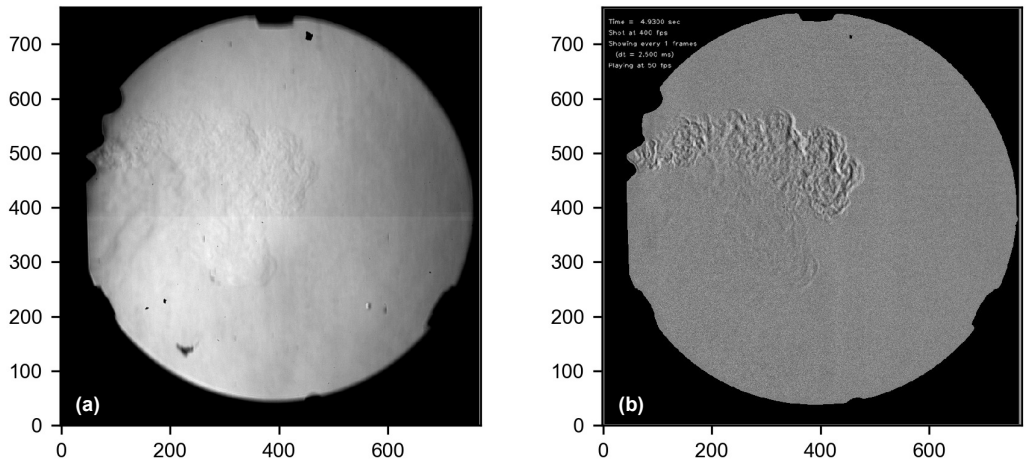

Figure 2: Raw schlieren image (left) and processed image to remove the background (right).

each pixel of one frame, and subtract the value of the same pixel of the next frame. This has for effect to assign to any pixels showing the still background a value close to 0. It also assigns to any pixel initially darker than the background a negative value. The latter was corrected by adding the value 128 to each pixel to make the background be medium gray. An example of the resulting image is shown on Figure 2b.

1.2 Audio

To complete the video records, audio was recorded on two devices. One was an Olympus LS10 model voice recorder, recording uncompressed 16 bits WAV files, at a sample rate of 44.1 kHz. The second was a National Instrument BNC data acquisition system (DAQ), recording the raw microphone voltage output voltage as 14 bits files, with a sampling rate of 44.1 kHz. The DAQ could be triggered together with the camera, allowing for precise synchronization between audio and video records.
Finally a 94 dB tone was recorded on both devices for calibration in post-process.

To investigate the Lombard effect on speech, a noise level calibrated background noise track was played in the participant's ear through a headset.

1.3 Experimental procedure

One experiment was done as follow. The participant was asked to seat in a way his/her face was at the edge of the schlieren field of view.
The Olympus LS10 voice recorder was turned on first, followed by the camera and the DAQ that were triggered simultaneously. A *clap* was then emitted using two plastic rods, in order to synchronize the high fidelity audio signals of the voice recorder with the DAQ signal, and thus with the video.
Approximately 3 seconds later, the participant was asked to pronounce the following 4 sentences, spaced by a time interval of approximately 3 seconds :

1. Peter Piper picked a peck
2. Where were you a year ago
3. She sells seashells by the sea
4. Mama made more lemon jam

Overall, the audio and video sequence were approximately 25 seconds long for a given background noise level. After 25 seconds, the camera and the DAQ stop recording, and the voice recorder is turned off.

2 Flow field extraction

2.1 Motion detection

The first step of flow field extraction consists in identifying regions where the jet is located. The result will be used to save computational resources when performing particle imagery velocimetry as described in 2.2, by performing it only in regions where the jet is located, as well as to infer the jet size evolution over time.

On the videos, the area the jet occupies corresponds to the area where significant motion could be observed. These areas can be identified using a simple motion detection filter as described in [1], applied to small regions of interest (ROI) of N-by-M pixels covering the whole frame.
The principle is the following. A pair of consecutive frames is chosen. The value of each pixel in a ROI is given by $g_1(i,j)$ and $g_2(i,j)$ respectively for the first and the second frame, for integers values $i \in [0, N-1]$ and $j \in [0, M-1]$, .
The root mean square (RMS) gray-level difference in the ROI between the two consecutive frames is given by

$$\phi = \sqrt{\frac{1}{N \times M} \sum_{i=0}^{N-1} \sum_{j=0}^{M-1} [g_2(i,j) - g_1(i,j)]^2} \tag{1}$$

This operation is applied on the overall frame such that the field of ϕ can be constructed. The results show some regions of the frame where ϕ is small, corresponding to regions where the first and second frame are almost identical. Regions in which the first and second frame are different show larger values of ϕ, suggesting that motion occurred.

A threshold value of ϕ is chosen, above or below which motion is assumed to occur or not, respectively. In practice, finding a single threshold for all frames of an experiments is difficult, owing to to slight variations of the average value of ϕ that may exist between several frames.
This difficulty is overcome by choosing a threshold value for $\bar{\phi} = \phi/(\phi)_{\text{average}}$, the value of ϕ normalized by its averaged value on a whole frame.
As a result $\bar{\phi}$ has for value 1 at its average. Typical thresholds chosen for identifying motion were taken for $\bar{\phi} \simeq 1.2 - 1.4$, for ROIs chosen of size 32×32 pixels square.

2.2 Particle image velocimetry (PIV)

Details of the flow involved by the jet, like the local flow velocity and direction, could be estimated using a particle image velocimetry (PIV) like method, applied to schlieren images.

Particle image velocimetry (PIV) is a common method used in experimental fluid mechanics. It consists in reconstructing a flow field by tracking the motion of groups of particles seeded in the flow with time.
To do so, two consecutive images of a given plane in the flow are captured at a short time interval. The local flow direction and magnitude are then determined by comparing small regions of the flow, located at the same position on the two frames. The method is illustrated in Figure 3, applied to a counter-clockwise vortex.

Two images of the vortex seeded with white particles at two different times are shown on Figure 3 (a) and (b). The region where the flow magnitude and direction are wanted is identified by the red squares drawn on each frame, and will be denoted as the *seeking region*, assigned to the second frame.
An enlarged view of the seeking region for each frame is shown as a solid red square on Figures 3 (c) and (d). On the same view is represented in dashed red square what is denoted as the *mask*. It contains the pattern of particles of interest in the first frame, and should be of a size smaller or equal to the seeking region.
To determine the magnitude and flow direction, one need to determine by what amount the mask containing the particles of the first frame should be shifted, in the vertical and horizontal directions, to correlate with the particles of the second frame in the seeking region.
The appropriate shift was found in practice by finding the minimum of the least square difference between the seeking region and the mask, by shifting the mask horizontally and vertically. This operation is repeated on other seeking regions to reconstruct the flow field.

This method was adapted to schlieren images, where correlation between 2 frames was found instead of particles. A mask size of 32 by 32 pixels and seeking regions of size 64 by 64 pixels were found appropriate to reconstruct to determine the local flow velocity. A distance of 7 pixels horizontally and vertically between the center of 2 seeking regions was found appropriate to reconstruct the velocity field with high enough accuracy.

3 Results

3.1 Jet size

Figure 4 gives an example of the found contours of the jet, taking a threshold value of $\bar{\phi}$ equal to 1.35.
The number of pixels contained inside the region contoured in red representing the regions where motion occurred, i.e. where the jet is located, can be counted and the result gives a measure of the size of the jet. This can be done for each frame of the video and a time evolution of jet size could be plotted, as seen in Figure 5.

The time evolution of the jet size can be differentiated with time, so that a characteristic speed of the spreading of the jet could be deduced, expressed in pixels per second, as shown in 5. As a reference, this value is positive when the jet size increases, is negative when the jet size decreases.

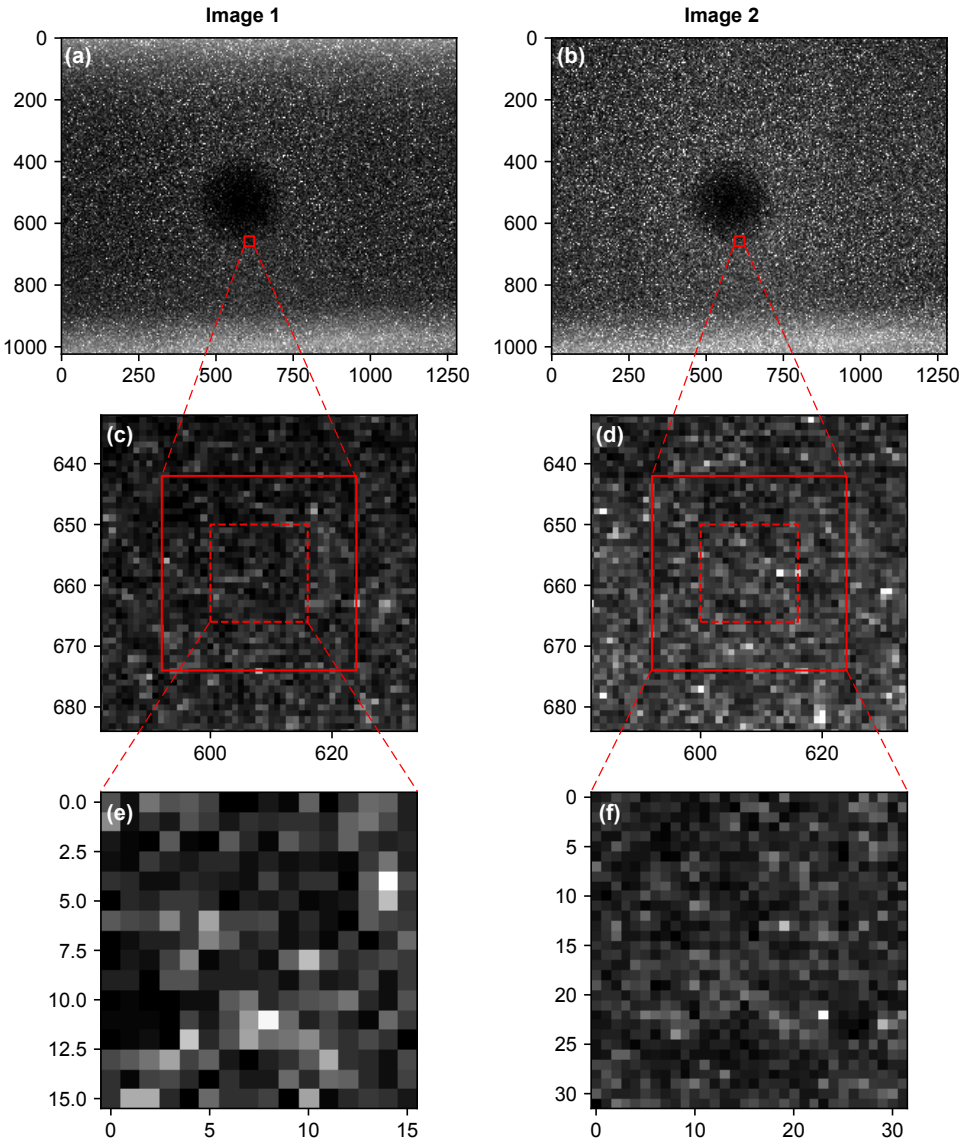

Figure 3: First (left column) and second (right column) images used to visualize the flow field generated by a vortex using PIV. Figures (a) and (b) are the global images. Figures (c) and (d) are zoomed in the relevant regions of interest for each image, i.e. the mask extracted from the first image (dashed red square), and the seeking area, extracted from the second image (solid red square). Figures (e) and (f) are the mask and the seeking region.

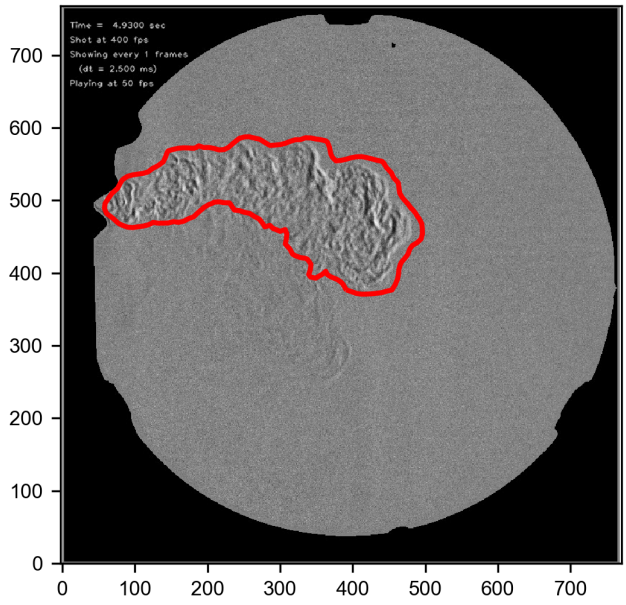

Figure 4: Contours (in red) of the jet determined using the motion detection filter.

Both plots were drawn together with the audio recorded by the DAQ, as a reference for defining instants when sentences are pronounced. It is relevant to mention that in between sentences, the size of the jet is not 0, but correspond to moments where the participant was breathing.

3.2 Flow field

An example of the flow field obtained using method described in section 2.2 is shown in Figure 6. The image on the top shows the magnitude of the flow velocity, and the image at the bottom shows the streamlines of the flow coming out of the mouth of the participant.

3.3 Jet carried momentum

The flow velocity being known, one can define as a measure of the jet velocity the average velocity of the flow at all points of the jet.
This jet velocity can then be multiplied by the size of the jet to provide a measure of the momentum carried by the jet.
The latter could then be used as a reference to discuss how far can a jet spread : a small jet going with a small velocity spreads less far than a large jet with a large velocity. In between lie small jets with large velocities and large jets with small velocities.
In Figure 7 are plotted both the average jet velocity in pixels per frame and the measure of the jet momentum, together with the audio recorded using the DAQ for reference.

3.4 Jet volumetric flow rate

A measure of the jet volumetric flow rate could be determined from the flow velocity profile, by measuring the amount of gas exhaled crossing a given boundary.
A reference figure for the calculations is given in Figure 8 for the notation, where the boundary considered was taken at $x = 200$ pixels. To determine the volume crossing a boundary, one needs to integrate the flow velocity over this boundary :

$$\dot{V} = \int_{y_{\text{bottom}}}^{y_{\text{top}}} u_x(x, y) dy$$

where u_x is the x-component of the local flow velocity Because the flow field measured using PIV-like method is discrete, the integral is approximated by a sum, and a measure of the volumetric flow rate crossing the boundary at location x is given by :

$$\dot{V} \simeq \sum_{i=0}^{N_y} u_x(x, y_i) \Delta y$$

where N_y is the total number of discrete points in the y-direction where the local velocity was measured, y_i the i^th discrete point in the y-direction, and Δy the distance between the center of two discrete points, equal to 7 in Figure 8.

As an example, the flow rate evolution over time crossing border $x = 200$ pixels is plotted on Figure 9, together with the audio recorded using the DAQ for reference.
A couple of remarks can be done from this plot. The first one concerns the amount of mass crossing a given boundary, that is expected to decrease the further the boundary is from the participant's mouth.
A second remark concerns the patterns observed when comparing the audio to the volumetric flow rate. It can be seen that the flow rates for a given sentence reach a maximum a few instants after the sentence is pronounced, and its maximum is larger when the sentence it succeeds does not provide a large flow rate.
This suggests that the maximum reached is due to air exhaled while breathing, that is large for sentences that did not require a lot of air to be pronounced.

3.5 Statistics

Statistics from single sentences can be done, and more global data at different background noise level playback can be done.
Figure 10 shows normalized statistics extracted from the experiments performed on participants 4 and 5.

The horizontal axis shows not at scale background noise level. The vertical axis represents values of different quantities introduced above, averaged on a single sentence.
To obtain these bar diagrams, the start and end time at which a sentence was pronounced was identified on the audio signals.
The average value of the quantity of interest over the time the sentence was pronounced was then calculated. This process was repeated for all sentences, at a given background noise level and plotted in Figure 10 in black, blue, red and white.

The process was repeated for all background noise level. A group average of the values associated to a given quantity for a single participant was calculated, then used to normalize the bar diagrams.
This was done in order to facilitate comparison between participants, by setting to value 1 the average speech volume associated to a single participant.

References

[1] KEGERISE, M. A., AND SETTLES, G. S. Schlieren Image Correlation Velocimetry and its Application to Free-Convection Flows. *9th International Symposium on Flow Visualization* (2000).

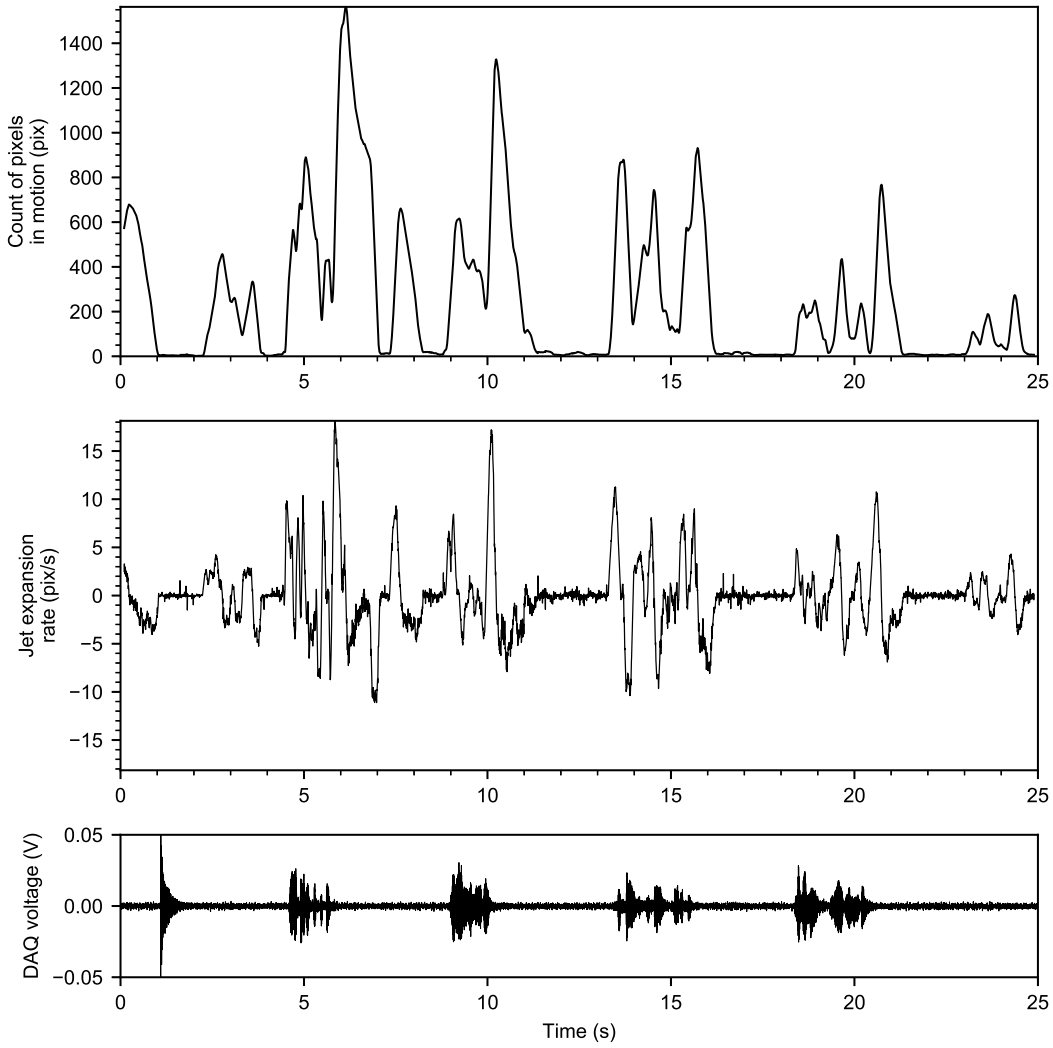

Figure 5: Jet size evolution and expansion rate over time. Audio signal recorded by the DAQ is also plotted as a reference for determining when a sentence was pronounced.

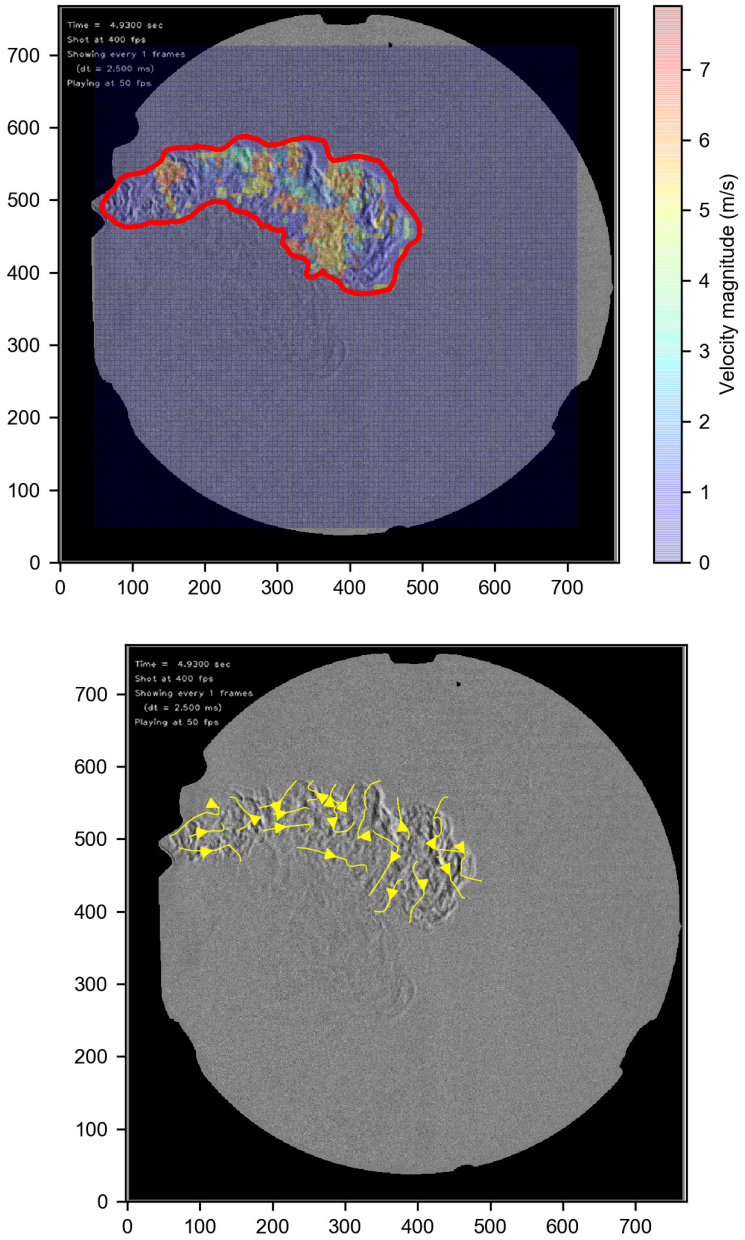

Figure 6: Magnitude of the velocity field (top) and streamlines (bottom), calculated using PIV-like method described in 2.2.

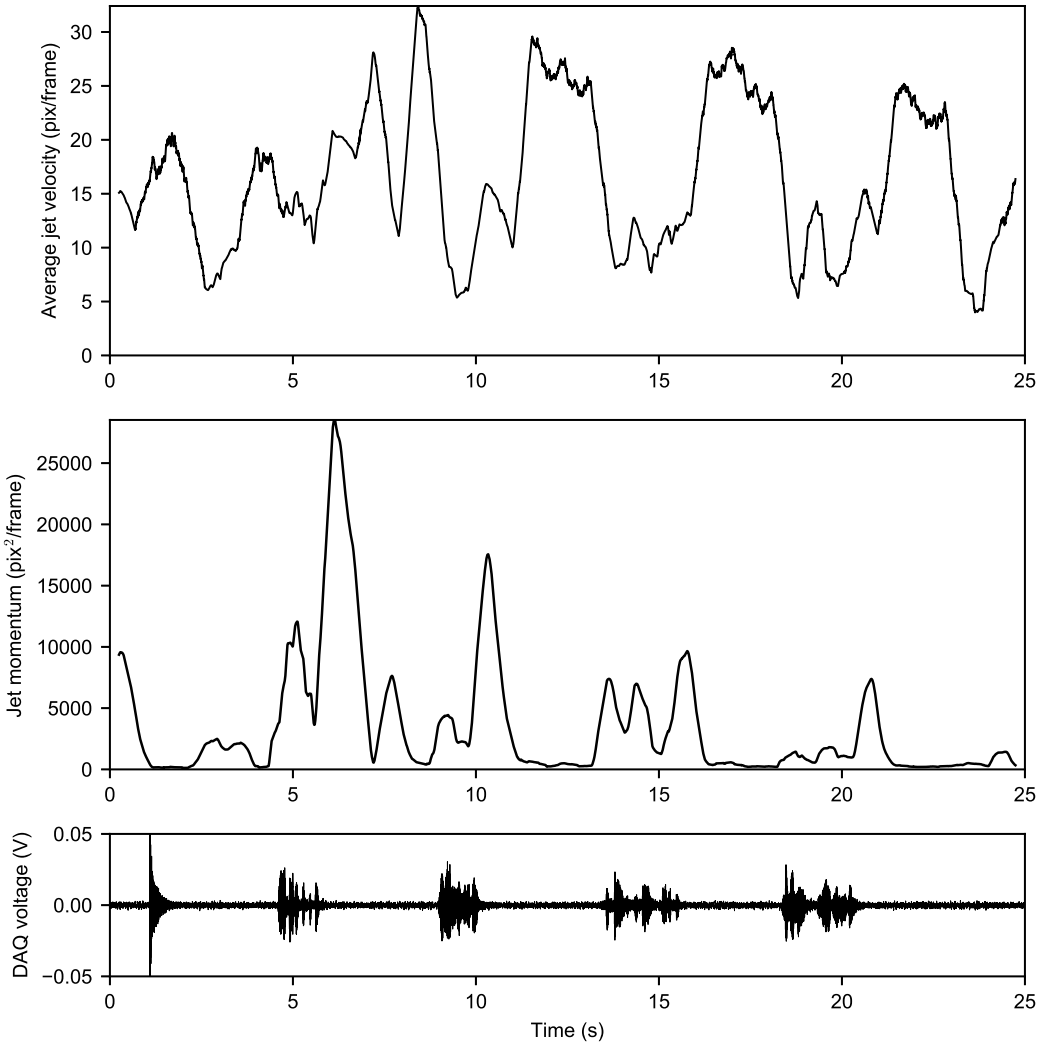

Figure 7: Example of the jet average velocity and momentum.

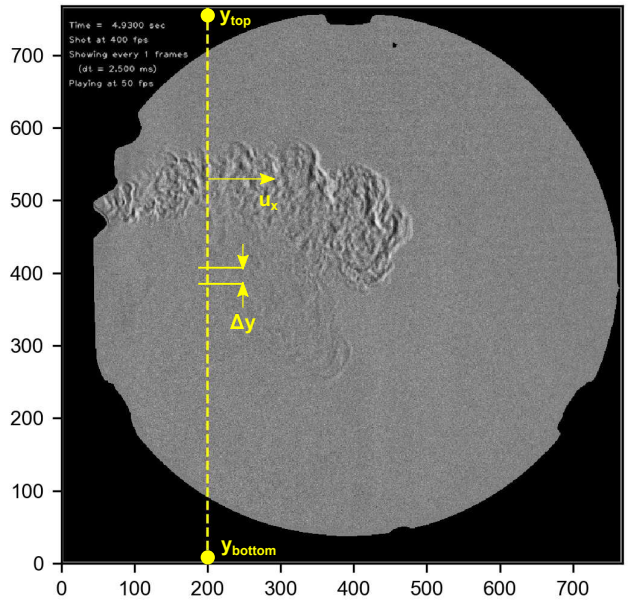

Figure 8: Schematic of the method used to evaluate the volumetric flow rate of human exhalation.

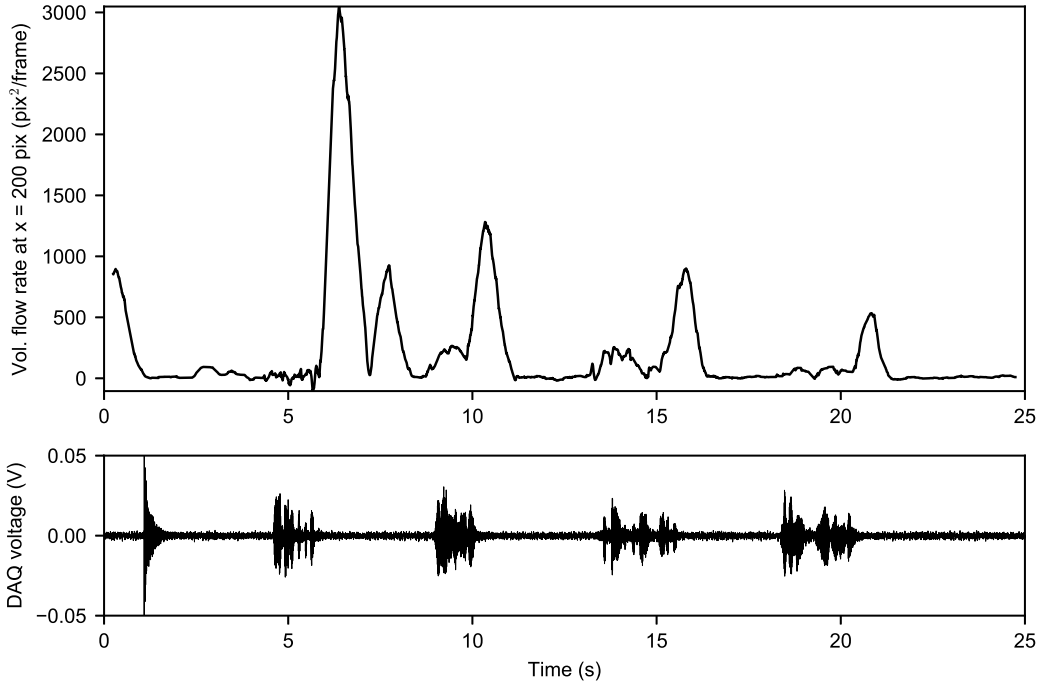

Figure 9: Jet volumetric flow rate at location $x = 200$ pixels.

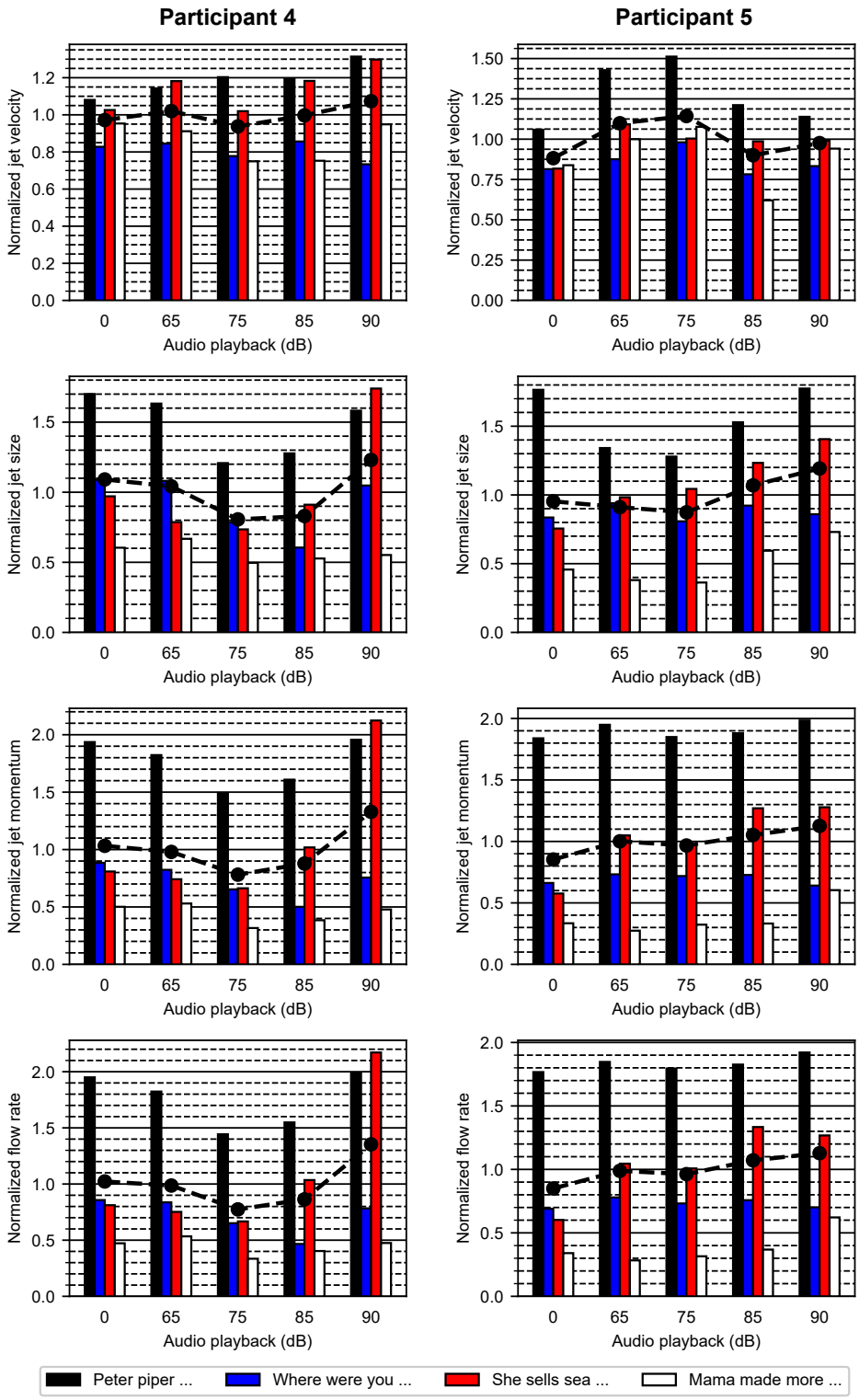

Figure 10: Statistics extracted from the flow measurements. Results are here presented normalized by the average value over the whole set of experiment associated to a single subject, for a given quantity.